UNIVERSITAT POLITÈCNICA DE CATALUNYA BARCELONATECH

PhD program in Electronic Engineering

Design and development of wireless nodes for the Internet of Things

Article-based thesis – Industrial doctorate

Doctoral thesis by:

Ripoll-Vercellone, Edgar

Thesis advisor:

Gasulla, Manel

Reverter, Ferran

Electronic circuits and transducers (e-CAT)

Department of Electronic Engineering

Castelldefels, February 2022

Dedicado a mis padres, Jorge y Silvana, quienes me dieron todo. Sin su sacrificio esto no hubiera sido posible.

Acknowledgements

Primero que todo, agradecer a mi familia por su amor y apoyo incondicional, no solo en estos años de doctorado, sino en toda mi vida. Una mención especial a mis padres, Silvana y Jorge, y a mis hermanos, Grecia y Leandro. Nuestra constante dedicación y ganas de crecer hizo que muchas veces estemos alejados físicamente, pero siempre juntos virtualmente. Son lo que más amo y me dan fuerzas para seguir adelante.

Gracias también a mis amigos que han estado siempre a mi lado, aun estando lejos. Gracias Ignacio porque juntos comenzamos a perseguir un sueño y curiosamente encontraste la convocatoria a este doctorado. Hubiera sido muy gracioso que yo encontrara la *job offer* de tu trabajo, pero no fue así, la encontraste vos mismo y todo salió mejor de lo que imaginamos. Gracias a mis amigos que sumé desde que llegué a Barcelona, han sido mi familia adoptiva en esta ciudad.

Debo agradecer al grupo de investigación e-CAT de la UPC por aportar su espacio y la instrumentación necesaria para llevar a cabo mi doctorado. En especial a mis directores de tesis Dr. Manel Gasulla y Dr. Ferran Reverter por su conocimiento y por guiarme durante todo el proceso. El objetivo no se hubiera cumplido sin su incalculable ayuda.

Me gustaría agradecer también a la empresa Idneo Technologies que me dio la oportunidad de desarrollar mi investigación. En especial a Jordi Aubert y a Vicent Ferrandiz, sus aportes a la tesis han sido imprescindibles. Gracias Jordi por recibirme y esforzarte por integrarme en mis primeros meses, es un gran gesto del que nunca me olvidaré.

Finally, I thank the different institutions for the funding received to develop this research: the EnSO (Energy for Smart Object) project under Grant Agreement No. 692482, the Secretariat of University and Research of the Ministry of Business and Knowledge of the Government of Catalonia, the Spanish Ministry of Economy and Competitiveness, the European Regional Development Fund under Project No. TEC2016-76991-P, the Department of Electronic Engineering of the UPC, and the Spanish State Research Agency (AEI).

Muchas gracias a todos por aguantar mi escasa interacción social que les he brindado para dedicar tiempo a mi carrera profesional. Gracias por animarme y escucharme en los peores momentos. Gracias por alegrarse y acompañarme en los mejores momentos. Gracias, gracias y gracias.

Abstract

The Internet of Things is a trending topic these days. It is improving people's daily lives, mainly because it greatly facilitates a wide variety of everyday household tasks. It also generates new business areas for new and well stablished companies. However, energy is often the major job stopper for broad adoption of this technology, which have three tight constraints: extremely cost oriented, long service life and small size.

As a consequence, developers must overcome many challenges related to the optimal management of the energy available to power a node. This management is not only limited to the power supply, but also comprises the smart energy consumption of the node. Three challenges are addressed in this work: the first associated with the node's sensing system, the second, with the power consumption when the node is not operating, and the third, with the energy harvesting. The contributions of this thesis are presented as an article-based dissertation of three fundamental journal publications and three conference articles, where each fundamental publication addresses one of the challenges.

The first contribution is related to the node's sensing system. Particularly, the electronic gas meters' sensing system. A novel sensing system for gas meters has been developed. It is based on a dual magnetic sensing: a) low-cost, low-power primary sensing via reed switches connected to the microcontroller's (MCU) digital inputs, and b) secondary sensing using Hall-effect sensors coupled to the MCU's analogue inputs. Furthermore, both sensing systems use an active and a passive element to provide an output that is immune to external interfering magnets. To establish the dependability of the prototype, it was implemented and evaluated under various test scenarios. In addition, the contribution is complemented with the design of a node that could be easily installed in old mechanical gas meters to upgrade them to smart ones. This study has gone some way towards improving the data collection process of gas meters. Taken together, these contributions meet the constraints of nodes for the IoT.

The second contribution of this research work has proposed, analyzed, and evaluated a contactless wake-up circuit for an MCU that makes use of a light-emitting diode (LED) operating as a photodetector and is lighted by a smartphone flashlight. This contribution contains a theoretical analysis as well as experimental data that support the circuit described. Two wake-up circuits were proposed: a) a simple one, but with limitations and b) a robust one, which requires extra stages. The circuit a) is the simplest, lowest-cost, smallest, and lowest-power solution for waking up an MCU found in the literature. It consists of only a resistor and an LED. Nevertheless, its limitation is the operation under ambient light conditions, which may cause unwanted turns-on and higher consumption to the node. The circuit b) comprises a high-pass filter and a voltage-level translator that connects the LED to the MCU through an appropriate resistor in parallel. When lighted by a switching flashlight, the LED produces a square voltage, which is translated into logic levels at the wake-up circuit output. A firmware embedded in the MCU also ensures that a specified series of logic pulses at a specific rate is received in order to activate the MCU. These additional

stages make it more robust against ambient light interferences. Note that LEDs manufacturers do not disclose information regarding how LEDs respond to light. It is critical for designers to understand the behavior of LEDs to create new applications in this field. Consequently, in order to select the most appropriate LED depending on the ambient interfering lights, this second contribution is complemented with the current-voltage characterization of several types of LEDs in two scenarios: outdoors and indoors.

Finally, in the third contribution, the energy challenge associated with the node's power source is addressed. Specifically, the energy harvesting of radiofrequency (RF) signals present in the environment is chosen among all available energy sources. Numerous RF energy harvesters have been proposed in this regard. The challenge is that the amount of RF energy that can be harvested in some realistic scenarios is relatively limited, needing the development of highly efficient harvesters. However, due to the non-linearities of the circuit, the research and simulation to obtain further insight into the harvesters' performance are difficult. A compact Thévenin model for a rectenna is proposed in this study. This model is used to create a high-efficiency RF harvester with a maximum power point tracker (MPPT). The investigated rectenna comprises an L matching network and a half-wave rectifier. The developed model is simpler and more compact than those previously proposed in the literature, and it contains explicit and simple analytical expressions of the Thévenin voltage (V_{oc}), resistance, and power efficiency. The rectenna is implemented and characterized from -30 to -10 dBm at 808 MHz. The experimental findings support the suggested model, demonstrating a linear current–voltage relationship as well as a maximum efficiency at $V_{oc}/2$, specifically 60% at -10 dBm. At the rectenna output, an MPPT was also employed to automatically work at the highest efficiency point, with an overall efficiency nearing 50% at -10 dBm. Further experiments were carried out, this time with a nearby transmitting antenna, to power a sensor node with a power demand of 4.2 µW.

The last two chapters review, analyze, comment on the obtained results in relation to the argument and the objectives of this thesis, and conclude the current research work.

Resumen

El Internet de las Cosas (IoT) es un tema tendencia en estos días. Está mejorando la vida diaria de las personas, principalmente porque facilita en gran medida una amplia variedad de tareas domésticas cotidianas. También genera nuevas áreas de negocio para empresas nuevas y consolidadas. Sin embargo, la energía es a menudo el principal obstáculo para la adopción generalizada de esta tecnología, que tiene tres restricciones estrictas: es extremadamente orientada a los costos, requiere una larga vida útil y un tamaño pequeño.

Como consecuencia, los desarrolladores deben superar muchos desafíos relacionados con la gestión óptima de la energía disponible para alimentar un nodo. Esta gestión no solo se limita a la fuente de alimentación, sino que también comprende el consumo energético inteligente del nodo. En este trabajo se abordan tres desafíos: el primero asociado con el sistema de detección del nodo, el segundo, con el consumo de energía cuando el nodo no está en funcionamiento, y el tercero, con la recolección de energía. Las contribuciones de esta tesis se presentan como un compendio de artículos de tres publicaciones fundamentales de revistas y tres artículos de conferencias, donde cada publicación fundamental aborda uno de los desafíos.

La primera contribución está relacionada con el sistema de detección del nodo. En particular, el sistema de detección de los contadores electrónicos de gas. Se ha desarrollado un nuevo sistema de detección para contadores de gas. Se basa en una detección magnética dual: a) detección primaria de bajo costo y baja potencia a través de interruptores de lengüeta conectados a entradas digitales del microcontrolador (MCU), y b) detección secundaria mediante sensores de efecto Hall acoplados a entradas analógicas de la MCU. Además, ambos sistemas de detección utilizan un elemento activo y uno pasivo para proporcionar una salida que es inmune a imanes externos que puedan interferir con la medición. Para corroborar la fiabilidad del prototipo, se implementó y evaluó en varios escenarios de prueba. Además, la contribución se complementa con el diseño de un nodo que podría instalarse fácilmente en contadores de gas mecánicos antiguos para actualizarlos a medidores inteligentes. Este estudio ha contribuido a mejorar el proceso de recopilación de datos de los contadores de gas. En conjunto, estas contribuciones cumplen con las limitaciones de los nodos para IoT.

La segunda contribución de este trabajo de investigación ha propuesto, analizado y evaluado un circuito de activación sin contacto para MCUs, que hace uso de un diodo emisor de luz (LED) que funciona como fotodetector y es iluminado por el flash de un móvil. Esta contribución contiene un análisis teórico, así como datos experimentales que sustentan el circuito descripto. Se propusieron dos circuitos de activación: a) uno simple, pero con limitaciones y b) uno robusto, que requiere etapas extra. El circuito a) es la solución más simple, de menor costo, más pequeña y de menor consumo para activar un MCU que se encuentra en la literatura. Consiste solo en una resistencia y un LED. Sin embargo, su limitación es el funcionamiento en condiciones de luz ambiental, que puede provocar activaciones no deseadas y un mayor

consumo del nodo. El circuito b) comprende un filtro pasa alto y un traductor de nivel de voltaje que conecta el LED al MCU a través de una resistencia apropiada en paralelo. Cuando se hace conmutar el flash, el LED produce una señal cuadrada, que se traduce en niveles lógicos en la salida del circuito de activación. Un firmware integrado en el MCU garantiza que se reciba una serie específica de pulsos lógicos a una cierta velocidad para activar el MCU. Estas etapas adicionales lo hacen más robusto contra las interferencias de la luz ambiental. Se debe resaltar que los fabricantes de LED no divulgan información sobre cómo responden los LED a la luz. Es fundamental que los diseñadores comprendan el comportamiento de los LED para crear nuevas aplicaciones en este campo. En consecuencia, para seleccionar el LED más adecuado en función de las luces ambientales interferentes, esta segunda aportación se complementa con la caracterización corriente vs. tensión de varios tipos de LED en dos escenarios: exterior e interior.

Finalmente, en la tercera contribución, se aborda el desafío energético asociado con la fuente de energía del nodo. Específicamente, la recolección de energía de señales de radiofrecuencia (RF) presentes en el medio ambiente se elige entre todas las fuentes de energía disponibles. En este respecto, se han propuesto numerosos recolectores de energía de RF. El desafío es que la cantidad de energía de RF que se puede recolectar en algunos escenarios realistas es relativamente limitada, lo que requiere el desarrollo de recolectores altamente eficientes. Sin embargo, debido a las no linealidades del circuito, la investigación y la simulación para obtener más información sobre el rendimiento de los recolectores de energía son difíciles. En este estudio se propone un modelo compacto de Thévenin para una rectenna. Este modelo se utiliza para crear un recolector de RF de alta eficiencia con un rastreador de punto de máxima potencia (MPPT). La rectenna investigada comprende una red de adaptación L y un rectificador de media onda. El modelo desarrollado es más simple y compacto que los propuestos previamente en la literatura, y contiene representaciones explícitas de la tensión (V_{oc}) y la resistencia de Thévenin y la eficiencia energética. La rectenna está implementada y caracterizada de -30 a -10 dBm a 808 MHz. Los hallazgos experimentales apoyan el modelo sugerido, demostrando una relación lineal entre la corriente y la tensión, así como una eficiencia máxima a $V_{oc}/2$, específicamente 60% a -10 dBm. En la salida de rectenna, también se empleó un MPPT para trabajar automáticamente en el punto de mayor eficiencia, con una eficiencia general cercana al 50% a -10 dBm. Se llevaron a cabo más experimentos, esta vez con una antena de transmisión cercana, para alimentar un nodo sensor con una demanda de potencia de 4.2 μW.

Los dos últimos capítulos revisan, analizan y comentan los resultados obtenidos en relación con la argumentación y los objetivos de esta tesis, y concluyen el trabajo de investigación actual.

Contents

Acknowledgements ..... **v**
Abstract ..... **vii**
Resumen ..... **ix**
Contents ..... **xii**

1 Introduction **1**

1.1 Motivation 2

1.2 Argument 2

1.3 Objectives 5

1.4 State of the art 5

1.4.1 Internet of Things 5

1.4.2 Wireless Sensor Node 7

1.4.3 Energy challenge 1: Low-power sensing system 17

1.4.4 Energy challenge 2: Low-power wake-up circuit 29

1.4.5 Energy challenge 3: High-efficiency energy harvester 35

1.5 Structure 40

1.6 Publications 41

2 Publications I & II **44**

2.1 Publication I: Conference proceeding I 45

2.2 Publication II: Journal Article I 45

3 Publications III, IV & V **55**

3.1 Publication III: Conference proceeding II 56

3.2 Publication IV: Conference proceeding III 56

3.3 Publication V: Journal Article II 56

4 Publication VI **68**

4.1 Publication VI: Journal Article III 69

5 Analysis of the results **84**

5.1 Energy challenge 1: Low-power sensing system 85

5.2 Energy challenge 2: Low-power wake-up circuit 95

5.3 Energy challenge 3: High-efficiency energy harvester 101

6 Conclusion and future work 106

6.1 Conclusions 107

6.2 Future work 109

6.2.1 Energy challenge 1: Low-power sensing system 109

6.2.2 Energy challenge 2: Low-power wake-up circuit 110

6.2.3 Energy challenge 3: High-efficiency energy harvester 110

7 References 112

1

Introduction

1.1 Motivation

This research work is carried out within the framework of an Industrial Doctorate program of the Generalitat de Catalunya. Within an Industrial Doctorate, the PhD student is enrolled in a university but bases his/her research in a strategic research project of a specific company. The research for this project is developed at the company Idneo Technologies S.L. jointly with the electronics Circuits and Transducers (e-CAT) research group of the Department of Electronic Engineering at the Universitat Politècnica de Catalunya. Idneo wants to become a leader in the emerging field of the Internet of Things (IoT) and this doctorate is part of its strategy to achieve it. Idneo, through national and international associations and forums, will follow this doctorate and other market initiatives to orientate research and development to the challenges faced on these initiatives and its related products/services.

The contributions of this thesis are presented as an article-based dissertation of three journal publications and three conference articles. This doctoral thesis will tackle issues commonly encountered when designing a wireless sensor node for the Internet of Things. The specific approach will be as general as possible to extrapolate the achieved results to other products and scenarios. Nevertheless, it does not exist a one-size-fits-all approach to solve these problems, that is why the author worked on different solutions for energy problems faced when designing an IoT device. The solutions depend on the form factor, the application, the environment where the node will be installed, the available energy to power the node, etc. Also, because of the company-specific work dynamic of the industrial doctorate, the focus of the investigation varied during the doctorate. The research projects were linked to clients, the company, or the research group interests, which led to a broad research field.

1.2 Argument

Broadly, several initiatives rely on Internet of Things (IoT) as enabling technologies [1]–[12]. Energy is often the major job stopper for broad adoption of this technology [13]–[16], in particular in very high-volume products, which have the following three tight constraints [17], [18]:

- Extremely cost oriented: Particularly when objects are disposable or have reduced life, the IoT node must be in line with the overall cost, which implies that IoT nodes of such products have to be extremely cheap [19].
- Long service life [19], [20]: they tend to be spread and may not be under control; therefore, maintenance such as replacing a battery is either not possible or economically not feasible [13], [14]. A long lifetime is required as it keeps maintenance and cost lower.

- Small size: they are destined to be ubiquitous [14].

The challenge is to power wireless nodes while complying with the three constraints. On the one hand, the lower the cost and the smaller the size, the lower the energy that can be stored or harvested. On the other hand, the longer the service life, the higher the energy needed. As a consequence, developers must overcome many issues related to the optimal management of the energy available to power a node. This management is not only limited to the power supply, but also comprises the smart energy consumption of the node. These issues will be referred from now on as *energy challenges*. Three challenges will be addressed here: the first associated with the node's sensing system, the second, with the power consumption when the node is not operating, and the third, with the energy harvesting.

Firstly, the energy challenge tackled by this thesis is related to the node's sensing system. Particularly, considering the employer partner interests, the aim is the design of a low-power sensing system for gas meters. This challenge will be referred herein as *low-power sensing system*. Historically, the measurement of the gas usage of residential communities is performed with mechanical gas meters [21]. Even though the gas meters' performance proved to be highly reliable for over 20 years, the collection process of the measurement data is done periodically one-by-one by a company provider technician [22]–[26]. Therefore, the process is slow, costly, and prone not only to human mistakes, but to fraud, too [22]. Moreover, the gas meters suffer all kind of tampering attempts by the users, which cannot be detected by the gas meters, since they do not have any smart device to register them.

Smart gas meters are becoming an alternative to the traditional mechanical meters [27]. There are two types of smart gas meters: electronic gas meters and add-on nodes. The first one requires replacing all the old meters by these new electronic gas meters. This option takes a lot of work, cost, and time [24]. The second is an add-on node that upgrades the old meters to smart ones, without the need to replace them. It is a challenge for either of these smart gas meters to match or improve the reliability and service life of traditional gas meters, to be free from tampering fraud, or at least detect them, and to improve collection process of data. In addition, the smart gas meters must still comply with the three constraints for IoT nodes. A low-cost, small size, and low-power measurement technique insensitive to external tampering attempts is required.

Secondly, the energy challenge tackled by this thesis is related to the power consumption when the node is not operating. This challenge will be referred here as *low-power wake-up circuit*. In some applications, several months can pass between the assembly and the activation of the sensor node. Furthermore, the node case is usually permanently sealed. Hence, this prevents adding the power supply later to active the node. Moreover, adding a switch or a button only to turn it on once increases cost, number of components and size. A wireless wake-up source is needed so the node can remain at its lowest power mode until a signal wakes it up.

Many wireless wake-up technologies that can be used for this purpose exist. The main ones are RF, optical and magnetic. RF wake-up sources have been widely investigated. Piyare et al. [28] developed a survey of 75 different researches. All of these require one or two antennas to achieve this, which increases the size and cost of the node. A magnetically-actuated sensor is an alternative. However, it requires the node to have a sensor only for this purpose. Besides, the reader should be able to generate a magnetic field. Finally, optical wake-up mechanisms are a promising alternative for short-range line-of-sight applications. Studies have been done in this field, finding the main issues in the ambient light interference and complex circuits that do not comply with the constraints of nodes for the IoT.

Thirdly, the energy challenge associated with the node's power source will be addressed. This challenge will be referred herein as *high-efficiency energy harvester*. Currently, two main alternatives are used for providing energy to the IoT node: the use of primary batteries or environmental energy harvesting [13], [14], [19], [20]. Primary batteries lead to simpler designs because, depending on the electrical characteristics of the device, the battery might match the voltage range of the node components. If that is not the case, a DC-to-DC (DC-DC) voltage converter is required, for example a linear or a switching regulator. The downside of the primary batteries is they have a limited energy budget. Their use is feasible whenever the available energy is enough to power the IoT node during a cost-effective period of time. Contrariwise, energy harvesting leads to more complex designs [14]. Despite the design complexity, the available energy is unlimited. The downside is that the available average power is limited and needs to be higher than the average power required by the IoT node to ensure the device remains powered [29].

From the point of view of the power supply and due to demands within the scope of the industrial doctorate and the research group, energy harvesting is the topic selected. Specifically, from all the sources of energy, the harvesting of the radiofrequency (RF) signals available in the environment or intentionally radiated by a nearby RF source is selected. In that sense, countless RF energy harvesters have been extensively proposed [30]–[39]. The problem is the RF energy that can be harvested in some practical scenarios is very limited, so highly efficient harvesters must be designed [40]. However, the study and simulation to gain more insight into the harvesters' performance are complex because of the non-linearities of the circuit [41]. Several models have been proposed in the literature. Some models are complex and require additional simulations or extensive calculations [42], others, are simpler but are inferred from experimental data [43]. Therefore, there is a need for a novel and simpler analytical model to fully characterize the RF energy transducer, which will ease the design of highly efficient harvesters.

1.3 Objectives

Given the industrial doctorate context, the aim of this thesis is to address different topics concerning the design and implementation of nodes for the IoT. Three objectives have been formulated, one for each energy challenge mentioned in the previous section:

- Objective 1: Define a feasible sensing system alternative for smart gas meters. This objective includes the design and implementation of a low-power, small size, and low-cost sensing system insensitive to external tampering and the improvement of the collection process of the data of gas meters.
- Objective 2: Optimization of the IoT node power consumption when this is not operating. This objective involves the analysis, characterization, and evaluation of a simple low-power wireless system for waking up nodes.
- Objective 3: Analysis, design, and implementation of a high-efficiency RF energy harvester. This objective includes characterizing and proposing a simple model of the transducer and then applying that model to design a highly efficient RF energy harvester.

1.4 State of the art

This section presents the context and background of wireless nodes for the IoT. Firstly, the IoT topic is introduced. The definition, applications examples, and an overview of the IoT's elements are provided. Secondly, the focus is on wireless nodes for the IoT, where a detailed explanation of the modules they comprise is given. Thirdly, the three energy challenges are addressed: low-power sensing system, low-power wake-up circuit, and high-efficiency energy harvester.

1.4.1 Internet of Things

The Internet of Things is a trending topic these days [14]. The ISO/IEC[1] defined the IoT as "an infrastructure of interconnected objects, people, systems and information resources together with intelligent services to allow them to process information of the physical and the virtual world and react" [44]. This is improving people's daily lives, mainly because it greatly facilitates a wide variety of everyday household tasks [45].

The IoT generates new business areas for new and well stablished companies [14], [46], too. For example, in the healthcare sector, many wearable sensors are being developed, such as glasses, wristbands, hearing aids, and systems for tracking and managing assets in hospitals [47]. The healthcare

[1] ISO/IEC (International Organization for Standardization and International Electrotechnical Commission): Organized the Joint Technical Committee, which is the standards development environment where experts come together to develop worldwide Information and Communications Technology (ICT) standards for business and consumer applications.

sector benefits because it can implement constant and reliable monitoring of most of its internal processes, tools, and resources. Patients also benefit because the new technologies allow concrete tracking of their passage through the healthcare system, monitoring the availability and use of medications and, in some cases, gauge body signs associated with the effectiveness of treatment and rehabilitation. In the Smart Society field, we find utility meters, secure authentication wearables and electronic seals or locks. Moreover, in the Mobility and Production areas, some examples are industrial assets monitoring, indoor localization and navigation support and wireless condition monitoring [48].

In [49], IoT remote monitoring systems for the mining, rail and construction industries are implemented. The use of the IoT resources in mining allow a significant increase in safety in exploration and extractive activities. Basically, they allow to establish real time remote measurements and monitoring with minimal human intervention. In addition, operating costs are reduced in this way. Most common sensors in this industry are geophones, piezometers, and toxic gas detectors [50]. These sensors work in combination in Wireless Sensor Networks (WSNs). Rail and construction industries also benefit from IoT devices, as they can use them to monitor assets in real time and program timely maintenance activities [51]. On the other hand, construction mostly uses IoT technology to ensure workers safety through alarm and monitoring systems to reduce accidents [52], [53].

Lastly, IoT are also widely implemented in the retail sector [54]. Currently, retail sector uses various IoT nodes and software to optimize service processes through various functions: contributing to an augmented and unique shopping experience based on proximity sensors; or establishing food tracking systems to ensure maximum freshness of meats and fruits.

Currently, the above examples show intensive uses of IoT nodes for different modalities of asset monitoring. This is associated with supply chains, maintenance scheduling, and user distribution. It is also used to substantially increase worker safety. In those applications, not only wireless sensors nodes are required, but also a system able to organize and handle the information these nodes constantly gather.

A generic IoT system consists of three mains elements: the Edge, the Gateway (GW) and the Cloud. Figure 1 shows a generic architecture of an IoT system. The IoT system allows connecting the wireless sensor nodes into the Cloud using a methodology that promotes scalability, interoperability, and security all the way from the edge to the Cloud.

The *Edge* is the integration between the physical and the computation world. It usually includes: “things” (physical devices); wireless sensor nodes, forming WSNs; actuators; gateways, which connect different WSNs [55]. A WSN is a set of nodes organized into a network. In IoT systems, the things have a variety of sensors deployed in homes, automobiles, or factories [56]. The WSN has adopted the same kind of topologies than traditional networks: star, mesh, grid, circular, bus, tree, and ring [57].

The *Gateway* is a device that serves multiple functions. It acts as a bridge between the nodes and the Cloud [58]. It forwards the information coming from the nodes and sends it to the Cloud and vice versa. In addition, it may provide both hardware and software level of security to lock down the WSN of the internet of things. Besides, it can process data and transform it to actions in real time, resulting in a closed loop control.

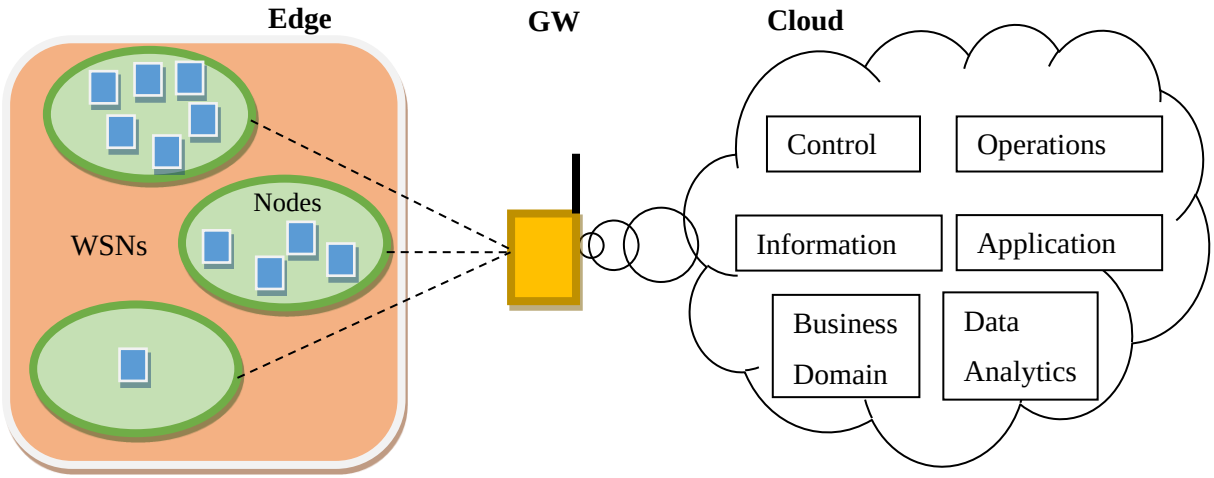

Figure 1: Architecture of a generic IoT system

The *Cloud* is a platform where the data is stored and processed. It contains the system infrastructure, and it allows the interaction with the users. It provides the computing capability that enables to perform big data analytics for the IoT solution [55]. The Cloud can have the same information, which was collected at the edge for a particular deployment but expanded through a set of assets from around the world. It can turn basic data into information that can become valuable insights into how the IoT system is functioning in the field. It enables to extract the value through the analytics capabilities.

This section has attempted to provide a brief overview of the IoT, which includes: the Edge, the GW, and the Cloud. The following part of this dissertation moves on to describe in greater detail the nodes for the IoT.

1.4.2 Wireless Sensor Node

A wireless node of the IoT is an electronic device, which spends most of the time in standby mode (or sleep mode) and only wakes up to perform a quick defined task [14]. This task is usually sensing, processing, and transmitting information [59]. This results in a typical current consumption profile as show in Figure 2. During time interval $t_{1\text{-}2}$, the node is sensing and processing the data, while consuming a current i_2. During $t_{2\text{-}3}$, the node transmits the information while consuming i_3. In general, transmitting the information is the most power-hungry function. The current i_1 is the node consumption in sleep mode, usually in the order of µA or even less. Finally, T is the task period, which, depending on the application, might be in the order of seconds, minutes or even days.

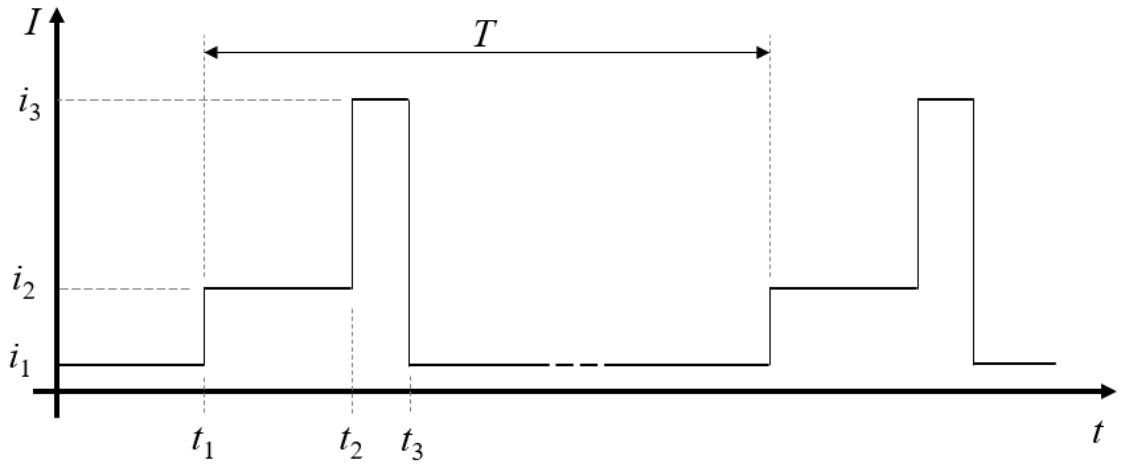

Figure 2: Generic current consumption profile of a wireless node.

Figure 3 shows the block diagram of a generic wireless sensor node. It commonly consists of four modules: power, sensor, control and communication [59]–[62]. These 4 modules will first be quickly outlined here:

- Power module: provides electrical energy to the rest of the modules. It usually integrates a power source and, optionally, a power conditioning circuit.
- Control module: responsible of making the node a smart object. It usually includes a processor, the interfaces to connect with the other modules, the clock, and the memory unit. This is generally done with a low-power microcontroller (MCU). It controls all the other modules, and it processes the information [61].
- Communication module: sends and receives data using a transceiver.
- Sensor module: transforms a physical or chemical quantity into an electrical signal. Also, it includes the analog signal conditioning circuit so that the microcontroller can process the signal.

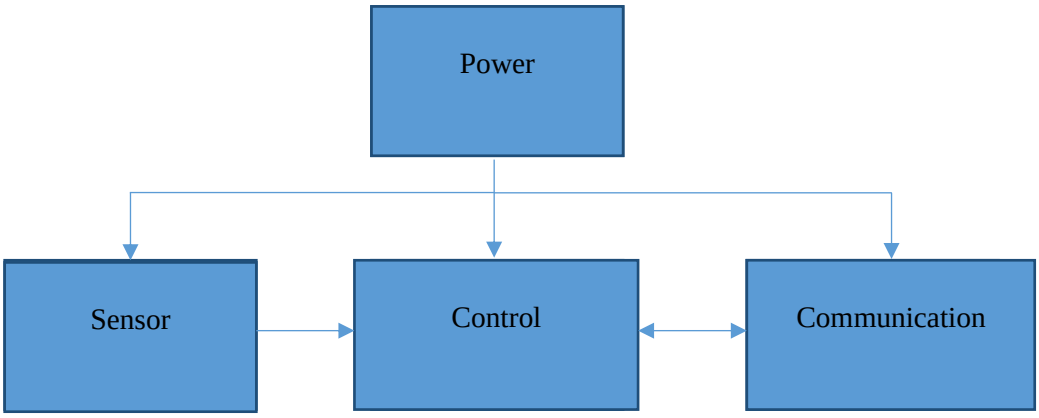

Figure 3: Block diagram of a generic wireless sensor node

The design and implementation of wireless sensor nodes for the Internet of Things requires paying exceptional attention to their sources of energy consumption in order to extend their lifetime

[13], [14], [63]. Consequently, every module of a node is examined in the following subsections. The definition, functions, characteristics, and an overview of recent advances in power consumption optimization of the node's modules are described.

1.4.2.1 Power Module

Two types of power source are considered for sensor nodes: batteries and energy harvesting. A more detailed account of batteries is given in this subsection, which includes theory, classification, and techniques for optimizing the available energy. The topic energy harvesting will be addressed in depth in Section 1.4.5.

Nodes need energy mainly for acquiring (sensing), processing and sending the information. When choosing the right power source for a node, some aspects have to be taken into account, for example, the required lifetime of the node, the environment where is located, the restrictions of size and cost, etc. Due to the large number of nodes in a WSN and the difficult physical accessibility to them, the option of changing batteries when they are drained it may not be feasible. So, it is not convenient to waste energy in the sensor node and special care must be taken to manage power in a highly efficient manner.

Batteries

The use of batteries is the most common way of powering the nodes. Batteries are chemical devices that store energy. They are commonly built with a liquid electrolyte and two electrodes (positive and negative), which through the reduction-oxidation reaction of the electrolyte with metals (electrodes), convert chemical energy to electrical energy [64].

There are many kinds of batteries. They can be classified in primary and secondary batteries. Primary batteries can be used only once, i.e., when their energy is depleted. They have to be thrown away (and recycled) because they cannot be recharged. Contrarily, secondary batteries (commonly called rechargeable batteries) can be used a certain amount of charge and discharge cycles. They have lower power density than primary batteries [59], so their use in wireless nodes is only justified if the node is powered by energy harvesting.

Regardless of the great number of battery manufacturers [65]–[69], there is a standard for the battery sizes and voltages. Common nominal voltages for primary and secondary batteries are: 1.2 V, 1.5 V, 3 V and 3.6 V. With the possibility to connect them in series to reach a higher voltage, of course. Conventional primary and secondary battery chemistries are Lithium-Ion (Li-ion), Lithium-Manganese dioxide (Li-MnO_2), Lithium-Iron disulfide (Li-FeS_2), Alkaline, Nickel-Cadmium (Ni-Cd), and Nickel-Metal hydride (Ni-MH). Lithium-based batteries have become popular for powering IoT devices since they have considerably more energy density and the voltage remain quite constant while discharging [70], [71].

The liquid electrolytes found in batteries, especially the ones containing lithium, are extremely volatile and highly flammable. These electrolytes also must not be exposed to air, earth, or water since they are highly contaminant. Moreover, if a thermal runaway occurs, the electrolyte creates safety hazards [64], [72]. An alternative to liquid-electrolyte batteries are solid-state batteries [73]. They are safer because they do not contain liquid chemicals. Nevertheless, their power density is much lower, and the manufacturing cost is considerably higher than liquid-electrolyte batteries [64], [72]. Therefore, the use of solid-state batteries is appropriate only if the application requires them rather than liquid-state ones. For example, medical applications or environmentally hazard applications that might cause a thermal runaway to liquid-state batteries.

Power conditioning circuit

The node power conditioning circuit will depend on the battery voltage and the node's voltage requirements. Common node's required voltages are: 1.8 – 3.3 V, 3.6 V and 5 V. If the voltage requirement matches the battery voltage, it is possible to connect the proper battery directly to the node. Otherwise, a DC-DC converter is required. DC-DC converters are electronic circuits that converts a source of direct current (DC) from one voltage level to another. Low power DC-DC converters can be linear regulators, which dissipate unwanted power as heat, or switching regulators, which convert the voltage by transferring power in discrete energy packets by using the energy-storing capabilities of inductive and capacitive components. An extended theoretical description about the operating principle of DC-DC converters can be found in [74], [75].

Connecting the battery directly to the node might not be the most energy efficient way, even if the node voltage requirement matches the battery voltage. Sometimes, it can be more efficient to use a step-down switching converter configured to make the node work at a lower admissible voltage. Nowadays, switching converters have considerably improved their efficiencies, even at low-current consumption [76]–[78]. Their quiescent current has been reduced to a couple of nanoamperes. Moreover, when the battery voltage decreases to a certain threshold over the target voltage, it automatically disables the commutation and internally bypasses itself.

For example, a node voltage requirement range goes from 1.8 – 3.3 V and the selected battery is a 3 V coin cell CR2032. As mentioned before, one option is to connect the battery directly to the node. Another option is to connect it through a highly efficient step-down configured to 2.1 V (considering that output ripple of a switching converter can reach up to a couple of hundreds of millivolts). This working voltage lowers the power consumption of the node.

An important remark is that usually recently-purchased batteries, with a certain nominal voltage, have an output voltage of hundreds of millivolts higher than the nominal one. For example, 3.3 V for 3

V batteries or 4.2 V for 3.6 V batteries. This may affect in the overall lifetime efficiency since switching converters are more efficient while the input and output voltage difference is lower. Therefore, a thorough study has to be made to choose the right output voltage, which depends on the components and functionalities of the node. The right output voltage will optimize the conversion efficiency with the node power consumption. This technique is more complex than connecting the battery directly to the node, but it can significantly increase the lifetime of the node.

Novel switching converters allow many other techniques to be used to dynamically increase the power efficiency. For example, there are off-the-shelf switching converters that can dynamically change its output voltage. Given the periodicity of the node's tasks (sensing, processing, transmitting, and sleeping), it is possible to configure the power supply voltage depending on the task. The voltage can be configured to its lower value when the node goes to sleep. Then, increase it to a higher value that endures the voltage drops due to current hungry tasks, such as sensing and transmitting.

Low Drop Out (LDO) voltage regulators are commonly used, too. They are linear DC-DC converters. Sometimes preferred over switching converters because of their lower cost and the fact they do not need an inductor. However, their power efficiencies are lower than switching converters, especially when voltage differences are large. Occasionally, LDOs are used together with a switching converter. The purpose is to clean up the ripple out of the voltage supply after the switching converter.

Energy Harvesting

It is not always possible to place a battery in the IoT device. Many reasons exist such as battery lifetime, size, or environment requirements (places where it is not allowed, or recommended, to put a battery, like human pacemaker, hospitals, etc.) Energy harvesting is an alternative to supply these kinds of demands. This technology can be also used to recharge batteries and extend the lifetime of the device [79] and to power batteryless devices (which usually are of the kind power-only-when-there-is-energy.)

Energy harvesting is a method that takes advantage of the energy available from the environment and transforms it to electrical energy [59]. Under the right conditions, this technology allows the nodes to run permanently. The downside is the increase in the complexity of the circuit that entails conditioning the voltage to properly power the nodes [14]. Another inconvenient is that the amount of energy that provides the harvester is typically small and highly variable over time. This creates uncertainties that make the forecast of autonomy difficult. When the energy availability is approximately regular, it is possible to accumulate it and store it for later use in a secondary battery or a supercapacitor [80]. If the energy availability is not frequent, more than one energy-harvesting source can be included to power the node.

Powering wireless nodes with energy harvesting normally implies a larger size, cost, and a greater number of components than the primary battery solution. However, with this solution, no

maintenance is required, and the possibility of perpetual work is feasible. The topic energy harvesting will be addressed deeper in Section 1.4.5.

1.4.2.2 Control Module

The main component of the control module is the MCU, which is generally a low-power version. It is responsible of making the node a smart object. It usually includes a processor (CPU), the interfaces to connect with the other modules, the clock, and the storage unit. It controls all the other modules, and it processes the information [61]. The power consumption of a microcontroller depends on the amount of computational operation needed to carry out the algorithm, the MCU architecture and the clock speed.

The optimization of energy consumption in microcontrollers is a key aspect for the node lifetime or even their survival in case they take its power from energy-harvesting sources [13]. Lately, technology advances in microcontrollers allowed improvements in the subject of low-power consumption. New techniques have been developed, such as Dynamic Power Management (DPM) and Dynamic Voltage and Frequency Scaling (DVFS). The appearance of those techniques resulted in a diversity of low-power modes (LPMs), also called sleep modes, for microcontrollers. Due to the large diversity of variables, the selection of the correct mode has become a complicated task. First of all, there are many MCU manufacturers, which fabricate MCU with different architectures and create specific features for their MCUs. Therefore, the management of the internal modules of the MCU differ from one manufacturer to another. Second, there are a lot of internal modules in an MCU. Each one with many specific configurations and power modes.

Many Operating Systems (OS) for microcontrollers were developed in order to facilitate the programming process. However, they may not be as optimal in the sense of energy efficiency because they generalize some common features. Algorithms are needed to optimally run the most accurate LPM and still satisfy the application requirements.

Dynamic Power Management

Dynamic Power Management is a technique that helps a single sensor node or a wireless sensor network to save energy by switching to different energy consumption states at run time. Those states can be defined in different ways. In [61], the authors make a review of some algorithms that carry out the DPM. For example, strategies for configuring the MCU of a node in sleep mode based on its activity [81]–[84]. At network level, the authors mention a cooperative DPM technique in which many nodes get involved in the decision of going to sleep based on a timeout [85]; or in which the WSN makes a prediction of the position of the target [86].

Another approach of this technique is to individually select the operating mode of the different modules that integrate the node, such as sensors or transceivers [87]. In [88], the energy consumption states are determined by power gating the internal peripherals of the MCU.

Dynamic Voltage and Frequency Scaling

Dynamic Voltage and Frequency Scaling is a technique used for reducing the energy consumption by changing the CPU voltage and frequency. This technique is also applied for power saving of other devices, such as multimedia servers [89]. The drawback of this method is the loss of performance. Since MCUs are based on CMOS logic, they have a voltage-dependent maximum operating frequency. This means that reducing the voltage supply implies slower transition stages of transistors, i.e., lower clock frequency and slower computational operations [90], [91]. This power management technique allows the processor to run at a custom voltage and frequency in order to meet the right performance, which still meets the application requirements [92].

Operating Systems for Low-Power MCUs

Since the MCU dynamically manages the power consumption, those algorithms must be contained in the OS. TinyOS [93] was one of the first to carry out the power management. When the scheduler stack does not have tasks to execute, the lowest power mode is selected based on the status and control registers. Besides, they proposed different policies for switching on and off the resources (MCU peripherals and external modules). However, writing applications in TinyOS is particularly complex. On top of that, it is coded in a dialect of C, called NesC. As a result, the learning curve is very steep.

RIOT OS [94] also automatically determines the LPM. The MCU is switched to an idle thread when there are not pending task to execute. Nevertheless, RIOT concentrates only in the MCU power states, but it is not implemented alongside with a DPM algorithm.

Another usable OS for energy management is Contiki [95]. Contiki is an OS designed for very small computational systems (usually up to 8-bit processing) but has been developed to support MCUs and embedded systems. Contiki is composed by a considerably light code, which allows an almost negligible power consumption [96]. In this sense, a dual purpose is fulfilled, since the node operates through a portable, multitasking, and open-source system compatible with a large number of sensors and Wi-Fi network protocols, but with minimal power usage due to its low memory and processing requirements.

Batteryless nodes often are run by special kind of OS that are aware of the energy left before it powers down [97]. This requires the ability to detect the amount of energy recharged by an energy harvesting power module, and to measure what is available in the absence of the ambient energy source. Batteryless nodes seek to obtain energy from the environment itself in order to operate. These devices typically guarantee a virtually infinite operating time, so they require OSs that can efficiently manage data during extended periods. An example of this is Shepherd [98], a system that allows compensating

for batteryless nodes problems. This open-source OS memorizes energy traces between 3 µA to 50 µA with a frequency of 100 KHz to track the energy level of each node in the system.

1.4.2.3 Communication Module

Nodes of the IoT need to transmit the information they sense. This task takes place in the communication module of the diagram block showed in Figure 3. This is the most power-hungry module of a node [14], [16], [19]. The power consumed depends on many factors, such as the communications technology, the protocol implemented, the range of communication, etc. RF and optical communication technologies will be analyzed here, considering the energy costs derived from the use of these systems.

RF technology communicates systems through radio waves, usually choosing a specific bandwidth. This same technology supports systems such as radio and wireless cellular communication. Usually, wireless communication on nodes of the IoT is achieved by RF waves in the unlicensed ISM radio band[2] frequencies. Different standards are used, such as Near Field Communication (NFC) [99], Bluetooth Low Energy (BLE) [100], [101], Sigfox® [102], [103], LoRa [103], and Zigbee [101]. Custom made protocol are also developed using RF transceivers, which perform standard signal modulations, like FSK, ASK, OOK, etc. [104]–[107]. Cellular communication is another RF technology that was recently customized for nodes in order to reduce the required transmission power. LTE-M and NB-IoT are cellular-based standards that, depending on the RF output power and the network settings, require from 200 to 850 mW to transmit information [108]–[112]. Even though these protocols require high current peaks to transmit (around 400 mA [108], [109], [111], [113]), the power consumption is lower than the one required in other cellular-based protocols used for larger amount of data transmission [114], like GPRS (from 0.5 to 3 W and 2 A current peaks), WCDMA (from 1.6 to 2.7 W), LTE-CAT 1 (from 1 to 3.1 W), and LTE-CAT 4 (from 1 to 2.6 W) [115]–[121].

Optical communication allows systems to communicate using perceivable and non-perceivable light signals that turn on and off very quickly, so this can be interpreted as binary signals by a sensor. Light is received by surfaces or specialized sensors connected to transducers that convert light oscillations into data. Light-based communication is also a viable option for low consumption node connectivity because it allows the data to be sent and received with extremely low power consumption (tens of mW and even µW [122]–[124]). The drawback of this technology is that requires line-of-sight between the emitter and the receiver.

Most frequent optical communication technologies used in IoT wireless networks are free space optical (FSO), visible light communications (VLC), optical camera communications (OCC) and wireless networking with light, usually referred to as Li-Fi. The most common way of light-based communication is with infrared LEDs and a photodiode [125], [126]. LED-to-LED communication was also studied, the

[2] ISM radio bands are portions of the radio spectrum destined to industrial, scientific, and medical applications.

results show that this technology, among the other light communication options, is highly energy efficient and significantly lower in cost [127], [128]. On the contrary, Li-Fi wireless networks need high-resource systems [129]. This kind of network allows considerable data transmission rates (about 100 times faster than Wi-Fi), as it uses ultraviolet or infrared light.

Henrie et al. [130] proposed a novel LED-based circuit that can communicate with another devices. Particularly, the LED device can be connected directly to the input of a PC and fit into any port. The proposed circuit uses an infrared LED as an emitter and a phototransistor as a receiver, showing that a bidirectional circuit for wireless data transmission can be created through this type of devices. In this research this mechanism was used to test the connectivity between the PC and sound input and output peripherals.

At this point, it can be understood that both RF and optical communication represent low-power options for ensuring communication between nodes. However, they are also susceptible to adopting ways to further optimize energy utilization. DPM technology allows significant energy savings by controlling the switching on and off of the network's communication module. This can be easily done by using the *chip enable* pin of the transceiver. For example, the communication module should be powered only when a message is needed to be transmitted. This paradigm changed the way communications was done, generating new communication protocols. Only when a node turns on the transceiver to send a data, it is possible for a GW to talk with the node. Otherwise, the communication is powered down to save energy. The disadvantage of this method is that it is not possible to send information to a node other than a small reception period. Low-power wide-area networking (LPWAN) protocols are based upon this methodology. Sigfox®, LoRaWAN®, LTE-M and NB-IoT are examples of protocols have been created based on LPWAN. Furthermore, other protocols were modified to make them compatible with the IoT constraints, for example, the Bluetooth Low Energy (BLE).

It is important to note that, even with the power consumption optimization in LTE-M and NB-IoT, the high current peaks necessary for data transmission and the varying latency call into doubt the idea that battery-powered nodes may have a 10-year lifespan. The power consumption estimates for NB-IoT given by the developers of this technology are specified for a best-case scenario [131]. However, power consumption doubles if coverage is limited. In [132], the authors estimated 12.8 years of battery life with the following 3 considerations: 1) a 27.7 Wh battery, 2) sending a message once a day, and 3) assuming that all the available battery capacity is allocated to the cellular module. Despite the large size of the battery chosen by the authors, it does not even withstand the average current required for transmission without dangerously dropping the voltage by more than 600 mV [133]. This behavior neglects the power supply guidelines established by cellular modules manufacturers [109]–[113]. Alobaidy et al. [108] documented the power consumption of an NB-IoT cellular module throughout transmission. Using the same 3 considerations as in the previous work [132], the maximum achievable

battery life would be around 9.1 years. According to Mekki et al. [114], despite the studies conducted by cellular modules manufacturers, the paucity of NB-IoT commercial deployments raises concerns about the actual battery lifetime and performance of this technology under real-world settings. Therefore, a detailed analysis is required in each particular use case to assess cellular communication feasibility in highly constrained IoT nodes.

1.4.2.4 Sensor Module

A sensor transforms a physical or chemical quantity into an electrical signal. There are different kind of sensors. One way to classify them is by the output type: analog, ON/OFF and digital. A brief description is provided in the following paragraphs.

Analog sensors either change their own impedance (such as resistance, capacitance, and inductance) so a circuit transform it into a readable signal for the control module, or directly outputs a current/voltage signal. Usually, these signals are of low amplitude and noisy. Consequently, a signal conditioning circuit is required to amplify and filter these signals.

ON/OFF sensors have a switch as an output. This can be achieved by relays or a mechanical switch. Sometimes, ON/OFF sensors provide two outputs: normally open (NO) and close (NC). Sensors of this type, if properly connected, do not consume while no actions are performed.

Digital sensors have transistor-driven output signals. The output can be push-pull, open drain/collector (if the transistors are MOSFET or BJT, respectively) or a peripheral interface (usually a serial communication). Common serial communication standards are: Universal Synchronous Asynchronous Receiver Transmitter (USART), Local Interconnect Network (LIN), Serial Peripheral Interface (SPI), and Inter-Integrated Circuit (I^2C). This kind of sensors are embedded in the form of integrated circuits (IC). These ICs have been improved to incorporate new features that efficiently manage the power consumption. Besides, the ICs already incorporate the analog-to-digital converter (ADC), the signal conditioning circuit, the filters, and the amplifiers, thus resulting in the concept of *smart sensor*. These improvements allow nodes to have less discrete components, thus making them smaller.

The energy consumption used for the sensing conversion varies depending on the type of sensor. Many efforts have been made to create new sensing methods and integrated circuits (IC) compatible with the requirements of nodes for the IoT, i.e., simpler and lower cost designs [134]–[140]. In [134], [135] the authors implemented the DPM technique for the sensor module, i.e., the sensors and all the associated circuit are powered only when needed. In [134], a duty-cycled excitation for Wheatstone bridges was proposed, offering energy savings compared to static biasing. In [135], the authors improved this technique by increasing the duty-cycle frequency and lowering the instantaneous battery current. Moreover, they designed a new ADC that achieves a 2.5 pJ/conversion-step figure of merit (FoM). In

[136], the authors designed an ADC with an optimized architecture of the voltage reference generator and a better power efficiency comparator maintaining the same noise performance as typical architectures. Results showed a 2.4 fJ/conv-step FoM.

An alternative to ADCs was addressed in [137]–[140] using a timer-based converter. The works detailed in [137]–[139] are focused on applications where sensors output amplitude-modulated signals. In those applications, the demodulation is conventionally carried out using an analog circuit (rectifier, mixer, and low-pass filter) together with an ADC. However, the authors proposed and implemented a digital timer-based demodulator. This novel demodulator is compatible with the digital timer modules typically embedded into MCUs. The main advantage for an MCU-based design is that the power consumption of a time-to-digital converter is lower than that of an ADC. In [140], a timer-based low-power and low-cost measurement system for interfacing capacitively-coupled resistive sensors was presented.

1.4.2.5 Summary

The previously subsections gave the reader the support and background on the IoT topic, providing deeper detail into the internal modules of a wireless IoT node. All the modules described before drain energy from the power source in more or less proportions. One of the main challenges when facing the deployment of an IoT system is the capability of the wireless sensor nodes to run for a long time without changing the batteries. This can be done both by reducing the power consumption as much as possible and by optimum managing the available energy of the power module. As a consequence, researchers are continuously proposing for new integrated circuits, methods, and techniques for optimizing the node's modules functionalities. This thesis continues in that regard as to design and implement different techniques to optimize the energy issues for the IoT nodes.

There are many topics to be addressed in the design of wireless nodes for the internet of things. The approach followed in this work was to tackle different energy challenges that developers must overcome when designing an IoT node. In the following sections, three energy challenges will be addressed.

1.4.3 Energy challenge 1: Low-power sensing system

As it was mentioned before, the first energy challenge tackled by this thesis is related to the node's sensing system. Many emergent researches for developing innovative methods to replace, or upgrade, conventional sensing systems was commented in the subsection 1.4.2.4. Here, the author will

focus on household smart gas meters' sensing system, considering the employer partner interests in the industrial doctorate. A smart gas meter is a utility (gas) meter that incorporates an electronic device that integrates the physical and the computation world. It is the Edge element of an IoT system, as explained in Section 1.4.1.

First, a brief overview about Smart Grids will be given. Next, the actual challenges faced by gas suppliers, grid operators and service providers to deploy this new technology will be outlined. Three issues were identified:

1) the rollout of this new technology will entail substantial costs, technical challenges, and risks;
2) nodes must be immune to tampering fraud, or at least detect them; and
3) smart gas meters must still comply with the three constraints for IoT nodes.

Hence, having noticed the market needs in this field, the gas meters will be studied. This includes listing the types of gas meters and mention the standards they must comply. Following, the state of the art of smart gas meters is discussed in two subsections. First, the literature review is focused on the most relevant novel sensor systems applied to smart gas meters. Second, it is focused on the different techniques to detect tampering fraud. Each subsection will provide an analysis where the different solutions are linked to the identified challenges.

1.4.3.1 Smart Grids and Smart Cities

One of the potential areas of development for the IoT, in terms of energy management, is reflected in the smart cities' paradigm. Smart cities are human environments in which the vast majority of traditional services such as mobility, citizen information, or public and social services, are offered and monitored through digital mechanisms that increase their efficiency. Obviously, this requires efficient management of the energy that supports it. Therefore, research on Smart Grids becomes more relevant since this system enables efficient energy management in all IoT nodes used for this purpose. Smart grids are automated computer systems that respond to fluctuating energy production, and intelligently address fluctuating demand [141]. A smart grid has a number of circuits that monitor and measure energy consumption and make automated decisions, making energy consumption more efficient, more demand-driven and less costly [142]. Besides, it generates new business models for the energy providers, changing the utility sector paradigm [143].

Smart homes implement an unpredictable and diverse amount of IoT, home automation and computing mechanisms [27]. Examples of this are air-conditioners, lamps, tablets, consumer electronics, utility meters, among others, which can be monitored and controlled remotely, or can automate their operation based on decisions made algorithmically from information obtained from environmental

sensors. This is also true for the services that can be provided to the citizen in public transport infrastructures.

Currently, some of the most widely used nodes are in electricity meters given the advantage they can be continuously connected to the network. These systems are responsible for evaluating power transfer and energy consumption within a network. These, which are in essence simple machines, are the basis for more complex systems with computational structures that store, and process large amounts of data based on energy monitoring. Following, the challenges faced for deploying smart gas meters, which have to be autonomous, are addressed.

1.4.3.2 Challenges for deploying smart gas meters

Historically, the measurement of the gas usage of residential communities is performed with mechanical gas meters [21]. Endesa is one of the electricity and gas providers in Spain and they do not have gas meters that provide data remotely, but a technician stops by every home every one or two months to take the reading [23]. The same happens with many other providers [22], [24]–[26]. Therefore, the process is slow, costly, and prone not only to human mistakes, but to fraud, too [22]. The gas meters can suffer from all kinds of tampering attempts by the users, which cannot be detected by the gas meters, since they do not have any smart device to register it. It is inevitable that all utilities in people's home are going to be smart, send real-time consumption and facilitate the provider management. Smart meters are a key component for the deployment of the Smart Grid [27]. However, the rollout of this new technology will entail substantial costs, technical challenges, and risks [24]. There are two types of smart gas meters: electronic and add-on gas meters. Both incorporate an electronic device (an IoT node) that integrates the physical and the computation world. The difference is the first one embeds the node in the gas meter. In the second one, a node is attached to the old gas meter (mechanical gas meter).

A study on behalf of the German Federal Ministry of Economics and Technology for defining a regulated and market-driven roll-out strategy of smart electricity meters was made by the firm Ernst & Young [144], a multinational professional service network that offers consulting services. Even though the study talks about smart electricity meters, the data can be extrapolated to estimate similar technical challenges and costs associated for deploying smart gas meters. The firm estimated that, depending on the assumptions made, if the 80% roll-out is targeted in a ten-year period, it would require the installation of 4.3 million smart metering systems per year, i.e., more than 10000 installations per day. It is evident that an installation that is performed in a short amount of time is preferable, otherwise a great number of technicians are required to achieve that target. In addition, they estimate that the total cost to cover the deployment is around 9 to 20 billion euros. Hence, a low cost per smart meter should be sought. A small variation in the cost of the smart meter will result in a great difference in the total

cost, given the great number of sensors units required for a complete roll-out. They propose the funding of the roll-out should be made by end-consumers. All other market participants (energy suppliers, grid operators and service providers) should not be responsible for a fraction of the roll-out costs. However, they first have to make a substantial investment in information technology (IT)[3] systems and process amendments for benefiting from the smart metering system.

The extrapolation of the information given by Ernst & Young appears justified in view of the pilot test the company Nedgia has performed. Nedgia is another Spanish energy provider that is making a pilot test of remote measurement devices in all the supply points in a small town in Spain [145]. They claim the prototype installation is carried out rapidly and it does not require to interrupt the service in any time. Only if the mechanical gas meter is not compatible with the device, the technician replaces it and install the prototype in a gas meter compatible with the system. Their approach corresponds with the roll-out strategy suggested by Ernst & Young.

Reuse the existing mechanical gas meter and install an add-on node so it can operate as a smart meter is preferable and many researchers are looking for that solution as it will be discussed in depth in the subsection 1.4.3.4. The add-on smart meters benefit of the accuracy and the long-term stability of the conventional gas meters and the advantages (traceability, security, reliability, and easier management) of the node upgrade. Contrariwise, electronic gas meters require the replacement of all the gas meters by the new smart gas meters. The developed solution should be low-cost, easily deployed, and immune to tampering fraud.

1.4.3.3 Gas Meters

To better understand the literature review of innovative smart gas meters, a brief description of gas meters will be first given here. There exist many types of mechanical gas meters, such as, rotary displacement gas meters, turbine gas meters, ultrasonic gas meters, and diaphragm gas meters. They differ between each other in the operating principle used for measuring the gas. Typically, diaphragm gas meters are installed in household premises, and they are the ones this work focuses on.

It is important to explain how diaphragm gas meters show the reading in the totalizer. The totalizer may come in different versions: dial, imperial, and metric. Figure 4 (a) shows a dial totalizer. It is found in old gas meters, and, as its name implies, it records the gas consumption using dials. In Figure 4 (b) an imperial totalizer is shown. It incorporates a mechanical index together with a dial, and every complete rotation of the dial indicates a cubic foot of gas consumed. Finally, metric meters are the modern version of gas meter's totalizers, they record the consumption in a mechanical index as

[3] IT: "The use of computers and telecommunications equipment (with their associated microelectronics) to send, receive, store and manipulate data" [204].

illustrated in Figure 4 (c). Some metric totalizers integrate a magnet in the mechanical index. From now on, if a metric totalizer is mentioned it is assumed that a magnet is integrated.

Gas meters have to follow different directives and standards depending on their geographical use. For instance, the equipment for potentially explosive atmospheres (ATEX) directives have their origin and are applicable in the European Union. The ATEX directives describe what type of equipment and environment is allowed for working in an explosive atmosphere. Other organisms, like the European Committee for Standardization (CEN), require gas meters with battery powered devices to comply with specified standards, such as the EN 16314:2013 [146].

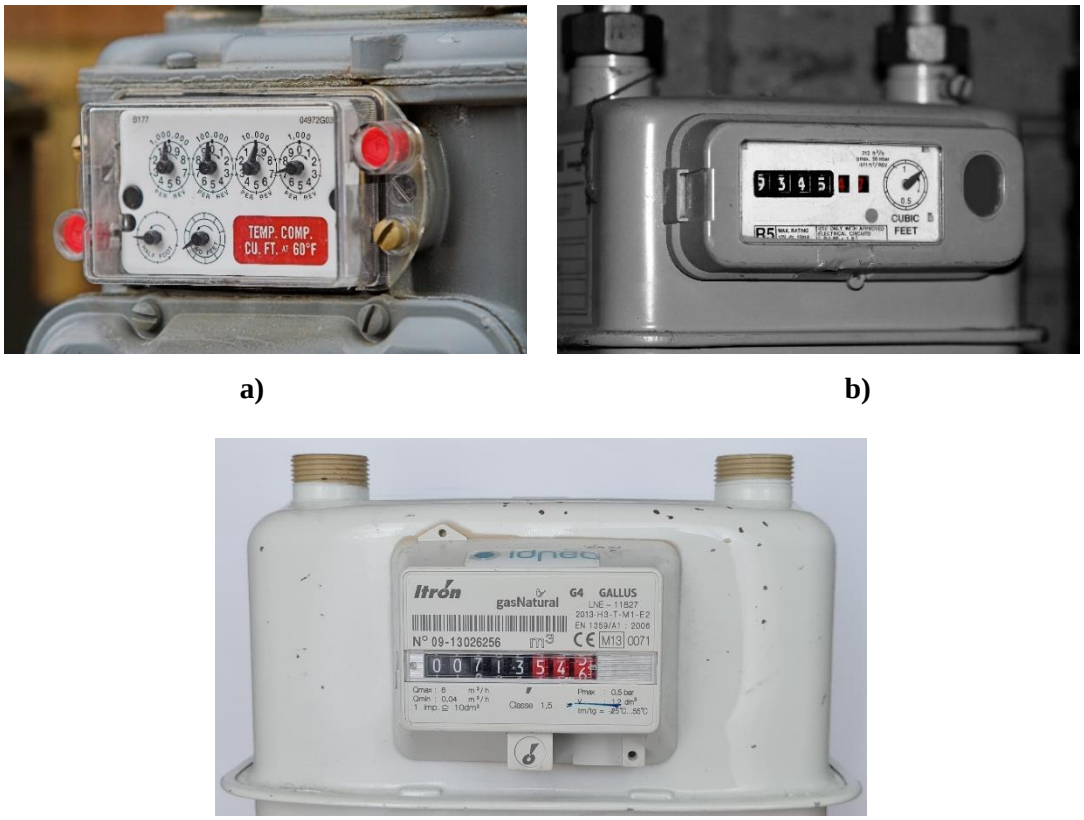

a) **b)**

c)

Figure 4: Pictures of different totalizers: (a) dial [147]**, (b) imperial** [148]**, and (c) metric.**

1.4.3.4 Sensor systems applied to smart gas meters

In this subsection, the literature review is focused on the research done for designing novel add-on sensor systems applied to smart gas meters. Basically, two approaches are proposed for developing an add-on node. On the one hand, researchers conducted investigations into the field of the imaging processing, as can be seen in [25], [45], [149], [150]. On the other hand, the designs take advantage of the magnet integrated in the metric totalizer using magnetic sensors. Examples of this kind of designs

are [24], [26], [151]–[153]. Following, the different approaches are detailed, and a discussion is provided at the end of the subsection.

Starting with imaging processing approaches, Puttnies et al. proposed in [45] a universal solution for measuring all utilities meters (gas, electricity, and water). Their approach consists of measuring the utility meter's totalizer using computer vision. It is compatible with all meters, providing they have a metric totalizer. Their contribution is a novel algorithm for detecting the regions of interest with auto-alignment, which makes it more robust regarding the camera placement. The camera was positioned in 9 different positions, being the closest one at 25 cm from the meter. This takes a lot of space, and, in many cases, it will not fit inside the cabinet where the mechanical meter is installed. It is not specified if the source of energy are batteries or a network connection. Moreover, they did not perform an energy study to verify the feasibility of the solution. The prototype costs 30 $, consisting of a Raspberry Pi, a camera, and a lens. This cost does not include the required infrastructure to install the camera in front of the mechanical meter.

In [149] the authors present a camera vision solution for gas meters with metric totalizers. The prototype consists of a camera module, an infrared light source, a control board, and a communication module. The prototype is enclosed in a case and attached to the totalizer. To keep the enclosure thin, they opted to place the camera perpendicular to the totalizer and mount a mirror to reflect the mechanical index. They claim the system is low-cost, but they only specified the cost of the camera, but not the rest of the components. The prototype is battery powered but an energy study was not performed.

In [150] an automated add-on gas meter monitoring approach using optical imagining was proposed. In this case, the visual solution is compatible with imperial totalizers. The prototype consists of a camera, a white LED light source and a Raspberry PI. The camera and the LED are enclosed and attached to the totalizer. It takes 5 seconds to perform a measure, which is not convenient for autonomous devices. The target is to perform a quick defined task and then go to sleep mode. The authors did not specify the cost nor performed an energy analysis.

In [25] a gas meter reading system based on image recognition and Zigbee communication is proposed. The system consists of two parts: 1) the Community multimedia Zigbee network, which comprises the sensor nodes and the community terminal, and 2) the Gas Accounting System, which is the server in charge of receiving all the images from the sensors and processing them. The sensors are distributed forming a multi-hop wireless mesh network topology, connected to the internet through the community terminal. The sensor nodes send a picture every month. The cost of the sensor node is around 25 €, but there is not an estimation of the community terminal. They did not perform an energy consumption analysis.

Jiang et al. used a different technology in [151] for developing a low-power wireless gas meter sensor. They proposed a gas meter sensor based on reed switches for detecting the magnet fixed in the

mechanical index of metric totalizers. Their approach is mainly theoretical, and no experimental measurements were made. The low-power consumption design recommendations are a bit trivial. The theoretical energy consumption analysis results show the battery-powered device can last between 3 to 5 years. They added many energy-hungry features that an edge element should not have to prolong the lifetime, like a motor to close the flow valve or a buzzer. The installation of the device will not be fast and easy since the service will have to be cut to add the valve. A study of the cost was not done.

In [152], the authors propose a solution of a Smart Grid for gas metering. The design is based in a star topology, where a central node, called Access Point (AP), receives the data via RF coming from the peripheral nodes and it communicates with a commercially available embedded control personal computer (PC). The PC sends the data to internet and perform other functionalities, such as sending alerts. The node is attached directly to a metric totalizer and measures the gas flow using a reed switch. They claim the proposed system is low-cost, but a cost estimation of the system is not described. They state the solution is low-cost only because the node and the AP hardware and firmware are custom designed. They did not consider the cost of the PC. Regarding the energy consumption, based on experimental test, the lifetime of the node was estimated to almost 10 years. Either the capacity of the battery nor the consumption of the sensor was specified.

In [26], Wiratama et al. implemented an add-on node for metric totalizers. Although, the focus was on the design of an automated gas billing system. The gas usage volume was measured using a Hall-effect sensor, instead of a reed switch. The node provides other measurements, such as, inlet and outlet pressure and temperature. Those measurements are performed in the gas tube. Hence, even though the device reused the already installed gas meter, adding the other features increases the installation complexity because the technician should cut the service to install the system. The device was powered by a 24 V battery connected to a charger to the network.

In [24], a non-intrusive device, called the retrofit module, that can be installed in commercial gas meters is proposed. The retrofit module is basically an improved totalizer. It comprises an encoder built with 10 magnetically actuated reed switches placed radially in a fixed angle, a compound gear train consisting of five gears, and a neodymium magnet fitted in the final driven gear. In order to install the retrofit module, the original totalizer must be removed. The magnet rotates above the reed switches, producing 90 closings per meter's gear shaft[4] revolution. This allows a high-resolution measurement of the gas consumption at expense of adding gears and many reed switches, increasing the cost and size of the module. Having high-resolution measurements allowed them to perform an algorithm to determine the gas appliance usage (furnace, water heater, dryer, or gas stove).

The retrofit module cost and the installation procedure are studied in a previous work [153]. In that work, they demonstrated the feasibility of the measurement technique by using a high-resolution

[4] Gear shaft: It is the axle of the gears, which provides the rotation to the compound train gear.

rotational optical encoder. They state the module costs 20-30 $, not including the battery. The installation time of the device is estimated to 15 minutes without the need of cutting the service. They did not report the energy consumption of their solution. This novel module is useful for gas meters totalizers that 1) do not have an integrated magnet, and 2) can be detached to install their proposed retrofit module. The second condition, to the best of the author's knowledge, is not possible for metric totalizers.

Discussion

Two relevant approaches were proposed in the literature to design a sensing system to upgrade a mechanical gas meter to a smart one: imaging processing and using magnetic sensors. However, most of the previous works did not evaluate the energy consumption of the node, which is the major job stopper for deploying the IoT. The exceptions are [151] and [152]. In [151], only a theoretical energy consumption analysis was provided. In [152], the authors experimentally estimated the autonomy based on the number of packages sent, without considering the power consumed in sleep mode. Regardless the methodology for estimating the autonomy could be improved, the results showed an operating life from 3 to 10 years.

There is not data about the power consumption of the image processing approach, but it can be inferred that is more than the second approach. Image processing needs a powerful MCU that performs the algorithm that reads the gas consumption based on the images. If the algorithm is calculated in the cloud the node needs to wirelessly send an image, i.e., sending more bytes, and consequently, more consumption, whereas the other approach only has to send a couple of bytes. The camera consumes more than a reed switch or a Hall-effect sensor. It would not reach that autonomy unless it is powered by bulky battery packs or by connecting the node to the network.

Regarding the size of the node, the first approach needs a proper positioning of the camera to get a correct image. The works showed a bigger size of the nodes, so big that it is questionable the feasibility of installing the nodes in residential gas meters. The second approach results in smaller node sizes.

Finally, regarding cost, and similarly to the analysis made for the power consumption, it can be inferred that the first approach is more expensive than the second one. From the point of view of the energy consumption, if more energy is needed to operate for the same time, it means more or bigger batteries, which add costs. More powerful MCU are more expensive. The camera is more expensive than the magnetic sensor.

One of the challenges was the add-on nodes should be installed quickly and easily. Therefore, solutions that require cutting the tube, unmounting the totalizer, or attaching a structure to the meter are preferably avoidable.

1.4.3.5 Techniques to detect tampering fraud

In this subsection, the literature review is focused on the different techniques to detect fraud due to meter tampering in magnetic-sensor-based add-on nodes. Babuta et al. presented in [154] a survey on power and energy measurement devices, providing the current situation of energy theft. While they focus on electricity smart meters, the analysis can be extrapolated to all utility meters, including gas meters. The authors stated that security issues can come from cyber-attack threats to the smart grid system or from the meter itself. Vulnerabilities related to the edge are called Non-Technical Losses (NTL) [154], [155].This work will focus on techniques for detecting NTL. The literature review has been done for all utility meters, since many of the designs solve the same types of tampering attempts, such as node's enclosure tampering (e.g. in [156]–[159]) and altering the reading using external interfering magnets, i.e. magnetic tampering (e.g. in [159]–[162]). Following, the different approaches are detailed, and a discussion is provided at the end of the subsection.

Conventionally, node's enclosure tampering is detected using mechanical methods, i.e., a switch button pressed against the lead when the case is closed [156]. However, the switch can wear out over time. In [157], the authors patented an electronic technique for detecting the opening or displacement of the meter's metallic case using an arrange of two magnetizable elements, such as inductors. They are magnetized at opposite polarities when the meter's case is closed. Nevertheless, if a tampering attempt is performed, the inductors magnetize at the same polarity. The MCU continuously polls the sensors to evaluate their polarities. The company Texas Instruments reported what seems to be an implementation of the previous patent ([157]) in a white paper [156]. The design was implemented in a three-phase electricity meter. They claim that the system warns the service providers when the case is opened or moved by as little as 4 mm. The magnetizable elements are implemented as flat printed circuit board (PCB) coils. Measurements show that, while sampling at 1 Hz, the inductive sensors consume only 2 µA.

In [158], the patented technique utilizes the piezoelectric properties of a ceramic capacitor, that uses barium titanate as principal dielectric constituent, to detect the physical movement of a utility meter. The invention is extended to any transducer that converts mechanical movement into electrical energy. Since the invention is mainly designed for an electricity meter, the sensor is always powered from the electrical grid.

In [159], the authors worked on both types of tampering attempts. In particular, this work applies the solution to a water meter, but it can be extended to utility meters that have a rotary magnet to register the utility usage. To detect the case tampering, the meter includes a magnetometer. This allows to indicate whether the meter has been dislodged from the measurement chamber. In the case the reading

is being altered, a Hall-effect sensor is used to detect if an external magnetic field surpasses a threshold. The sensors are periodically powered to perform a measurement.

In [160], a solution for magnetic tampering detection using ON/OFF Hall-effect sensors is reported. The solution was applied in an electricity meter; hence the system is not wireless but connected to the electrical grid to power the sensor. The solution consists of detecting high magnetic fields near the transformers, which in some electricity meters are used as power supply and/or as current sensor. Two sets of three Hall-effect sensors were used for a three-phase electricity meter. One set was placed near the power supply transformers and the other one near the current transformers. The Hall-effect sensors are powered only to perform the measurement. A magnetic tampering is considered when a magnetic field of ±6.9 mT is detected. In that moment, the timestamp is stored, and a defined metrology penalty is applied because it assumes that the current consumed is larger than the one measured.

In [161], the company Tormene Group, which develops gas meters, presents a series of rotary displacement gas meters for industrial applications. They can optionally be equipped with an add-on node. The node comprises a rotary magnet and magnetic sensors (Wiegand sensors) to measure the gas flow. They based the tampering protection against externally applied magnetic fields on covering the sensors and the magnet with an aluminum frame. By heavily shielding the gas meter, they assure magnetic fields up to 500 mT will not produce artifacts in the measurement. Besides, a Hall-effect sensor is also placed to record if someone is trying to manipulate the reading. Regarding energy consumption, 12 years lifetime is guaranteed with one AA cell battery, but there are no theoretical or experimental analyses to really back that up.

In [162] a patent is presented claiming a method for detecting a magnetic tampering in an electricity meter. This invention utilizes a Hall-effect sensor to generate an interrupt in an MCU when a magnetic field exceeds a defined first threshold. The MCU proceeds to perform several measurements of the magnetic field to be sure that the interrupt was not generated because of electrical noise. If all the measurements exceed the first threshold, they are compared with a second higher threshold. If this condition is met, then an alarm indicates an unauthorized interference. On the contrary, if the Hall-effect sensor measurements values are between the first and the second threshold, an additional step is performed to verify the abnormality. In this case, the meter's current transformers are used to detect a load imbalance. If the distortion of 20% is reached, then the alarm fires off.

Discussion

Two relevant cases of utility meter tampering were reviewed in the previous subsection: node's enclosure tampering and altering the reading using external interfering magnets. Other types of energy theft were not covered. For instance, cyber-attack threats to the smart grid system, bypassing the meter, etc. Following, the previous approaches are discussed and verified with the issues for deploying a Smart Grid mentioned at the beginning of section 1.4.3.

Usually, the approaches reviewed are not only hardware, but they work along with an algorithm to avoid false positives. The algorithms can be simple like processing the sensor data and conclude whether a tampering is being detected [156], [157] or sophisticated like detecting irregular trends of energy usage [154], [160], [162].

Regarding the node's enclosure tampering, the approaches reviewed were conventional mechanical buttons, magnetizable elements, the piezoelectric properties of a ceramic capacitor, and a magnetometer. Since most of them were implemented in electricity meters and are powered from the mains, the authors did not pay much attention in the power consumption. The exception was [156], which reported a consumption of 2 µA. The only zero-consumption solution is a normally closed button, i.e., while remained pressed, the circuit is open.

Most of the reviewed designs require complex and large circuitry to detect the node's enclosure tampering. This corresponds to larger cost and size. The smallest and lowest-cost approaches are the button and the magnetometer. The components themselves are cheap (around 1 €). Besides, they only need an extra resistor, for the button, or a couple of decoupling capacitors, for the magnetometer, to work.

Regarding altering the reading using external interfering magnets, the approaches are heavily shielding the enclosure and using magnetic sensors. Shielding the enclosure works only because the totalizer was completely replaced. In an add-on-based smart gas meter, this is not possible because the totalizer cannot be removed. All the other approaches consist of detecting if a magnetic field surpasses a threshold. The main difference between them is that the threshold can be defined by the MCU if the sensor is analog, or by the sensor if it is ON/OFF. As a result, all the proposed solutions have a similar size and cost. The difference is in the power consumption, where using a ON/OFF sensor allows the MCU to attend the external interrupt when a magnetic field activates the sensor, instead of periodically performing a measurement.

Regarding the challenge of detecting tampering fraud, there is a drawback identified, which is that, in the event of tampering, the gas consumption measurement is lost until a field intervention is done. In other words, the techniques only detect the tampering, but the node is not able to measure the actual consumption while the tampering is happening. Even if the node has direct communication with the cloud, the only thing that can be done is to speed up the field intervention. Finally, an additional limitation is that the approaches are mainly industrial but there is no scientific evidence to support those methods or techniques.

1.4.3.6 Summary and general discussion

In this section, the first energy challenge, related to the node's sensing system, was addressed. In particular, household smart gas meters' sensing system. The section started giving an overview of Smart Grids and the challenges faced to deploy that concept. Three issues were emphasized:

1) the rollout of this new technology will entail substantial costs, technical challenges, and risks;
2) nodes must be immune to tampering fraud, or at least detect them; and
3) smart gas meters must still comply with the three constraints for IoT nodes.

Based on the identified issues, reusing the existing mechanical gas meter and install an add-on node so it can operate as a smart meter is a feasible solution. Next, a brief theory about current gas meters was provided. Of all the listed types of meters, this work focuses on diaphragm gas meters with metric totalizers that integrate a magnet in their mechanical index.

Following, the literature review was presented. First, the research of novel sensor systems applied to add-on-based smart gas meter. Two relevant approaches were proposed in the literature to design a sensing system to upgrade a mechanical gas meter to a smart one: imaging processing and using magnetic sensors. Being the second approach feasible, low-cost, small size and low-power consumption solution. It is also appropriate for add-on nodes since it allows a rapid installation.

Second, it was focused on the different techniques to detect tampering fraud. Two relevant cases of utility meter tampering were reviewed: node's enclosure tampering and altering the reading using external interfering magnets. For the first case, it was concluded that a mechanical button or a magnetometer approach is compatible with the constraints of the nodes for the IoT. For the second case, like the previous challenge, the use of magnetic sensors seems the most appropriate for IoT applications. However, the proposed solutions only detect the tampering, but the actual consumption is lost until a field intervention is done. Besides, more scientific evidence is needed to support those methods or techniques.

In summary, many researchers have been interested in this field. However, the solutions proposed in the literature do not effectively deal with the three issues simultaneously. Based on the works reviewed, using magnetic sensors to develop a sensor system of the add-on node is in the right direction for a solution that solves those issues. The developed solution should be low-cost, easily deployed, immune to tampering fraud, and still comply with the three constraints for IoT nodes.

1.4.4 Energy challenge 2: Low-power wake-up circuit

The second energy challenge tackled by this thesis is related to the power consumption when the node is not operating. In Section 1.4.2 the nodes for the IoT were studied. Techniques for optimizing the node's power-hungry modules consumption were described. Also, methods for managing the available energy of the node's power supply. However, always from the point of view of the active operation. The study of the shelf life is not usually considered. In the following subsections, a review of how researchers are currently dealing with this issue is provided. The implemented technologies will be compared and a suitable one, considering the constraints of a node of the IoT, will be selected. Next, the circumstances that hinder the progress of the selected technology are reviewed. Finally, a summary and a discussion of the section are provided.

1.4.4.1 Wake-up techniques

Enclosing sensors in sealed packages can raise operational issues in the field because is not possible to add the power supply later. This means the battery starts draining from the moment the node is assembled. In some applications, several months or years can pass between the assembly and the activation of a node. Therefore, a wireless wake-up source is needed to activate the node.

Budampati et al. [163] focused their work on sensors, systems, and methods for activating nodes in the field. The patent is targeted to sealed nodes enclosed with a battery. Their idea for activating a node consists of a pre-defined trigger, applied by an external agent, which closes a switch connecting the battery to the node. The node draws almost no power until is activated, thus increasing the shelf life. Their idea is that the activation mechanism can be powered either by the battery or an energy harvesting source. However, the proposal is broad and vague, since the authors did not specify what technology is used for activating the node, what kind of triggering or what is the protocol for detecting it, either hardware or firmware. They did not talk either what is that stimulus, or the activation mechanism. Only the idea was proposed.

Adding a switch or button only for turning on a node increases cost, number of components and size. Smaller alternatives to switches or buttons are intelligent load switches [164]. They are ICs designed to be connected in series with the battery, so the device is at shutdown for shipping. Despite they do not physically disconnect the battery from the node, as switches do, they have low leakage current at shutdown. However, intelligent load switches still need an external electrical signal to activate them.

A solution that does not the need to add a switch (mechanical or intelligent) is using the DPM technique to shut down all the modules of a node, except the MCU and the wake-up source. The MCU is then configured to the lowest power mode that still allows it to detect a wake-up signal.

Either if a switch is added or not, a contactless wake-up source is needed so the node consumes as little power as possible, until a signal wakes it up. It was mentioned in Section 1.4.2.3 different wireless communication technologies (i.e. RF, magnetic field, and optical communication), which can also be employed as a wake-up mechanism. A considerable effort has been devoted to find different ways to wirelessly activate a hermetically isolated device. Piyare et al. [28] made a thorough survey on wake-up systems using RF transceivers. Hall et al. [63] reported two circuits to turn-on active RF identification (RFID) labels. The patents [165], [166] were presented describing ideas, techniques, and methodologies for waking up nodes using different technologies, such as magnetic fields and optical communication. An optical wake-up system was proposed in [18], too. The mentioned works are detailed in the following paragraphs.

RF technology is the most common way of wireless wake-up source. This is because many nodes come with a RF transceiver. Piyare et al. [28] exhaustively researched the state-of-the-art of wake-up RF transceivers, or as the author defined it, wake-up radios (WuRs). The authors analyzed 75 WuRs. The main classification of WuRs is based on the power source since it has the most significant impact on its purpose of saving energy. The WuRs can be active, passive, or semi-active. Active WuRs are continuously powered by the node's power supply. Even though they are the most power consuming WuR, the operational range is large. Passive WuR harvest the energy from the ambient environment or from the wake-up signal. Contrarily to active WuRs, passive ones have the shortest operational range, but they do not take energy from the node. Finally, in semi-passive WuRs some components are continuously powered while others remain passive. Regarding power consumption, out of the 75 reviewed prototypes, 23 WuRs achieved a power consumption below 10 μW. The lowest power consumption has been achieved by 3 of them and it was around 100 nW. Generally, to achieve extreme low power consumption, dual radios are utilized. One is the main transceiver, which is kept off during periods of inactivity. The other is the WuR, that generates the wake-up interrupt to the MCU. There are many trade-offs regarding the WuRs characteristics: sensitivity vs. power consumption, data rate vs. power consumption, antenna size vs. range. Therefore, the different applications will set the requirements to choose the appropriate WuR.

Hall et al. [63] worked on a wake-up solution using RF, too. The authors proposed a turn-on circuit that connects the battery only when the communication is happening. The field of application are active RFID labels that use their own power supply to independently generate a reply. Their work consists of simulating two turn-on circuits with the goal of designing a nano-circuit in a wafer. Both turn-on circuits are rectifiers. One capable of directly activating a transistor. The other, generating a voltage, which, compared with an internal reference voltage, activates a transistor. The transistor is a p-channel FET used as an active battery switch, like an intelligent load switch. The tag's antenna is used both to communicate and to generate the energy to activate the turn-on circuit. They do not study what happens if the interrogator is too close to the device, since an overvoltage protection may be needed.

Also, no protection against unwanted turns-on. And it only works if the interrogator is providing enough energy to activate the FET. They did not consider a clamping circuit to keep the FET activated while answering from sudden losses of energy-transmission from the interrogator. The circuit was simulated but not measured. They did not perform a study on how the circuit affects the performance of the antenna.

Knapp et al. [165] worked on an alternative to RFID tags. They patented a self-powered data tag but using optical communication. The tag uses an LED to receive and transmit information, and even to power itself. The LED is connected to a complex circuit that has three functions: power conditioning, signal conditioning and driving the LED. The power conditioning part filters the modulated light, emitted by a reader, to produce a DC voltage to power the tag and to get the received data. Capacitors store the DC energy that allows the tag to transmit data. However, this idea seems unfeasible in a practical scenario since the power generated by an LED operating as a photodiode is in the order of nanowatts, as it will be detailed later. The energy needed, only to turn on an LED, is around 3 orders of magnitude higher than the one generated by the same LED. Therefore, it would take a lot of time to gather that energy. Besides, the capacitor size required to storage the energy would be huge, even though they say they need a 1 nF capacitor and 1 μA to turn on an LED. Nevertheless, the circuit designed to perform the signal conditioning and driving the LED, if applied to a battery powered node, is robust. The drawback is that the circuit is far from simple, small, and low power.

Another optical-based solution was approached by Sifuentes et al. [18], who worked on vehicle detectors for parking occupancy and traffic flow. Their wake-up approach consists of a dual sensor system. One sensor is low power, but prone to false detection, and the other, consumes more, but it is more reliable. Both sensors, together with a power-efficient event-based software, achieve a low-power solution. The operation principle consists of a light dependent resistor (LDR), an optical sensor, which, once covered by an object, wakes-up a magnetic sensor that distinguish if that object is a ferromagnetic object, i.e., a car. The LDR is always on and activates an external interruption pin of the MCU waking it up from a low power mode. The MCU, in turn, senses the input with an ADC and then activates the magnetic sensor to verify if the object is a car.

The use of magnetic fields is another way to wirelessly activate a node. This idea was patented by Karren et al. [166]. The method consists of magnetically actuating a reed switch sensor. They focused on hermetically sealed circuits, in particular, those used for forcing the complete discharge of batteries. In their work, the battery is enclosed within a housing, together with the reed-switch-based circuit. A magnetic signal closes the reed switch and connects the battery to a low value resistor until it is completely depleted. A silicon-controlled rectifier (SCR) is used to keep the battery connected to the load if the magnetic field is taken away.

Choosing the technology

It is evident there is a strong interest for designing and researching circuits for waking up hermetically-sealed electronic devices in many fields of application. The mentioned wake-up circuits are not completely aligned with the constraints of IoT nodes. They are complex, power hungry, and they use many components. Otherwise, if they are simple and low-power, they do not add any protection on unwanted turns-on.

There are a lot of wake-up approaches with RF. One of the problems is that many of them need two antennas, one for performing the main communication and the other for waking up. Approaches that use only one antenna are the ones that consume more power. A wireless alternative for devices that do not use RF communication, or an antenna is needed.

Magnetic field is a fair option, but a better alternative to Karren et al. [166] design is required. A protection against unwanted turn-ons is mandatory, and reed switches are not designed to switch fast. Therefore, little can be done to develop a robust protection communication protocol. Hall-effect sensors are another kind of magnetic field sensors. Because they are semiconductor-based sensors, they have a better timing response than mechanically-actuated reed switch sensors. In this case, if Hall-effect sensors were used, instead of reed switches, the drawback comes from the reader side (the wake-up source), which should have a coil that generates the magnetic signal. This kind of methodology entails a higher degree of complexity to the system.

Optical communication is a promising alternative for applications were short-range communications and line of sight are an option. Optical sensors are photodiodes, phototransistors, photoFETs [167], solaristors [168], and LDRs. There are several options but only a few of them are commonly found in nodes and using them for nothing more than waking up the node would increase its size and cost. Phototransistors, PhotoFETs, solaristors are used only when the application requires them. Besides, they are more expensive than photodiodes. The LDR-based solution approached by Sifuentes et al. [18], is feasible but again requires adding a component that is not usually found in nodes. Besides, LDRs commonly contain Cadmium-Sulfide (CdS) and Cadmium-Selenide (CdSe). The use of those materials is severely restricted in Europe due to the RoHS[5] ban on cadmium. Lead-Sulfide (PbS) and Lead-Selenide (PbSe) based LDRs are RoHS compliant, but they are not commercially found, and they are expensive. LDRs do not come in surface-mount technology (SMT) packages, but they are available in 4.1 mm, 5 mm, 12 mm, 20 mm and over through-hole packages. This takes too much space for a component that is only used once.

[5] RoHS means "Restriction of Certain Hazardous Substances". It is an EU regulation to protect the environment and public health. This restriction is anchored in EU Directive 2011/65/EU [205]. If an electrical or electronic equipment is RoHS-certified, confirms the proportion of hazardous substances is limited to the maximum allowed.

Photodiodes are cheap, widely available, small and can be easily integrated in nodes. They come in all sizes and packages. The most common are infrared photosensors with peak sensitivity around 900 nm. Photodiodes are usually encapsulated in opaque housings, filtering the light below the near-infrared (NIR) region. Less frequently, they come with optical filters for a specific light spectrum region. If no optical filter is placed, they detect the whole light spectrum.

LEDs can also work as photodiodes, as was seen in Section 1.4.2.3 [126], [127], but with two main advantages: they are cheaper and already available in nodes for signaling purposes, which would not involve the extra size and cost of adding a new device for this task. The drawback is LEDs are not physically optimized to work as photosensors. LEDs are manufactured in a way that emit light when electrical current flows through them. However, photodiodes are optimized to generate electrical current in presence of light. Photodiodes have a wide surface detection area for this purpose, whereas LEDs do not, so lower electrical power is generated. Hence, a thorough study is required to design a circuit that maximizes the performance of LEDs working as photodetectors. The circuit must still comply with the constraints of IoT nodes.

1.4.4.2 Problems using LEDs as photosensors

Two main problems hinder the design of an optimal solution using LEDs as photosensors. One is particular for LEDs, and the other, is linked to optical communication technology. The first one is the insufficient information about LEDs operating as photodetectors since manufacturers do not provide it. The second one is the inherent ambient light interference. Following, a review of how those problems were addressed in the literature is provided.

LEDs characterization

Manufacturers do not characterize LEDs working as photodetectors. It is also important, when choosing one, to be aware of the current-voltage characteristics to design an optimal circuit that maximizes the performance of LEDs working as photodetectors. Kowalczyk et al. characterized through-hole LEDs as photoreceptors in [169]. They measured the spectral responsivity of 9 LEDs. The authors rubbed out the LEDs' lenses so they light would not concentrate on one point and affect the measurement. Recently, Sticklus et al. characterized LEDs in [170], too. They performed the characterization of off-the-shelf SMD LEDs. In this work, LEDs' lens was not modified. In both works, the authors experimentally investigated the spectral and temporal characteristics of off-the-shelf LEDs working as photodetectors. Results showed the LEDs' spectral responsivity varies depending on the materials they are fabricated. The responsivity peak is produced below the peak emission wavelength. Moreover, the peak and the width of the spectral responsivity, and the overlap with the emission spectrum differ from one LED to another, even if they are the same color. However, this data is still insufficient to design the circuit. The current-voltage characteristics are not provided. The characterization of the LED should be done for every use case to optimize the design.

Ambient light interference

There is a challenge to communicate using light in bright environments. The problem is that the photosensor either gets saturated or considerably reduces their sensitivity in presence of ambient light [171], [172]. The optical communication should be robust even in fluctuating ambient light conditions. Studies show that ambient interference behaves as a DC offset in the received signal [173]–[176]. Basically, there are two approaches to overcome the ambient light interference: cancel the DC offset and modulate the signal. Next, a review of research done in this subject is provided.

Yin et al. approached this problem in [173] with a hardware and software combination. First, they designed a circuit that adaptively adds an offset based on the ambient light. The offset was dynamically adapted using an algorithm programmed in the MCU. Second, the authors elaborated a communication protocol optimized for reducing the signal-to-noise ratio (SNR). Results show a reliable and robust communication with almost zero system error rate under different ambient light conditions and distance from emitter to receiver. The drawback is the code overhead in the MCU and the complex hardware needed to accomplish this. The prototype consumes 315 mA when running and it cost around 45 $.

In [174], the authors proposed a method to fade the effect from ambient noise by recognizing the rising edge of the encoded light pulse from the fluctuated ambient light. Moreover, their explanation of the ambient light sensitivity consists of the fact that ambient light is low frequency (DC for sunlight and <120Hz for commercial LED lamp), while they use modulated light for transmission. And second, the limited field of view of photodiodes, thus the perceived ambient light is largely attenuated. However, this does not cancel the entire interference from the ambient light leading to further effort of the node on the edge detection accuracy. Moreover, the ambient light still can saturate the photodiode if direct light hits it. The authors do not give details of the power consumption in reception mode but hint that is power-consuming.

Heydariaan et al. [177] developed their solution using OpenVLC1.0. The communication modulation is OOK. They evaluated its performance under various ambient light conditions (1 lx, 120 lx and 300 lx), which corresponds with indoor lighting. They used both a low-power LED (3 mm) and a photodiode as receptors. Higher data rate was achieved with higher modulation frequency. Communication was considerably compromised at 300 lx.

Zhao et al. [175] proposed an improvement in OOK modulation novel method of a VLC receiver immune to the ambient light interference. The method is based on cancelling the DC offset generated by the ambient light from the photosensor. To accomplish this, the receiver needs 4 operational amplifiers, which are power hungry. They did not perform an analysis of the power consumption or under dynamic ambient light environment, for example, when lights are suddenly turned on or a window is opened.

Bonnie Baker wrote a white paper about photosensing with ambient background [176]. Once again, a DC restoration circuit adaptively cancel the offset voltage below the signal frequency. Besides, it cuts off the DC voltage of the signal, reducing its amplitude to half the value. Two operational amplifiers were used to accomplish that. No power consumption analysis was performed.

The works mentioned before are mainly focused on optical communication as the principal communication technology of the node. Consequently, some parameters are prioritized above the ones interested in this work, such as simplicity, size, and power consumption. The works previously reviewed looked to optimize other parameters, like bandwidth or communication range. This entails a larger complexity in the design and a larger consumption of the circuit. A simple optical wake-up method should be designed to comply the constraints of an IoT node.

1.4.4.3 Summary

In this section, the second energy challenge, related to the power consumption when the node is not operating, was addressed. A literature review was done regarding that. Several technologies are used for waking up nodes of the IoT: RF, magnetic fields, and optical. Researchers mainly focused on wake-up techniques using RF communication. One of the problems is that many of them need two antennas and approaches that use only one antenna are the ones that consume more power. There is a necessity for a wake-up node method that does not use the RF spectrum.

Optical communication is a promising alternative. Among the different photodetectors commercially available, using LEDs as photodetectors were chosen given their advantages: ultra-low-cost, comes in all different packages, and they are already present in most devices for signaling purposes.

In order to design a wake-up system, special care must be considered for optimizing the performance of the LED working as photodetector, since they are not manufactured to perform that function. Two problems hinder the design of an optimal circuit: the lack of information of LEDs operating as photodetectors and the ambient light interference. Firstly, LEDs should be characterized because manufacturers do not provide this information. Secondly, problems with the ambient light interference of optical communication must be addressed in a way it still complies with the constraints of the IoT nodes.

1.4.5 Energy challenge 3: High-efficiency energy harvester

The third energy challenge tackled by this thesis is related to the node power supply. In Section 1.4.2.1 the power module was studied. This included batteries or an energy harvester as a power source, and the power conditioning circuit. In this section, RF energy harvesting will be addressed. First, an

introduction about energy harvesting technology will be given. Next, a brief overview of different sources of energy harvesting will be listed. The list will conclude with a more detailed description of RF as source of energy harvesting. Finally, the summary of the Section is provided.

Developers must overcome a major problem related to the optimal management of the energy available to power a node. It was mentioned in Section 1.4.2.1 that primary batteries are the principal way of powering nodes. However, their energy is limited. Moreover, there are applications where the use of this component is prohibited because they are highly contaminant, volatile, and flammable. An alternative to primary batteries to lengthen a node operating live is energy harvesting.

Over the years, new technologies for energy harvesting have been developed and slowly started to being widely spread over different applications. Harvesting the available "free" energy from the environment is one of the methods to increase the lifetime of nodes. Despite the hardware design complexity, the available energy is unlimited. The downside is that the available *average* power is limited, which needs to be higher than the average power required by the IoT node to ensure the device remains powered.

An energy-harvesting-based power module is shown in Figure 5 [14]. It successfully summarizes the elements needed for different ambient sources and the options for powering the node. The power module harvesting system requires:

- The ambient energy and its appropriate harvester (or transducer), which have to be well chosen depending on the operating environment of the node, the form-factor constraints and the power budget needed;
- the power conditioning circuit, which is not easy to implement since the output voltage and/or current of an energy harvester is not stable. Also, the output power of the harvester can be quite low, so the power conditioning circuit has to optimize the power delivery as much as possible. A common approach to achieve this is the maximum power point tracking (MPPT). It consists of dynamically changing the input impedance of the load to optimize the operating point of the harvester and, as consequence, get as much power as possible;
- and the energy storage, that must be efficient to save the dynamic and unpredictable energy from the harvester.

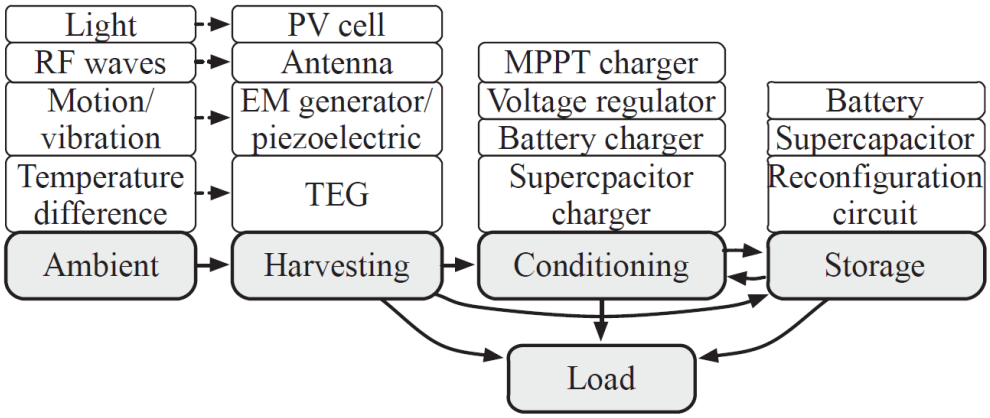

Figure 5: Elements of an energy-harvesting-based power module.

Source [14]

There are several ambient energy sources that can be used to generate electrical energy, such as radiant (optical and radiofrequency), mechanical (vibrations, pressure, and stress-strain), thermal, etc. [59], [60], [178]. Following, various ambient energy sources are briefly overviewed.

1.4.5.1 Thermal Energy Harvesting

Thermal energy harvesting relies its operating principle in the Seebeck effect. The thermoelectric generator (TEG) generates electrical power by a temperature difference between its faces [59], [60], [179]. More theoretical information is provided in [180].

This type of technology is costly, bulky and the output energy is low in terms of the efficiency. This makes them to be used in specific applications where advantages outweigh the drawbacks or in combination with other sources of energy harvesting. For example, a self-powered node for health care applications is presented in [79]. The node measures patients' vital parameters and send them to the cloud. In this case, a photovoltaic-thermoelectric hybrid energy harvester was used. The combination of two power sources allows the system to last longer. A flexible PV from Sundance Solar was used, so it adapts to the arm of the person that it is wearing the node. The TEG size is 4 cm x 4 cm and generates energy from the body heat of the patient.

Recent research used a TEG to extend the battery life of a node embedded in a connector to predict the maintenance of a cable. Results showed 5.430 mW of harvested power for a 43.56 ˚C temperature gradient of an 80mm x 40mm TEG [181].

1.4.5.2 Mechanical Energy Harvesting

Mechanical energy can be scavenged through piezoelectric, electromagnetic, and electrostatic mechanisms. Sources of energy could be pressure, vibrations, and stress-strain. Each source would need a different mechanism to harvest the energy. A more insightful theoretical description can be found in [59], [60], [179], [182]. Recent research achieved a maximum output power of 1.19 mW for a wind

speed of 2.1 m/s using a piezoelectric energy harvester [183]. Kinetic energy can be scavenged from the human body for power generation which will enhance the advancement of wearable electronics. For instance, in [184], an electromagnetic energy harvester generated 4.2 mW when it was placed at a person's ankle and walking at a normal walking frequency of 1 Hz.

1.4.5.3 Optical Energy Harvesting

It is one of the most popular sources of energy harvesting due to its high-power density [79], [80]. There are different ambient sources of optical energy: the sun, in the first place, but also artificial light. A photovoltaic panel (PV) is the transducer that converts the optical energy in electrical energy. Researchers have been investigating in great depth different materials for optimizing the PVs to operate under several circumstances, such as for indoors or outdoors applications [185], [186]; rigid or flexible requirements [187]; and specific dimensions or shape [188].

Different use cases of IoT nodes powered with PVs include a rechargeable battery or a super-capacitor that is used as an energy buffer [80]. In [80], Mohsen et al. utilize a solar harvester to prolong the lifetime of the battery. The power management consist of a 3800 mAh lithium-ion battery charged by two flexible PV connected in parallel. The node is continuously monitoring patients' vital parameters, as heart rate, body temperature, and blood oxygen level, and periodically sending the data to the cloud through Wi-Fi. With an average power consumption of 20.23 mW, the node lasts about 28 hours.

In [189] a PV was used to not only provide energy to a batteryless autonomous wireless node, but also to sense the ambient light. The data is sent via BLE to a base station (gateway), which in turn sends it to the cloud. The storage element is a capacitor, calculated to be large enough to provide energy to the microcontroller to supply the current peaks as to perform the transmission. The average consumed power is provided by the PV. The node can still operate in an ambient light intensity down to 200 lux, which is an indoor level of light.

1.4.5.4 Radiofrequency Energy Harvesting

Radio frequency signals are electronics waves, generated by a transmitter, that travel through a medium, usually air, for communication purposes or to deliberately power a node. RF energy harvesting has been widely proposed, especially over the last 30 years with the increase of the wireless signals [41]. Nodes can be benefited from RF energy that is deliberately generated to power them, like RFID tags [37], or from ambient RF energy present in the environment, like digital TV, radio, satellite, Wi-Fi or cellular signals [190]–[192].

A detailed block diagram of an RF harvester is shown in Figure 6 [41], [190], [191], [193]. It consists of the antenna, the matching network, the rectifier, and the power conditioning circuit. The antenna is the transducer as it converts radiated energy to electrical energy. The matching network has the double function of matching the impedance of the circuit and the antenna and acting as a signal pre-

amplifier. The rectifier has the double function of converting the alternating signal to a DC voltage and boosting the voltage. Finally, the conditioning circuit regulates the voltage to the value necessary to power the load, which can be an energy storage and the sensor node. The matching network, the rectifier and the power conditioning blocks will be detailed in the following paragraphs.

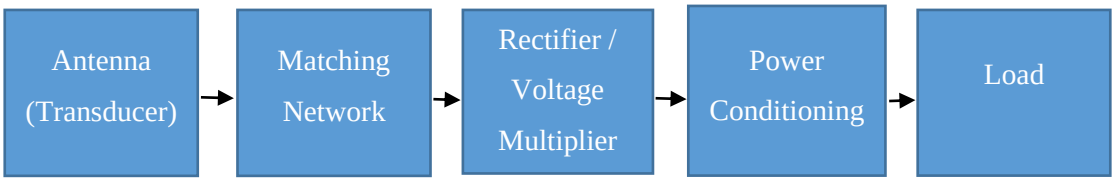

Figure 6: Block diagram of a RF harvester.

The RF energy that can be harvested is very limited. The electrical power scavenged by the antenna is around 100 µW or less [194]. Therefore, the voltage generated by the antenna can be lower or about the voltage required to directly bias the rectifier's diodes (or MOS transistors). Consequently, the matching network must transfer the maximum power from the antenna to the rectifier and boost the voltage in the most optimal way. One technique to achieve this is called passive LC voltage boosting [37], [40], [195], [196]. A passive LC network that, using resonant amplification, boosts the signal's voltage amplitude, increasing the efficiency of the rectifier.

The RF signal cannot directly power the node, but it has to be converted first in DC voltage. The rectifier is the less efficient stage of the block diagram. It is inherently a source of power loss due to biasing the diodes (or MOS transistors), and this limits the efficiency of the overall harvester. There are several circuit configurations to make a rectifier. The basic ones are half-wave or full-wave rectifiers, which consists of diodes and capacitors. They do not provide any gain and their output voltage is proportional to the input. Sometimes, the matching network output voltage must be amplified again because the values obtained are not enough to power the node and adding a rectifier with losses considerably decrease the efficiency. In those cases, the rectifier stage is designed to achieve the double target of amplify the voltage and to convert the AC signal to DC. Common configuration for achieving this is through multistage rectifiers, also known as Dickson and Villard voltage cascades. They are the simplest and most common voltage multipliers. They can be implemented using discrete components and ICs. There is not a significant efficiency difference between them. However, for small signal analysis, Dickson configuration results in easier nonlinear impedance analysis. The higher the number of stages in the rectifier the higher the voltage multiplication, but also the power losses, the parasitic capacitance, and the sensitivity (minimum operating input power level). However, too few multiplier stages may result in not enough voltage to power the node. A tradeoff has to be made between the required voltage and the power losses.

Finally, after the rectifier, a power conditioning circuit is placed. High-efficiency converters are preferred over LDOs, Zener diodes or any other voltage limiter that only sinks the excessive available

power on itself [197]. While all the available energy should be profited and not wasted, a voltage limiter circuit could be used for over-voltage protection purposes. Depending on the application, the power conditioning circuit could be a DC-DC switching converter, a MPPT regulator, a battery charger, and/or a supercapacitor driver. Special care should be taken when using a voltage regulator since its efficiency significantly decreases under light-load conditions. The reason for this is that voltage regulators need a quiescent current to operate. Hence, if that current is similar to the load consumption, the voltage regulator efficiency is severely reduced.

1.4.5.5 Summary

In this section, the third energy challenge, related to the node power supply, was introduced. From the point of view of the power supply and due to interests and expertise of the research group, energy harvesting is the topic selected. First, an introduction about the energy harvesting technology was given. A general block diagram of an energy-harvesting-based power module was described. Next, a brief overview of different sources of energy harvesting and the recent advances in the literature was listed. This included thermal, mechanical, optical and RF energy harvesting. The list concluded with a more detailed description of RF as source of energy harvesting.

Specifically, from all the sources of energy, the harvesting of the RF signals available in the environment was described. A detailed block diagram of an RF harvester was shown. This includes the antenna, the matching network, the rectifier, and the power conditioning circuit. The setback for this power supply is that the RF energy that can be harvested is very limited. Therefore, highly efficient harvesters must be designed. Nevertheless, the mismatch between the antenna and the rectifier is non-linear. The mismatch varies with the input power and the frequency, which makes it difficult to achieve a good sensitivity and efficiency over a wide range. Consequently, the challenge is to properly model the power module to obtain the most optimal harvester design. The final stage of the power module is the power conditioning circuit. It was reviewed that the RF harvester could be highly benefited from a MPPT because it dynamically changes the input impedance of the load to optimize the operating point of the harvester and, as consequence, get as much power as possible. Special care should be taken when using DC-DC converters since they need a quiescent current to operate.

1.5 Structure

The state-of-the-art review was given in the previous sections. Cost, long operating life, and size are the three principal constraints of nodes for the IoT. Providing energy to the constrained nodes is a

major job stopper for the deployment of the IoT. The approach followed in this thesis was to tackle three energy challenges concerning the design and implementation of nodes for the IoT.

This article-based thesis consists of a set of three papers. Those papers were developed during the doctoral work as a result of accomplishing the objectives set for the thesis. In addition, three conference publications were added in this article-based thesis as they allow a better understanding of the thesis work. In that sense, after the introductory Chapter 1, this document is organized as follows.

- Chapter 2 corresponds to one conference paper and one journal paper. It presents the articles related to the sensing system alternative for smart gas meters. First, an add-on gas meter device is described, together with its development and measurements. Second, a more robust, secure, low-cost, and low-energy consumption measurement system is developed and presented.
- Chapter 3 corresponds to two conference papers and one journal paper. It is devoted to the papers related to the power consumption when the node is not operating, using a LED-based wake up circuit. The publication addressed the idea proposal, the characterization of LEDs working as photodiode and the study and design of the circuit that wakes the MCU up.
- Chapter 4 correspond to one journal paper. It contains the publications dedicated to the node's power supply using RF energy harvesting. A Thévenin model of a rectenna is studied and then applied to power an autonomous sensor.
- Chapter 5 summarizes the thesis results. It analyzes and discusses the contributions of the research.
- Finally, chapter 6 concludes the article-based doctoral thesis and enumerates future work suggestions, identifying interesting topics.

1.6 Publications

The publications that comprehend this thesis are thematically coherent with the objectives of the thesis and the research plan and listed below. They were published during the years 2017 to 2021. The articles were published in relevant journals and conferences in the field of the sensors, instrumentation, and measurement science.

- *Publication I. Conference proceeding I:* "An Add-On Electronic Device to Upgrade Mechanical Gas Meters into Electronic Ones" [198]. It is reproduced in Chapter 2, section 2.1.
- *Publication II. Journal article I:* "Electronic reading of a mechanical gas meter based on a dual magnetic sensing" [199]. It is reproduced in Chapter 2, section 2.2.

- *Publication III. Conference proceeding II:* “Using LEDs for Visible Light Communication and as a Wake-up Mechanism in the Internet of Things" [200]. It is reproduced in Chapter 3, section 3.1.
- *Publication IV. Conference proceeding III:* “Experimental characterization of off-the-shelf LEDs as photodetectors for waking up microcontrollers” [201]. It is reproduced in Chapter 3, section 3.2.
- *Publication V. Journal article II:* "LED-Based Wake-Up Circuit for Microcontrollers" [202]. It is reproduced in Chapter 3, section 3.3.
- *Publication VI. Journal article III:* “A Compact Thévenin Model for a Rectenna and Its Application to an RF Harvester with MPPT” [203]. It is reproduced in Chapter 4, section 4.1.

PUBLICATIONS

2

Publications I & II

2.1 Publication I: Conference proceeding I

E. Ripoll-Vercellone, V. Ferrandiz, and M. Gasulla, "An Add-On Electronic Device to Upgrade Mechanical Gas Meters into Electronic Ones," *Proceedings Eurosensors*, vol. 2, no. 13, 2018, doi: 10.3390/proceedings2131094.

2.2 Publication II: Journal Article I

proceedings

MDPI

Extended Abstract

An add-on electronic device to upgrade mechanical gas meters into electronic ones

Edgar Ripoll-Vercellone [1,2,*], Vicent Ferrandiz [1] and Manel Gasulla [2]

[1] Idneo Technologies, Mollet del Vallès 08100, Spain
[2] e-CAT Group, Dept. Electronic Eng., Universitat Politècnica de Catalunya, Castelldefels 08860, Spain
* Correspondence: edgar.ripoll.vercellone@upc.edu; Tel.: +34-650-34-2256

Presented at the **Eurosensors 2018 Conference**, Graz, Austria, September 9–12, 2018.
Published: date

Abstract: Smart utilities enable more efficient energy consumption and distribution and are the key for smart homes development. We propose an electronic device that will be integrated as an add-on to already installed conventional gas meters as a first stage of smart metering rollout. The electronic device will measure the gas consumption and it will be managed by the user's or operator's smartphone via NFC. For the gas flow measurement, the electronic device takes advantage of the rotation of a permanent magnet fixed in an index drum.

Keywords: short-range networks; gas meter; smart utilities; smart society; Internet of Things

1. Introduction

Smart grids have been subject of study with the objective of optimizing the energy production and distribution as well as the management of the end users service, in terms of security, remote operations diagnostics, etc. Furthermore, they allow the consumers to manage their consumption according to the available information since they can read their consumption and prices with more detail [1]. Besides, it generates new business models for the energy providers such as the prepaid service [1-3].

Nowadays, most gas meters in Spain are mechanical, which hinders the achievement of smart grids for the gas sector [1]. The meters are periodically read by the user or an operator who takes a picture of the totalizer, which is prone to human mistakes and fraud billing [4]. However, their substitution by electronic gas meters is generally not economically feasible. The alternative solution proposed here is to attach an electronic device to the already installed meter (jointly forming a smart gas meter). The smart meters benefit of the accuracy and the long term stability of the conventional gas meters and the advantages (traceability, security, reliability and easier management) of the electronic upgrade. This solution is carried out within the European project "EnSO" (Energy for Smart Objects) [5].

2. Node Description

The add-on electronic device (node, hereafter) must have a long lifetime, small size and must be low cost [4]. In addition, the main required functionalities of the smart meter are: store gas consumption information in fixed periods (days, weeks, etc.); identify and register alarms (low battery, tampering, detect strong magnetic fields, repeated attempts to establish a communication, etc.); and communicate with smartphones through NFC (the user and operator use a smartphone application to perform the management and reading of the smart meter). Figure 1 shows a detailed block diagram. It consists of four main modules: power management, sensor/actuator, control and communication.

The power management module is designed for powering the node from a primary battery, solar cells or the NFC link. For this first version prototype, only primary batteries are considered, in particular coin cells.

The sensor/actuator module consists of three sensors (gas measurement, magnetic field and tamper detection) and one LED for indication purposes. The sensors are on/off switches. The operating principle of the gas measuring is based on that as the gas flows a transmission gear and a mechanical coupling transfer the reciprocating motion to the mechanical index, which has attached a permanent magnet in the index drum that represents the less significant digit. A reed switch is positioned in the edge of the node and is activated whenever the magnet passes in front of it. The resolution of the mechanical measure is 0.001 m^3, whereas the digital measure is 0.01 m^3, which corresponds to a complete turn of the index drum. Figure 2 (a) shows the node attached to a mechanical gas meter (Gallus 2000) [6]. On the other hand, a reed switch activates an alarm when a strong magnetic field is attempting to corrupt the gas measurement. Finally, the tamper detection consists of a button that is pressed against the case of the electronic device. If someone breaks the plastic case, the switch will be unpressed, generating an alarm.

The control module includes a STM32L0 series microcontroller, which gathers, stores and processes the information of the sensors and the communication module.

The communication module consists of a NFC transceiver. A smartphone is used to interconnect the smart meters with an Internet of Things platform, which is developed by a third-party company. The smartphone uses an android application for installation, configuration, activation, management and maintenance actions.

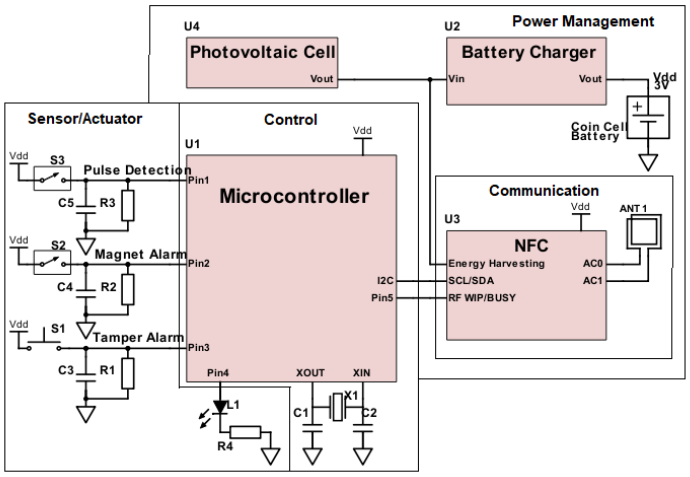

Figure 1. Block diagram of the add-on electronic device. It consists of four main modules: power management, sensor/actuator, control and communication.

Figure 2 (b) presents the printed circuit board (PCB) of the electronic device with a description of its elements. The dimensions of the node are 70 mm × 30 mm (without the solar cell). The estimated unitary cost is from 5 € to 7 € depending on the production volume.

4. Performance / Experimental Results

Performed tests using an emulated gas flow on an ITRON counter (Figure 2 (a)) validated a correct performance of the gas reading process. The magnetic field detection was validated by bringing a magnet closer to the sensor. The tamper detection was tested by opening the plastic case of the electronic device. Besides, extensive tests were also performed for assessing the reading range and reliability of the NFC communication and the operating lifetime of the node.

Regarding the tests of the NFC communication, in order to avoid magnetic interference, a plastic structure was used to hold both the smartphone and the node. The structure was placed on a clear laboratory table. Two smartphones models were used: the Huawei P8 Lite ALE-L21 and the Motorola Moto X Style XT1572. Three versions of the node were tested to evaluate the influence of some metallic parts: **1)** the original version (see Figure 2 (b)), **2)** the node with the battery holder and

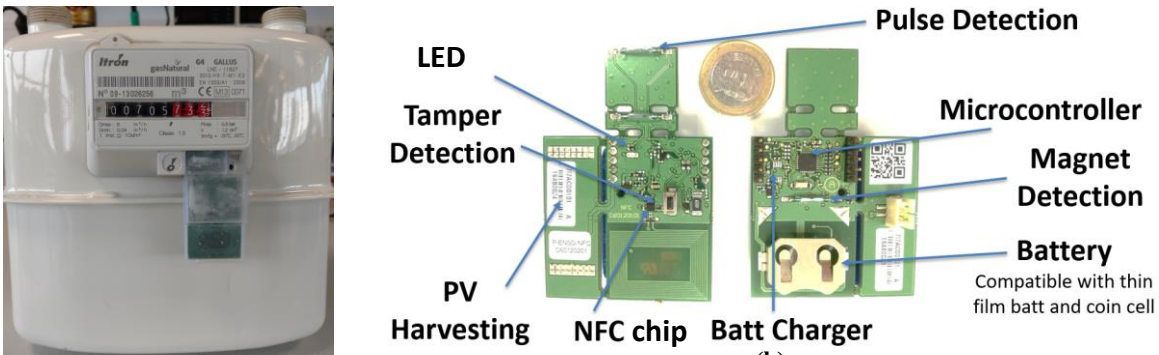

(**a**) (**b**)

Figure 2. (**a**) Tests carried out in a simulated environment, on an ITRON counter (Gallus 2000) [6]; (**b**) PCB of the node with a description of its elements.

all the copper removed from the back of the PCB coil and **3)** and the node with the copper removed from the back of the PCB coil and with a ferrite plane between the PCB coil and the battery holder. Version 2 was powered externally.

Table 1 summarizes the maximum range achieved with the different setups measured with a resolution of 0.5 cm. As can be seen, the battery holder and the copper placed below the PCB coil limit the communication range (version 1). For the Huawei smartphone the range is constrained to 1 cm, whereas without the battery holder and the copper (version 2) a range of 3.5 cm is achieved for both smartphones. The magnetic field distribution of version 3 is similar to the one of version 2, therefore the same communication range is achieved. As the battery must be within the board, version 2 is not feasible. However, a practical solution for version 1 to increase the communication range is to move the battery holder to a different location. When this is not possible due to size restrictions, a ferrite plane can be added between the metal plane and the PCB coil (version 3) at the expense of a higher cost of the node (about 0.5 € to 0.7 € for high volume production).

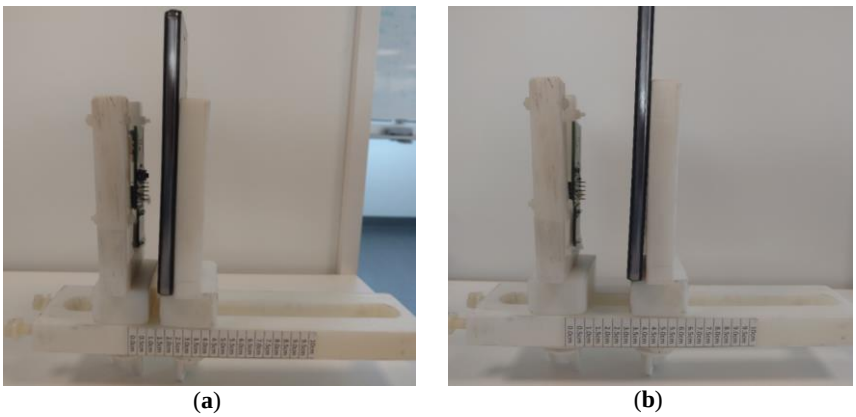

(**a**) (**b**)

Figure 3. Setup for testing the NFC communication range with the Huawei P8 Lite: (**a**) Version 1 at the limit distance of 1 cm; (**b**) Version 2 at the limit distance of 3.0 cm.

Table 1. Maximum Range. The ruler used for measure the distance has a resolution of 0.5cm.

Smartphone	Version 1	Version 2	Version 3
Huawei P8 Lite	1.0 cm	3.0 cm	3.0cm
Motorola Moto X Style	2.0 cm	3.5 cm	3.5cm

For the estimation of the operating lifetime of the node, the current profile of the power supply was measured with an oscilloscope current probe (Labdevice). The internal shunt resistor was replaced by other values (1 Ω and 39 Ω) to obtain a better resolution of the measurements. The idle current was measured with an Agilent 34461A. Table 2 shows the estimated average current consumption for each task based on the assumption of their periodicity. With a 230 mAh coin cell

battery, the lifetime of node is 600 days (about 20 months). This lifetime is insufficient for the application and a thorough analysis and redesign has to be done to extend it to more than four years.

Table 2. Average current consumption detailed by each task performed. A 3V coin cell battery powers the node. It is assumed that an NFC communication will take place every five days and one pulse detection will happen every 30 seconds.

	Task	Average Current [uA]	Consumption Percentage
Energy Consumption	*Idle Mode*	*12,60*	*78,88%*
	Pulse Detection	*3,2*	*20,03%*
	NFC Communication	*0,16*	*1,00%*
	Rest	*0,013*	*0,08%*
Autonomy	Battery 230 mah	*600*	*Days*
		1,64	**Years**

5. Future Work

Work is in progress regarding the design of a new version. The product specifications are redefined on the basis of the input from the developed prototype and previously described. This stage includes a new loop of development and validation solving all problems detected on the first prototype series and adding those new provided requirements. Two main features are going to be improved in the following version of the node. One of the goals is to extend the system autonomy as much as possible. Some hardware and software modifications have been studied in order to reach a lower consumption during the idle mode, which has the highest power consumption contribution (78.88%). It is estimated that the autonomy will be increased to more than four years by reducing the energy consumption in about five times. The second goal is to increase the NFC communication range. As it was mentioned in section 4, the battery holder and the copper generates considerable limitations for the PCB coil. Since adding a ferrite layer will significantly increase the cost of the product, the battery holder will be moved to a more appropriate location.

Acknowledgments: This work was supported by EnSO (Energy for Smart Objects), Grant Agreement No. 692482, Idneo Technologies S.L. and the Secretariat of University and Research of the Ministry of Business and Knowledge of the Government of Catalonia.

Conflicts of Interest: The authors declare no conflict of interest. The founding sponsors had no role in the design of the study; in the collection, analyses, or interpretation of data; in the writing of the manuscript, and in the decision to publish the results.

References

1. Q. Sun and H. Li and Z. Ma and C. Wang and J. Campillo and Q. Zhang and F. Wallin and J. Guo. A Comprehensive Review of Smart Energy Meters in Intelligent Energy Networks. *IEEE Internet of Things J.* **2016**, *3*, 464-479, DOI:10.1109/JIOT.2015.2512325.
2. S. Dong and S. Duan and Q. Yang and J. Zhang and G. Li and R. Tao. MEMS-Based Smart Gas Metering for Internet of Things. *IEEE Internet of Things J.* **2017**, *4*, 1295-1303, DOI: 10.1109/JIOT.2017.2676678.
3. R. Deng and Z. Yang and M. Y. Chow and J. Chen. A Survey on Demand Response in Smart Grids: Mathematical Models and Approaches. *IEEE Trans. Ind. Informat.* **2015**, *11*, 570-582, DOI: 10.1109/TII.2015.2414719.
4. Cascetta, F and Vigo, P. The future domestic gas meter: Review of current developments. *Measurement* **1994**, *13*, 129-145, DOI: 10.1016/0263-2241(94)90006-X.
5. Energy for Smart Objects (EnSO). Available online: http://enso-ecsel.eu/ (accessed on 02 May 2018).
6. Itron Gallus 2000 Residential Diaphragm Gas Meter product specification. Available online: https://www1.itron.com/local/Poland%20Product%20Portolio/GA-GALLUS-04-EN-02-14.pdf (accessed on 13 June 2018).

IOP Publishing Measurement Science and Technology
Meas. Sci. Technol. **32** (2021) 097001 (5pp) https://doi.org/10.1088/1361-6501/ac00e8

Technical Note

Electronic reading of a mechanical gas meter based on dual magnetic sensing

Edgar Ripoll-Vercellone, Manel Gasulla and Ferran Reverter*

Department of Electronic Engineering, Universitat Politècnica de Catalunya—BarcelonaTech, Castelldefels, Barcelona, Spain

E-mail: ferran.reverter@upc.edu

Received 4 February 2021, revised 20 April 2021
Accepted for publication 13 May 2021
Published 8 June 2021

Abstract

This article proposes a measurement system controlled by a microcontroller unit (MCU) for the electronic reading of a mechanical gas meter. The measurement relies on dual magnetic sensing: (a) low-cost low-power primary sensing based on reed switches connected to the digital inputs of the MCU and (b) secondary sensing based on Hall-effect sensors connected to the analogue inputs of the MCU. In addition, both sensing strategies have an active and a passive element to achieve an output that is insensitive to external interfering magnets. A prototype has been implemented and characterized under different test conditions to confirm its reliability.

Keywords: embedded system, gas meter, hall-effect sensor, magnetic sensor, microcontroller, reed switch

(Some figures may appear in colour only in the online journal)

1. Introduction

The application of information and communications technologies to the power grid has led to the concept of a smart grid [1], with corresponding benefits for energy production and distribution. In such a context, smart electronic meters, mainly for the electricity sector [2], have been designed and deployed at end-consumers' homes.

In the gas sector, most meters (see figure 1(a)) are still mechanical, and the reading of the mechanical index is carried out either by the end user or a worker from the gas company every one to two months. In order to avoid this type of manual reading and obtain a smarter meter, these mechanical gas meters can be complemented/upgraded with electronic measurement and communication systems. Many gas meters have a rotating magnet inside (from now on, *meter magnet*, as shown in figure 1(b)) that allows for electronic reading; this is the case for the diaphragm gas meters made by Itron and Elster–Honeywell, which are two of the main manufacturers. This meter magnet can be detected, for instance, through a low-cost reed switch connected to a microcontroller unit (MCU) [3, 4]. Its main limitation, however, is that the reading can be easily altered by an external interfering magnet. Other, more expensive, solutions have also been proposed in the literature for gas meters, such as optical encoders [5] and computer vision cameras [6].

The use of additional sensors to better extract the information of interest is quite common in electronic measurement systems [7, 8]. This has also been applied to utility meters, for example: (a) magnetic sensors (such as Hall-effect sensors) are employed in electricity meters to detect the tampering caused by external magnets [9, 10], and (b) magnetic sensors (such as reed switches) are proposed for detecting the theft or detachment of gas meters [11]. However, the detection of the meter magnet of a gas meter in the presence of an external interfering magnetic field is still a challenge. This is tackled herein by incorporating additional sensors into the basic reed switch-based configuration [3, 4].

* Author to whom any correspondence should be addressed.

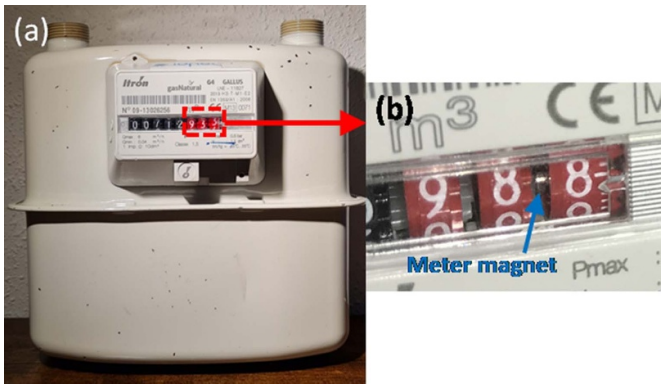

Figure 1. (a) Mechanical gas meter. (b) Meter magnet behind the least-significant drum of the mechanical index.

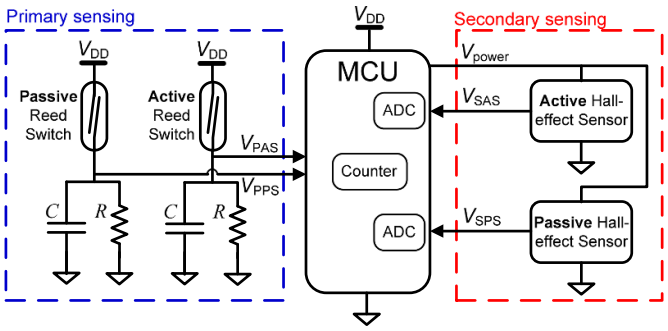

Figure 2. Schematic of the proposed circuit.

2. Electronic circuit

Figure 2 shows the proposed MCU-based circuit with dual magnetic sensing: (a) primary (default) sensing that relies on reed switches [3, 4], and (b) secondary sensing carried out by Hall-effect sensors. Both sensing strategies have active and passive elements, as employed in strain gauges to compensate for interfering effects [12]. The active elements are placed as close as possible to the position of the meter magnet to be very sensitive to it. The passive elements are placed at the minimum distance from the corresponding active element that provides a 'zero' sensitivity to the meter magnet. The shorter the distance, the more similar the effects of the interfering magnet on both sensors. Overall, the circuit has four sensors.

(a) The *primary active sensor* (PAS), which detects the meter magnet under normal conditions, i.e., without interfering effects.
(b) The *primary passive sensor* (PPS), which detects the interfering effects and, hence, activates the secondary sensing.
(c) The *secondary active sensor* (SAS), which monitors the meter magnet under unusual conditions, i.e. with interfering effects.
(d) The *secondary passive sensor* (SPS), which monitors the interfering effects under unusual conditions.

The PAS and PPS are connected, via an RC debouncing circuit, to digital inputs of the MCU with an external interrupt capability, while the SAS and SPS are connected to analogue inputs with an embedded analogue-to-digital converter (ADC). Except when the meter magnet is aligned with the SAS, the output voltages of the SAS and SPS (V_{SAS} and V_{SPS}, respectively) should be ideally the same. However, this is not practically true, due to the tolerance of the sensors and the fact that the interfering magnet will not equally affect both of them. The MCU also includes a digital counter that increases by one every time the meter magnet passes in front of the active sensors, thus counting the gas consumption with a resolution of 0.01 m^3.

With the aim of reducing the current consumption of the design, the SAS and SPS are only supplied when required. To achieve this, a digital output (V_{power} in figure 2) of the MCU provides a digital '1' to the supply voltage pin of these sensors only when the secondary sensing needs to be active. By default, V_{power} provides a digital '0' and, hence, these sensors do not consume energy.

Most of the commercial reed switches and Hall-effect sensors available on the market operate correctly in the industrial temperature range (i.e. from −40 °C to +85 °C), which is clearly wider than the expected operating range of the gas meter, even if it is placed outdoors. In addition, integrated Hall-effect sensors usually include temperature-compensation circuitry so that the analogue output is almost insensitive to temperature changes. The typical value of the temperature coefficient of the magnetic sensitivity is around 0.02% $°C^{-1}$ [13]. Accordingly, an extreme change of the ambient temperature of 50 °C would cause a change of 1% in the sensitivity and, hence, in the amplitude of the pulse generated by the presence of the meter magnet. This change is completely negligible for the application considered herein.

3. Firmware

A flowchart of the algorithm executed by the MCU is shown in figure 3. First, an 'Initialization and configuration' stage initialises the different peripherals of the MCU. In addition, the secondary sensing is temporarily activated with the aim of measuring V_{SPS} under 'at rest' conditions; its value is stored in the variable $V_{SPS,0}$. The flowchart next has five main stages.

- *Stage A*, which corresponds to normal operating conditions without the presence of an interfering magnet. The system relies on primary sensing, where the counter is increased by 1 at each rising edge of V_{PAS}, provided that V_{PPS} is '0'. If V_{PPS} is '1', the secondary sensing is activated.
- *Stage B*, which is intended to obtain the difference $V_{SAS} - V_{SPS}$ once V_{SPS} is stable, i.e., when the interfering magnet has a fixed position. Such a difference, which is stored in the variable ΔV_{ref}, is expected to be different from zero, since the interfering magnet will not equally affect SAS and SPS.
- *Stage C*, which checks the presence and/or movement of the interfering magnet. First, a double check of V_{PPS} and V_{SPS} confirms either the presence or absence of the interfering magnet. Second, any change of position of the interfering

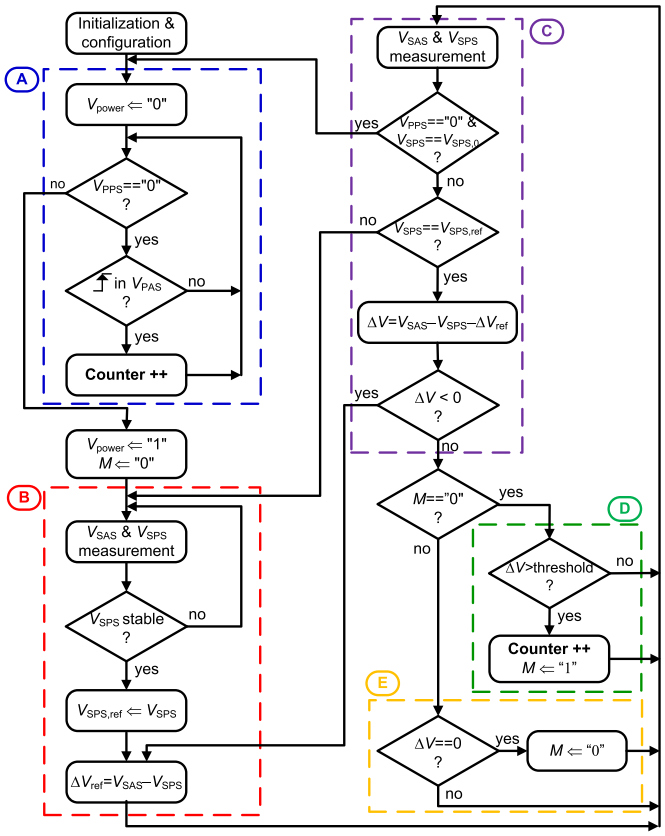

Figure 3. Flowchart of the algorithm executed by the MCU.

magnet is detected by comparing V_{SPS} with that obtained in stage B (stored in the variable $V_{SPS,\,ref}$). And third, the factor $\Delta V = V_{SAS}–V_{SPS}–\Delta V_{ref}$ is computed. We expect $\Delta V = 0$ under no effect of the meter magnet, and $\Delta V > 0$ under its effect. If $\Delta V < 0$, it means that ΔV_{ref} was computed in stage B with the meter magnet effects; if so, it has to be recalculated.

- *Stage D*, which detects the effects of the meter magnet on the SAS. When the meter magnet is aligned to the SAS, V_{SAS} increases and $\Delta V > 0$. If ΔV is higher than a certain threshold, then the counter is increased by one. In addition, an internal variable (M) is set to '1', which indicates that the meter magnet has already been detected by the secondary sensing.
- *Stage E*, which checks when the SAS is no longer under the effects of the meter magnet. This is inferred by comparing ΔV with zero. When this is the case, M is set again to '0' to be able to detect the next magnet–SAS alignment.

For a more stable algorithm, the values of V_{SAS} and V_{SPS} correspond to an average of ten measurements. In addition, the comparison between analogue voltages in figure 3 takes into account a certain level of uncertainty around the expected value. To optimize the energy consumption under unusual operating conditions, the MCU is by default in sleep mode, executes the algorithm every 50 ms, and enables the Hall-effect sensors (via the V_{power} signal) for 1 ms.

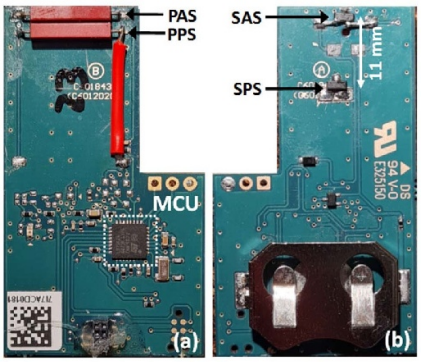

Figure 4. PCB developed: (a) top layer, and (b) bottom layer.

Table 1. Cost of the main components used to develop the design shown in figure 4, assuming high-volume production.

Component	Cost (€)
PCB	1.00
MCU	1.40
32 kHz crystal	0.26
Reed switches (×2)	0.69
Hall-effect sensors (×2)	0.63
Battery	0.16
Battery holder	0.17
TOTAL	4.32

4. Experimental results

A prototype of the circuit in figure 2 was developed using a printed circuit board (PCB), as shown in figure 4. The MCU (STM32L071KZU from STMicroelectronics) ran on a 32 kHz crystal oscillator. This MCU has an embedded 12-bit ADC with a resolution (or a least-significant bit, LSB) of 0.8 mV when the supply voltage (V_{DD}) is 3.3 V. The Hall-effect sensor (AH49ENTR-G1 from Diodes Incorporated, with a nominal sensitivity of 16 mV mT^{-1}) was selected to have a wide magnetic field range (±0.1 T) and, hence, avoid its saturation due to the interfering magnet. The reed switch was a CT10-2540-G1 from Coto Technology; R = 560 kΩ and C = 5.6 nF. Table 1 summarises the main costs of developing the proposed design.

The PCB had appropriate physical dimensions to be placed into the gas meter, as shown in figure 5. The primary sensing was placed at the top layer, whereas the secondary sensing was placed at the bottom, as shown in figure 4. The active sensors (PAS and SAS) were positioned at the border of the PCB to be as close as possible to the meter magnet; when the meter magnet was aligned, the distance to the active sensors was around 10 mm. On the other hand, the passive sensors (PPS and SPS) were placed at 2 and 11 mm, respectively, from the corresponding active elements. Using such distances, the PPS was insensitive to the meter magnet, while the SPS was at least ten times less sensitive to the meter magnet than the SAS.

To easily characterize the prototype, air was the gas injected into the meter inlet by an electric air pump. An external disc

Figure 5. Placement of the PCB shown in figure 4 into the gas meter: (a) without the protecting box, (b) with the protecting box.

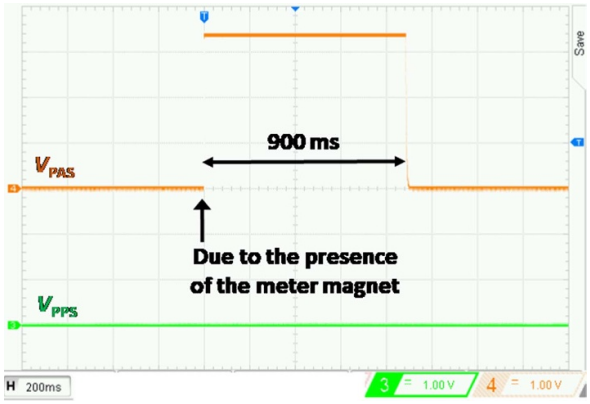

Figure 6. Waveforms acquired from the PAS and PPS when the meter magnet was detected without interfering magnetic effects.

magnet, with a diameter of 4.8 cm, was employed to generate the interfering magnetic field. This magnet was completely attached to the front, top, and side of the mechanical index of the meter; although attached, the minimum distance to the sensors was around 12 mm. In the worst testing scenario, this magnet caused (at the sensor position) an interfering magnetic field of 50 mT. On the other hand, the meter magnet generated (at the active sensor position) a magnetic field of 0.6 mT, which is 80 times lower than the previous one.

Figure 6 shows the experimental waveforms acquired by a digital oscilloscope without the effect of an interfering magnet. Under such conditions, the PPS provided a digital '0', while the PAS generated a rising edge, which increased the value of the counter by one, when the meter magnet became aligned with it. The signal provided by the PAS was activated for a time interval of 900 ms, which corresponds to a gas consumption of about 133 l min^{-1}. Of course, the lower the gas consumption, the longer the activation time.

The most critical interference scenario was when the interfering magnet was attached to the front of the mechanical index of the meter. Figure 7 shows the experimental waveforms of V_{SAS} and V_{SPS} when the interfering magnet was

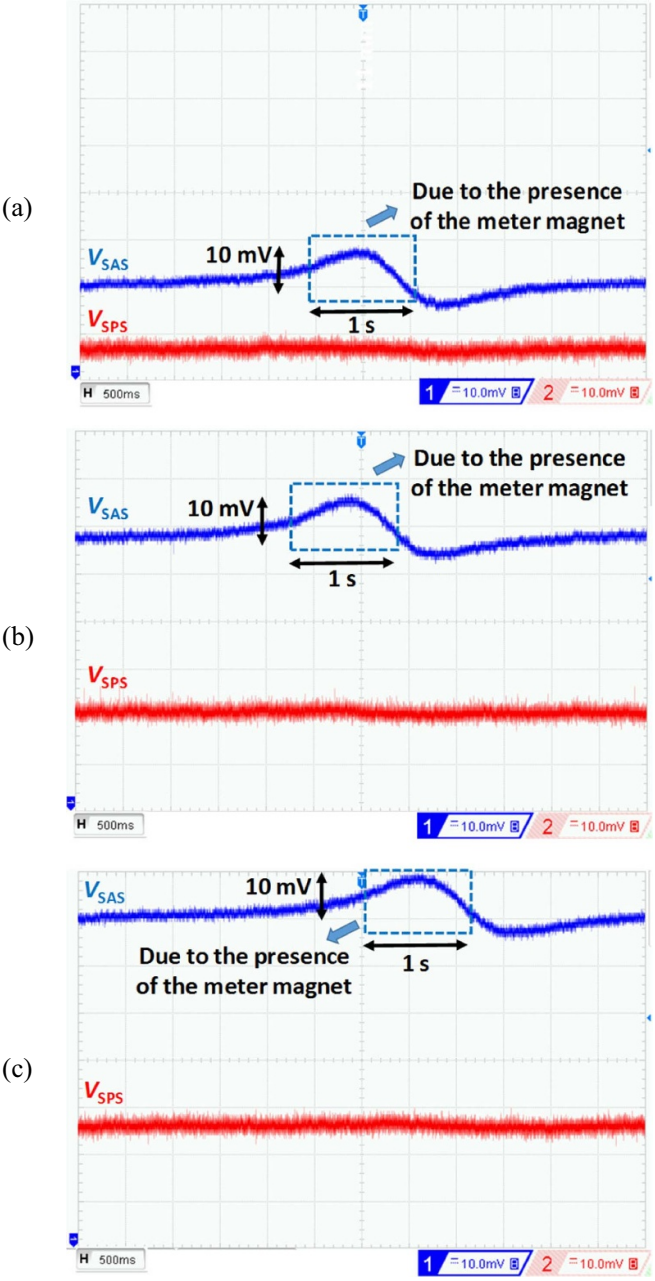

Figure 7. Waveforms acquired from the SAS and SPS when the meter magnet was detected and the interfering magnet was at three different positions at the front of the meter. The ground levels of channels 1 and 2 were moved down (not visible in the screenshots) to different positions to better appreciate the effects of the meter magnet on both signals, but they were at the same position for the three cases represented.

placed at three different front positions; the signals provided by PAS and PPS are not represented here, but they were a digital '1'. According to figure 7, when the meter magnet was aligned to SAS, V_{SAS} increased by 10 mV regardless of the position of the interfering magnet, whereas V_{SPS} was almost constant. An increase of 10 mV corresponds to a change of 12 LSB at the ADC output. From figure 7, we can also see that the baseline of V_{SAS} and V_{SPS} (and, hence, the difference

$V_{SAS} - V_{SPS}$) depended on the position of the interfering magnet, but this was dynamically corrected by the algorithm proposed in figure 3.

Under normal operating conditions and when the reed switches were open, the circuit in figure 2 had a current consumption of 5 μA, which was mainly due to the sleep mode of the MCU. However, when the secondary sensing was active, the average current consumption increased to 86 μA. Therefore, the robustness against interfering magnets comes at the expense of higher current consumption.

After proving the feasibility of the proposed measurement subsystem, this could be complemented by: (a) a communications subsystem using a low-power wide-area network technology, and (b) an energy harvester, such as a small-area photovoltaic panel, especially for those gas meters located outdoors. The energy consumption of the communications subsystem is expected to be higher than that of the measurement subsystem, but the sensor node could still be autonomous thanks to the energy harvester.

5. Conclusions

In the context of smart meters for smart grids, this article has proposed an MCU-based circuit for upgrading mechanical gas meters to electronic ones. The proposed circuit, together with a dynamically adjusted algorithm, is able to detect the meter magnet under the effects of an interfering magnet and, in addition, the interfering magnet itself does not cause an erroneous increase in the digital counter. Consequently, the proposed sensor system has been proven reliable in front of static magnetic fields generated by interfering magnets.

Data availability statement

The data that support the findings of this study are available upon reasonable request from the authors.

Acknowledgments

This work was supported by the Secretariat of University and Research of the Ministry of Business and Knowledge of the Government of Catalonia, and by the Spanish Ministry of Economy and Competitiveness and the European Regional Development Fund under Project No. TEC2016-76991-P.

ORCID iDs

Edgar Ripoll-Vercellone https://orcid.org/0000-0003-0013-5354
Manel Gasulla https://orcid.org/0000-0002-0364-6806
Ferran Reverter https://orcid.org/0000-0003-1653-0519

References

[1] Duarte D P, Nogueira R N and Bilro L B 2019 Semi-supervised Gaussian and t-distribution hybrid mixture model for water leak detection *Meas. Sci. Technol.* **30** 125109
[2] Rinaldi S, Ferrari P, Flammini A, Sisinni E and Vezzoli A 2019 Uncertainty analysis in time distribution mechanisms for OMS smart meters: the last-mile time synchronization issue *IEEE Trans. Instrum. Meas.* **68** 693–703
[3] Rorato O, Bertoldo S, Lucianaz C, Allegretti M and Notarpietro R 2013 An ad-hoc low cost wireless sensor network for smart gas metering *Wirel. Sens. Netw.* **5** 61–6
[4] Kot T 2015 Flow measurement with reed switches and BLE *App. Rep. TIDUB33* (Texas Instruments)
[5] Tewolde M, Longtin J P, Das S R and Sharma S 2013 Determining appliance energy usage with a high-resolution metering system for residential natural gas meters *Appl. Energy* **108** 363–72
[6] He Z, He Y, Yang Y and Gao M 2017 A low-cost direct reading system for gas meter based on machine vision *Proc. 12th IEEE Conf. Industrial Electronics and Applications* pp 1189–94
[7] Qiu S, Huang Y, He X, Sun Z, Liu P and Liu C 2015 A dual-mode proximity sensor with integrated capacitive and temperature sensing units *Meas. Sci. Technol.* **26** 105101
[8] Praveen Kumar T, Saimurugan M, Hari Haran R B, Siddharth S and Ramachandran K I 2019 A multi-sensor information fusion for fault diagnosis of a gearbox utilizing discrete wavelet features *Meas. Sci. Technol.* **30** 85101
[9] Keith Seal B and Martin B 2007 Magnetic field sensing for tamper identification *US Patent* 2007/0229256 A1
[10] Ramirez A D 2015 Magnetic tampering detection in a utility meter *US Patent* 2015/0002134 A1
[11] Yukihiro O 2012 Gas meter theft sensing device *Patent WO2012157264A1*
[12] Pallàs-Areny R and Webster J G 2001 *Sensors and Signal Conditioning* (New York: Wiley)
[13] Honeywell Inc Sensing and control *Hall Effect Sensing and Application* (available at: https://sensing.honeywell.com/hallbook.pdf)

3

Publications III, IV & V

3.1 Publication III: Conference proceeding II

Republished with permission of ACM (Association for Computing Machinery), from "Using LEDs for Visible Light Communication and as a Wake-up Mechanism in the Internet of Things," E. Ripoll Vercellone, V. Ferrandiz, J. Aubert, and M. Gasulla, *Proceedings of the 15th ACM Conference on Embedded Network Sensor Systems*, 2017, doi: 10.1145/3131672; permission conveyed through Copyright Clearance Center, Inc. (License ID: 1152030-1).

3.2 Publication IV: Conference proceeding III

IEEE copyright / credit notice: 2019 IEEE. Reprinted, with permission, from E. Ripoll-Vercellone, F. Reverter, V. Ferrandiz, and M. Gasulla, "Experimental characterization of off-the-shelf LEDs as photodetectors for waking up microcontrollers," in *I2MTC 2019 - 2019 IEEE International Instrumentation and Measurement Technology Conference, Proceedings*, 2019, vol. 2019-May. doi: 10.1109/I2MTC.2019.8826967.

3.3 Publication V: Journal Article II

IEEE copyright / credit notice: 2020 IEEE. Reprinted, with permission, from E. Ripoll-Vercellone, F. Reverter, and M. Gasulla, "LED-Based Wake-Up Circuit for Microcontrollers," *IEEE Transactions on Instrumentation and Measurement*, vol. 69, no. 9, 2020, doi: 10.1109/TIM.2020.3009340.

Demo Abstract: Using LEDs for Visible Light Communication and as a Wake-up Mechanism in the Internet of Things

Edgar Ripoll Vercellone
Universitat Politècnica de Catalunya
Idneo Technologies S.L.
edgar.ripoll.vercellone@upc.edu

Vicent Ferrandiz
Idneo Technologies S.L.
vicent.ferrandiz@idneo.com

Jordi Aubert
Idneo Technologies S.L.
jaubert@idneo.com

Manel Gasulla
Universitat Politècnica de Catalunya
manel.gasulla@upc.edu

ABSTRACT

The design and implementation of wireless sensor nodes for the Internet of Things require paying exceptional attention to their sources of energy consumption in order to extend their battery lifetime. These nodes spend most of the time in standby mode and they only wake up to perform a quick defined task, usually sensing and measuring or transmitting information. In this demo, LEDs are used for Visible Light Communication. A low-cost, small-size and low-power consumption LED-based interface circuit connected to an I/O microcontroller pin is proposed and tested. Moreover, this circuit also operates as a wake-up mechanism, aiding to achieve longer standby time and thus lower energy consumption. Our experiments are shown in actual commercial applications developed for a European project.

CCS CONCEPTS

• **Hardware** → **Sensors and actuators**; **Wireless devices**; • **Networks** → *Short-range networks*; Mobile networks; Wireless access networks;

KEYWORDS

Internet of Things, Visible Light Communication, Light Emitting Diodes, Energy Efficiency, Wake-up Mechanism.

ACM Reference Format:
Edgar Ripoll Vercellone, Vicent Ferrandiz, Jordi Aubert, and Manel Gasulla. 2017. Demo Abstract: Using LEDs for Visible Light Communication and as a Wake-up Mechanism in the Internet of Things. In *Proceedings of 15th ACM Conference on Embedded Networked Sensor Systems (SenSys'17).* ACM, New York, NY, USA, 2 pages. https://doi.org/10.1145/3131672.3136995

1 INTRODUCTION

The Internet of Things (IoT) is a trending topic these days, which proposes that every existing device or object (machines, consumer goods, vehicles, etc.) is able to gather and transmit information without human intervention. This is affecting people's daily lives and generating new business areas for companies. For example, in the Health area, many wearable sensors are being developed, such as glasses, wristbands, and hearing aids. In the Smart Society field we find utility meters, secure authentication wearables and electronic seals or locks. And in the Mobility and Production areas, some examples are industrial assets monitoring, indoor localization and navigation support and autonomous condition monitoring. In many of these applications, wireless sensors nodes are required.
This work is carried out within the European project "EnSO" (Energy for Smart Objects) [1], where some requirements are sought for the sensor nodes of the IoT; for instance, low cost, small size and low-power consumption. Paticularly, the use of LEDs can help fulfill those requirements. Here, a LED will be used in a sensor node for wireless communication purposes as well as a wake-up mechanisms when the node is in sleep mode.

2 USE OF THE LED AS EMITTER AND RECEIVER

2.1 Related Work

In the nodes of the IoT, wireless communication usually takes place through radiofrequency (RF) waves. Different standards are used, such as NFC, Bluetooth Low Energy, Zigbee, etc. However, these solutions need an antenna and a transceiver. As a consequence, they add size, power consumption and cost to the nodes. As an alternative, in applications where line-of-sight and short range between the emitter and receiver exist, Visible Light Communication (VLC) using LEDs can be a feasible solution, particularly if the sensor node needs one or more LEDs for signaling purposes anyway.
The use of LEDs both as a light emitter and receiver has been proposed in the literature, although not specifically for the nodes of the IoT requiring ultra-low power consumption. For example, in [2], a two-way LED communication was developed. In order to detect light, the microcontroller had to be awakened periodically, precharge the parasitic LED capacitance and discharge it via the photogenerated LED current. This process wastes too much energy. In [3], a dual-mode passive driver circuit is described. But, in this case, the usage of LEDs both for emission and for reception involves the microcontroller's ADC, which also implies an excessive power consumption.

SenSys'17, November 6–8, 2017, Delft, The Netherlands

ACM ISBN 978-1-4503-5459-2/17/11…$15.00
https://doi.org/10.1145/3131672.3136995

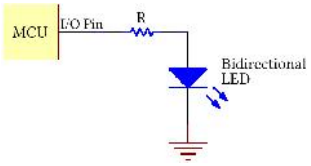

Figure 1: Circuit setup for LED bidirectional operation.

2.2 Description of the LED Circuit

Figure 1 shows the circuit we propose for VLC, where a LED is driven directly by a single microcontroller I/O pin. When the pin is configured as an output, the LED acts as emitter. Contrariwise, when the pin is configured as a (high-impedance) input, the LED operates at photovoltaic mode (unbiased) and acts as a light receiver. Whenever a beam of light hits the LED, a voltage builds up, whose level can be enough to be considered as a logic '1'. Otherwise, a logic '0' is read in absence of light.

Therefore, in spite of the simplicity of the circuit, a bidirectional communication using a LED can be established just by changing the microcontroller pin setting from output (LED as emitter) to input (LED as receiver). Futhermore, configuring the input as an external interruption, a contactless wake-up mechanism is created. So, the MCU can remain at its lowest power mode until a wake up light signal arrives and, afterwards, start a bidirectional communication. Hence, the microcontroller no longer has to wake up periodically to check whether a communication has to be set up. This leads to a significant reduction of the consumed energy since the time in standby mode is prolonged. In some applications, several months can pass between the startup of the sensor node and its first wireless communication. Besides, by using a single LED instead of an RF-based communication, a low-price and small area solution is achieved.

3 DEMONSTRATION

Figure 2 shows prototypes built for the EnSO project. The demonstration consists in the implementation of the above mentioned VLC and the wake-up mechanism using the circuit of Figure 1. This will be tested on the prototypes (sensor nodes) in three real use cases:

- **Electronic Seal:** Monitors and records tampering attempts.
- **Meter Supervisor:** Residential natural gas meter.
- **Smart Lock:** Keeps track of accesses and allows the creation of different kinds of hierarchy profiles.

In all of them, the external light source that communicates with the LED of Figure 1 will be a smartphone flash. The node will be at first in standby mode. Light codes will be sent from the smartphone flash to the LED of the sensor node to first wake up the node and then to send information. The node will also use the LED as an indicator once received the wake up signal and the messages. For example, in the Smart Lock demonstration, the LED will emit a specific light codification indicating whether the access code previously emitted from the smartphone was successful or not. For demonstration purposes, the sensor node will also be connected to a laptop through an USB cable. Depending on the application and

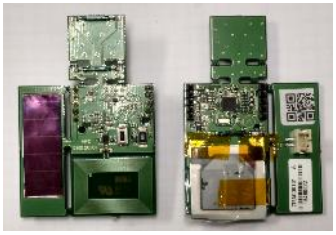

Figure 2: EnSO prototypes designed for testing several technologies; such as NFC, VLC, thin film batteries, etc.

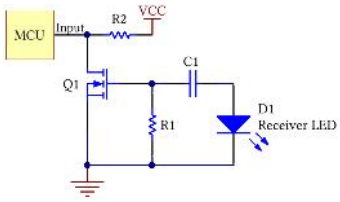

Figure 3: Interface circuit proposed to avoid high current consumption in case a constant light hits the LED.

the message code sent, a specific answer will be displayed in the laptop screen. The demonstration of a functionality of the Meter Supervisor can be seen at https://youtu.be/1fofwMxkPm8.

4 FUTURE WORK

The circuit simplicity of the Figure 1 has a downside. When a microcontroller I/O pin is configured as an input, current consumption is significant whenever the input voltage is around the transition between the logic levels. This may be due, for example, to the presence of a constant light beam, e.g. ambient light coming from artificial lights or from the sun.

In Figure 3, a interface circuit is proposed to solve that problem. It consists in a monostable multivibrator. It blocks low frequency signals and generates pulses (to the input pin of the microcontroller) when the LED receives a frequency modulated light signal, being the time lenght of the pulses determined by R_1 and C_1. Therefore, if a constant light hits the LED, zero current is drawn from the power supply.

Work is in progress regarding the implementation of the circuit of Figure 3 alongside with a bidirectional communication feature.

ACKNOWLEDGMENTS

This work was supported by EnSO (Energy for Smart Objects), Grant Agreement No.: 692482, Idneo Technologies S.L. and the Secretariat of University and Research of the Ministry of Business and Knowledge of the Government of Catalonia.

REFERENCES

[1] 2017. Enso - Energy for Smart Objects. (2017). http://www.enso-ecsel.eu/

[2] Paul Dietz, William Yerazunis, and Darren Leigh. 2003. *Very Low-Cost Sensing and Communication Using Bidirectional LEDs.* Springer Berlin Heidelberg, Berlin, Heidelberg, 175–191. https://doi.org/10.1007/978-3-540-39653-6_14

[3] S. Li, A. Pandharipande, and F. M. J. Willems. 2016. Daylight Sensing LED Lighting System. *IEEE Sensors Journal* 16, 9 (May 2016), 3216–3223. https://doi.org/10.1109/JSEN.2016.2520495

Experimental characterization of off-the-shelf LEDs as photodetectors for waking up microcontrollers

Edgar Ripoll-Vercellone
e-CAT Group, Dept. Electronic Eng.
Universitat Politècnica de Catalunya
Idneo Technologies S.A.U.
Barcelona, Spain
edgar.ripoll.vercellone@upc.edu

Ferran Reverter
e-CAT Group, Dept. Electronic Eng.
Universitat Politècnica de Catalunya
Castelldefels, Spain
ferran.reverter@upc.edu

Vicent Ferrandiz
Idneo Technologies S.A.U.
Mollet del Vallès, Spain
vicent.ferrandiz@idneo.com

Manel Gasulla
e-CAT Group, Dept. Electronic Eng.
Universitat Politècnica de Catalunya
Castelldefels, Spain
manel.gasulla@upc.edu

***Abstract*—The use of LEDs as photodetectors has been subject of study for a long time. However, LEDs manufacturers do not provide information about the response of LEDs to the light. It is essential for the designers of electronic devices to know what the behavior of LEDs is so as to develop new applications in this area. In this work, we propose the use of commercially off-the-shelf LEDs, illuminated by the flashlight of a smartphone, as a contactless wake-up system for microcontrollers that are in a sleep mode. In particular, the generated LED voltage is proposed as the wake-up signal. So, in order to choose the most suitable LED and depending of the main interfering light, the current-voltage (I-V) characterization of different kind of LEDs is performed for two scenarios: outdoors and indoors. It is demonstrated that placing a resistor in parallel with the LEDs allows a better discrimination between the LED voltage coming from the flashlight and that from the interfering lights. Results show that red and blue LEDs are more appropriate for outdoor and indoor applications, respectively.**

Keywords—LED, photodetector, microcontroller, wake-up system.

I. Introduction

The development of autonomous wireless electronic devices is a complex task. It is common that companies look for developing commercial products with a cost, size and power consumption as low as possible. Besides, energy efficiency must be taken into account from the very beginning of the project to guarantee the longest lifetime of the battery. For example, for some applications, depending on the required Ingress Protection Rating (IP Code, which classifies the degrees of protection provided by enclosures for electrical equipment as defined in IEC 60529), these devices are manufactured in sealed cases with the battery already integrated. However, they may stay in storage for months. So, in order to avoid draining the battery unnecessarily, there are several ways for activating a device at the right moment. A first solution is to add an on/off switch after the battery. A second solution is to configure the microcontroller unit (MCU) of the device in the lowest power mode and activate it by sending a signal through a switch pushbutton or a magnetically actuated reed switch. However, these solutions add a significant cost, size, difficulty in the mechanic design of the case or, sometimes, they are not even feasible given the constraints of the application. Besides, it is not convenient to increase the number of components just because they have to perform one single task only once in the lifetime of the device.

This work was supported by EnSO (Energy for Smart Objects) under Grant Agreement No. 692482, Idneo Technologies S.A.U., the Secretariat of Universities and Research of the Ministry of Business and Knowledge of the Government of Catalonia, the Spanish Ministry of Economy and Competitiveness and the European Regional Development Fund under project TEC2016-76991-P.

The use of LEDs as photodetectors can help fulfill those requirements. In particular, we propose the use of commercially off-the-shelf LEDs, illuminated with the flash light of a smartphone, as a contactless wake-up system of the MCU when it is in sleep mode. We have already researched on this subject, getting positive results [1]. There are several advantages with this solution: 1) LEDs can already be present for signaling purposes, 2) they are inexpensive and widely available, and 3) they are also small compared to mechanical or reed switches.

Several efforts have been done related to the use of LEDs as photodiodes [2], [3]. A photodiode generates a reverse current proportional to the incident light depending its spectral response curve on the material from which the diode is made. In ideal photodiodes, the upper cutoff wavelength is defined by the band gap energy, i.e. the responsivity is zero for photons with energy less than the band gap energy. On the other hand, the lower cutoff wavelength is a function of the absorption of the photons before they reach the sensitive region [4]. Nevertheless, manufacturers do not characterize LEDs as photodiodes and this knowledge is crucial to open new application fields, such as the proposed here. At this respect, some authors have characterized the performance of LEDs as photodetectors, concluding that their detection spectrum is wider and with a lower peak wavelength than that of the emission [4]-[6]. However, the current-voltage characteristics are not provided, which are necessary for the application proposed here.

This work tackles some of the previous issues. First, Section II proposes a generic interface circuit for waking up the MCU. Then, Section III describes the materials and methods to characterize the current-voltage characteristic of the selected LEDs as photodetectors, while, in Section IV, the experimental results are reported. Next, Section V discusses the results. Finally, conclusions are drawn in Section VI.

978-1-5386-3460-8/19/$31.00 ©2019 IEEE

II. Proposed Interface Circuit

Fig. 1 shows the proposed circuit, where the LED is working as a photodiode in photovoltaic mode and the I/O pin of the MCU is configured as a (high-impedance) input. First, let us suppose that the resistor R and the intermediate stage, consisting of a high-pass filter (HPF) and a voltage-level translator (VLT), is bypassed. So, assuming no bias current from the I/O pin, the LED is open-circuited. When no light is present, no voltage is generated across the LED and the MCU I/O pin reads a logic '0'. On the other hand, when light is present, a voltage is generated across the LED and the I/O pin will consider it as a logic '1' whenever the generated voltage surpasses the digital logic threshold.

In [1], we discussed that it is necessary to connect an interface circuit between the MCU I/O pin and the LED because the MCU current consumption (through its power supply pin) is significant whenever the input voltage at the I/O pin is around the transition between the logic levels. This voltage can be originated by interfering lights, such as sunlight or office light, which are low frequency (quasi-DC) signals. The HPF is used to block those interfering lights. Contrariwise, it lets pass signals of higher frequency to the MCU I/O pin, for example those coming from a switching flashlight, which is the signal of interest. The VLT may be needed to match the output signal voltage of the HPF to the logic levels of the MCU. Even so, interfering lights can also have sudden changes, which will generate voltage pulses that can wake up the MCU. For example, the autonomous device can be in darkness inside a room or a closed electrical cabinet and be suddenly illuminated when room lights switch on or the electrical cabinet is open, or it can just be outdoors in the shadow and suddenly be illuminated by sunlight. Placing a resistor in parallel with the LED, as shown in Fig. 1, can alleviate this issue, as will be discussed in Section V.

III. Materials And Methods

Table I summarizes the selected LEDs for this work: 2 red, 2 blue, 1 green and 1 white. Two of them (BLUE2 and RED2) were chosen with a higher emitting power level, although they are more expensive, expecting that they also present a higher sensitivity (generated photocurrent) because of its larger collecting area [5]. All LEDs have colorless-clear lenses (except the white LED because of its intrinsic phosphor layer) and flat top lens style. Each one was mounted in a 30 mm × 30 mm printed circuit board with a plug connected to the terminals of the LED.

Three sources of light were chosen, one being the signal of interest (smartphone flashlight) and the other two interfering lights (sunlight and office light). These interfering lights represent the interference the LEDs might find if they are placed in two dissimilar scenarios: outdoors and indoors. We assume direct sunlight outdoors and no sunlight indoors.

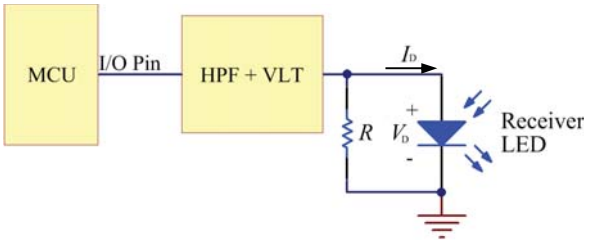

Fig. 1. Proposed interface circuit.

TABLE I. Selected LEDs for Characterization

Emitted Color	Part Number	Manufacturer	Emission Wavelength	Acronym
Blue	150060BS 75000	Wurth Electronics Inc.	470 nm	BLUE1
	L135-B475003500000	Lumileds	475 nm	BLUE2
Green	150060VS 75000	Wurth Electronics Inc.	528 nm	GREEN
Red	150060RS 75000	Wurth Electronics Inc.	625 nm	RED1
	ASMT-QHBD-AFH0E	Broadcom Limited	618 nm	RED2
White	CLM3C-WKW-CWBYA153	Cree Inc.	-	WHITE

The LED terminals were connected to a precision source/measure unit (SMU B2901A, Keysight), which allowed, for each LED and light source, the measurement of the LED current (I_D) while performing a LED voltage (V_D) sweep in steps of 100 mV. An additional characterization was performed in darkness. For the current measurement, an integration time of 10 PLC (power line cycles) was used, lasting each sweep about 7 seconds. To assess the repeatability, ten voltage sweeps were carried out with smartphone flash and office lights for BLUE1 and RED2. These LEDs were selected because they generate the lowest and highest values of I_D, as will be seen in Section IV. For the rest of cases, a single voltage sweep was performed.

As for the smartphone flashlight, a Motorola Moto X Style (XT1572) was used as the reference. However, in order to improve the repeatability of the measurements, an appropriate high-power white LED, emulating the smartphone flashlight, was used instead. The emission spectrum of the smartphone flashlight was measured with a spectrometer (AvaSpec-2048-SPU, Avantes) and then compared with that of high-power white LEDs with different color correlated temperature (CCT). The emission spectrum of the high-power white LED which best approximated that of the smartphone flash was the Lumileds L2C5-40701204E1300 model (the emitting LED from now on), with a CCT of 4000 K. Fig. 2 illustrates the similarity between the emission spectrums of the emitting LED and the smartphone flash. Fig. 3 shows the setup where the emitting LED is placed in a heat sink, fixed on top of a surface where the LEDs under test are placed. The light output level of the emitting LED was set (by regulating its forward current) to emulate the same irradiance received by the LED with the smartphone flash placed at a distance of 10 mm.

The sunlight characterizations were performed in a sunny day of autumn in Barcelona around midday. The LEDs were placed in an open space were the sunlight hit them directly. For the office light characterization, the LEDs were placed on a working table and lighted by compact fluorescent lamps (Osram DULUX D/E 26 W/840) placed on the office ceiling. These lamps also have a CCT of 4000 K. Finally, characterization in darkness was performed by placing the LEDs inside a closed box with only the measuring terminals accessible.

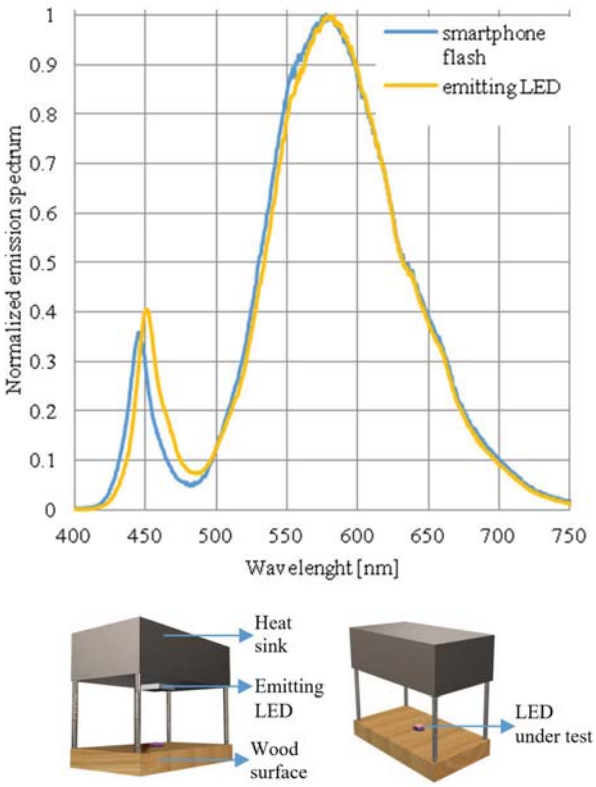

Fig. 3. Setup for emulating the smartphone flashlight.

IV. Experimental Results

Fig. 4 to Fig. 9 show the current-voltage (I-V) curves (I_D versus V_D, as defined in Fig. 1) for the LEDs of Table I and for the three lights under test. The light labeled as *Flash* corresponds to the emitting LED (setup of Fig. 3). As expected, in darkness the LEDs operated as diodes and no current was photogenerated; therefore, their results are not significant and they are not included.

Table II summarizes the values of the absolute photogenerated short-circuit current (I_{sc}, where $V_D = 0$) and of the open-circuit voltage (V_{oc}, where $I_D = 0$). The values of V_{oc} were calculated using a linear interpolation from the two adjacent data points above and below the abscissa axis. Several general conclusions can be drawn with respect to the values of I_{sc}: 1) values for the office light are about 3 orders of magnitude lower than for the other two lights, which is coherent with the proportionality of the photogenerated current with the light irradiance; 2) blue and white LEDs are more sensitive to sunlight than to flashlight, whereas the reverse is true for green and red LEDs; 3) red LEDs show a higher sensitivity than its blue counterparts; and 4) higher emitting-power blue and red LEDs are more sensitive than their lower emitting-power counterparts (about 2 and 1 order of magnitude, respectively), as suggested in Section III. Conclusions 2 and 3 are due to the lower peak wavelength of the LED detection spectrum with respect to that of the emission [4], [6]. As a result, blue LEDs skip most of the emission spectrum of the flashlight and thus show a low sensitivity to it. On the other hand, red LEDs have a higher overlap with the emission spectrums of the flashlight and sunlight and thus a higher sensitivity than blue LEDs. Finally, most white LEDs are fabricated from blue LEDs with a lens with a coated phosphor layer to spread the emitting spectrum; hence similar conclusions to blue LEDs can be drawn.

As for V_{oc}, the resulting values are: 1) significantly lower for office lights than for sun and flash lights, 2) equal or a little bit higher for blue and white LEDs with sunlight than with flashlight, whereas the reverse is true for green and red LEDs, and 3) higher for blue and white LEDs compared to green and red LEDs, the same that happens when those LEDs are used for emitting light. These conclusions are somehow related with that drawn for I_{sc}.

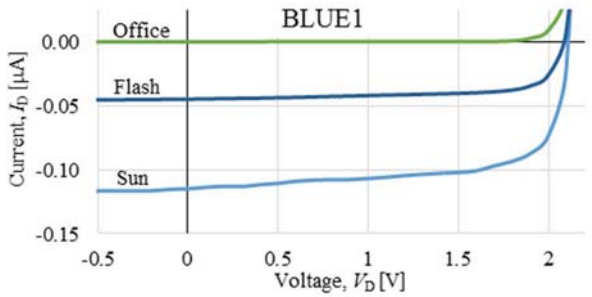

Fig. 4. I-V curves of the BLUE1 LED.

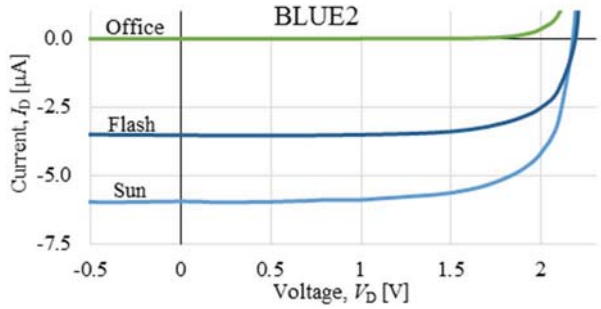

Fig. 5. I-V curves of the BLUE2 LED.

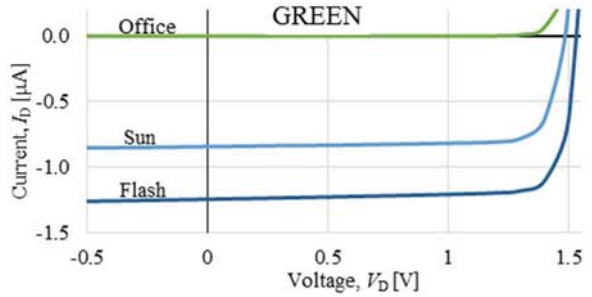

Fig. 6. I-V curves of the GREEN LED.

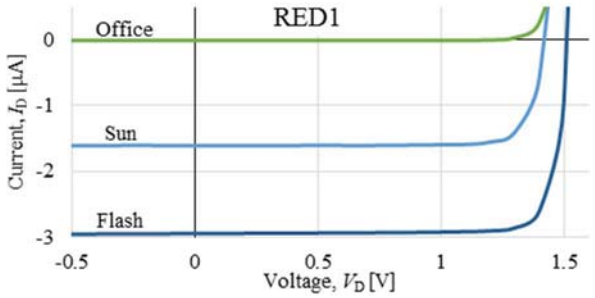

Fig. 7. I-V curves of the RED1 LED.

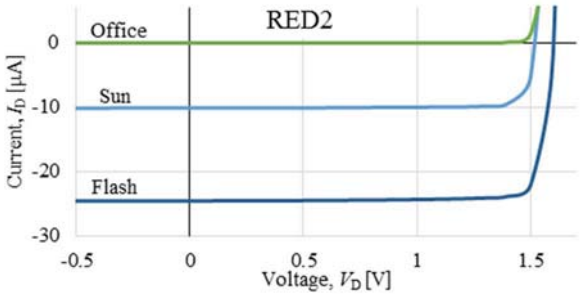

Fig. 8. I-V curves of the RED2 LED.

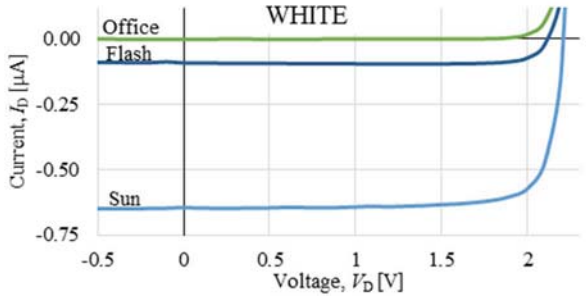

Fig. 9. I-V curves of the WHITE LED.

TABLE II. OPEN-CIRCUIT VOLTAGE AND SHORT-CIRCUIT CURRENT GENERATED BY THE LEDS

LED	Flash		Sun		Office	
	V_{oc} [V]	$\|I_{sc}\|$ [μA]	V_{oc} [V]	$\|I_{sc}\|$ [μA]	V_{oc} [V]	$\|I_{sc}\|$ [μA]
BLUE1	2.09[a]	0.044[a]	2.11	0.116	1.70[a]	3.0×10^{-4}[a]
BLUE2	2.18	3.54	2.18	5.95	1.53	7.5×10^{-3}
GREEN	1.52	1.25	1.47	0.845	1.19	1.6×10^{-3}
RED1	1.51	2.95	1.41	1.61	1.17	4.1×10^{-3}
RED2	1.60[a]	24.5[a]	1.51	10.1	1.32[a]	0.032[a]
WHITE	2.11	0.092	2.20	0.645	1.67	5.3×10^{-4}

[a] Average value of 10 measurements.

Repeatability results are summarized in Table III, where the standard deviations of V_{oc} (SD_V) and I_{sc} (SD_I) are shown. Values are given as a percentage with respect to the corresponding values of Table II. The values of SD_I were directly calculated from the 10 measured current values. On the other hand, given that V_{oc} was not directly measured, SD_V was calculated from the corresponding linear interpolations used to calculate V_{oc}. In all cases, SD_I was lower than the SMU uncertainty. For the case of BLUE1 and office lights SD_I was 1.94 %, much lower than the SMU uncertainty (±100 pA, ±33.7% of I_{sc}). Although this uncertainty is high, the inferred uncertainty on V_{oc} is only 1.3%.

TABLE III. STANDARD DEVIATION OF V_{OC} (SD_V) AND I_{SC} (SD_I) FOR BLUE1 AND RED2 LEDS

LED	Flash		Office	
	SD_V [%]	SD_I [%]	SD_V [%]	SD_I [%]
BLUE1	0.13	0.25	0.12	1.94
RED2	0.02	0.06	0.02	0.37

V. DISCUSSION

Photodetectors can work either in photoconductive or in photovoltaic mode, depending on the bias configuration. Here, LEDs are used as photodiodes and, based on the circuit of Fig. 1, they are used in the photovoltaic mode. The generated voltage (V_D) is the parameter of interest in order to serve as a wake-up signal for the I/O pin of the MCU. The aim is to achieve a significant voltage difference between the flashlight and the interfering lights, which should lead, with the aid of the intermediate stage of Fig. 1, to waking up the MCU only when flashlight illuminates the LED, even in presence of the interfering lights. One particular case is when no resistor is used, thus $V_D = V_{oc}$. According to Table II, the generated values of V_{oc} are quite similar on the same LED for the flashlight and sunlight (around 100 mV of difference maximum), which bans a good performance for the intended application. On the other hand, differences of V_{oc} between flashlight and office lights are higher, from 0.28 V to 0.65 V. In the following, we discuss how the addition of a resistor (R in Fig. 1) increases the voltage difference in both scenarios

The effect of placing a resistor R can be seen in Fig. 10 for the RED1 LED and for the case of sunlight as the interfering light. With respect to Fig. 7, the I-V characteristic of the resistor is added, the LED curve corresponding to office light is erased and only positive values of V_D are represented. Now, the operating voltages are not V_{oc} and arise from the intersections of the curves of the resistor and the LED. These are V_{sig} for the signal of interest (flashlight) and V_{int} for the interfering light (sunlight). In this way, the difference between the voltages corresponding to flashlight and sunlight greatly increases with respect to not using R.

The optimum value of R should be selected as the one that maximizes the difference between V_{sig} and V_{int}. This optimum value was estimated graphically and happens (approximately) when the resistor line intersects the knee of the flashlight LED curve. Considering that I_D at this optimum operating point is I_{sig}, the optimum load resistor was

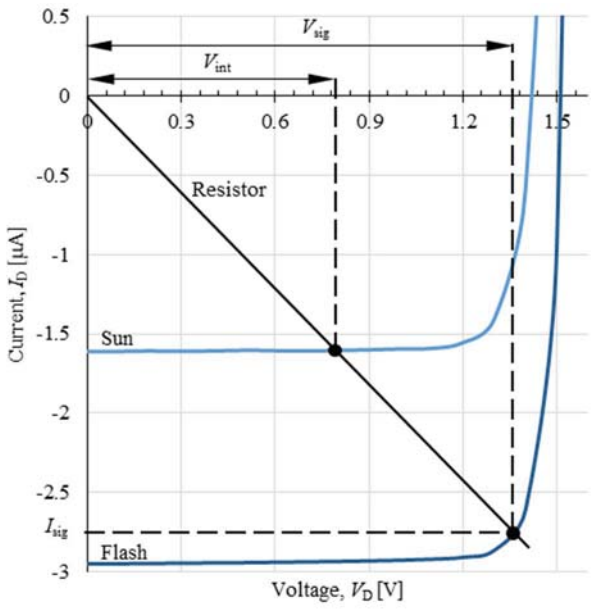

Fig. 10. Operating voltages for the signal of interest and the interfering light outdoors (sunlight) for the RED1 LED with the optimum resistor connected.

determined by

$$R = V_{sig} / |I_{sig}| \quad (1)$$

This solution is only feasible for LEDs with a higher current sensitivity to flashlight, i.e. for green and red LEDs. When applied on blue and white LEDs, V_{sig} will be lower than V_{int}, which bans their use.

When the office light is the main interfering source, the voltage difference can also be enlarged using an appropriate resistor as given by (1), as can be seen in Fig. 11 for the BLUE2 LED. Now, all the LEDs could be used but those that generate a higher voltage difference are blue and white LEDs.

Table IV summarizes the achieved voltage differences and the inferred values of the resistor at the optimum operating point of the LEDs; only the operational LEDs are given depending on the interfering light. For the outdoor scenario, RED2 LED offers the largest voltage difference (830 mV), which is much larger than that obtained without the resistor (90 mV, Table II). RED1 LED offers a lower cost and smaller size alternative but with a lower voltage difference, 580 mV. On the other hand, for the indoor scenario, blue and white LEDs offer the largest voltage differences, near 2 V. This voltage can be enough, depending on the MCU and its voltage supply, to be considered as a logic '1' and save the use of the VLT stage. Among those LEDs, BLUE1 is the lowest cost alternative. Nevertheless, the resulting value of the resistor (66 MΩ) is rather high, which results from its lower current sensitivity (low value of I_{sig}). On the other hand, green and red LEDs offer lower voltage differences but they can also be used outdoors with an appropriate VLT.

VI. Conclusions

In this paper, a contactless wake-up system for MCU using commercially available LEDs as photodiodes has been proposed. In particular, this work has been focused on the case in which the flashlight of a smartphone is used as the excitation source and the corresponding generated LED voltage is used as the wake up signal. However, interfering lights could also wake up the microcontroller

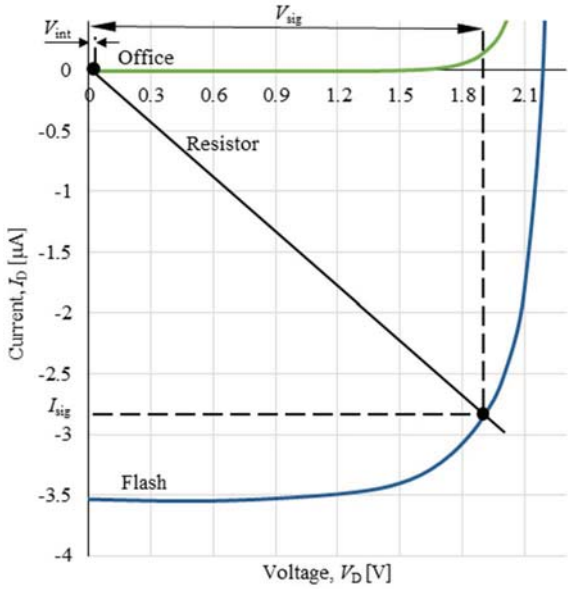

Fig. 11. Operating voltages for the signal of interest and the interfering light indoors (office light) for the BLUE2 LED with the optimum resistor connected.

TABLE IV. Voltages generated at the optimum operation point and the required resistance values

Scenario	LED	V_{sig} [V]	V_{int} [V]	$V_{sig} - V_{int}$ [V]	R [MΩ]
Outdoors	GREEN	1.36	0.96	0.40	1.2
	RED1	1.36	0.78	0.58	0.49
	RED2	1.47	0.64	0.83	0.063
Indoors	BLUE1	1.97	0.011	1.96	66
	BLUE2	1.90	0.025	1.87	0.40
	WHITE	2.00	0.031	1.97	28
	GREEN	1.36	0.003	1.36	1.2
	RED1	1.36	0.003	1.36	0.49
	RED2	1.47	0.005	1.47	0.063

Considering the lack of information from the LED manufacturers, an I-V characterization of some LEDs of different colors has been performed. The characterization has been carried out with the signal of interest (the smartphone flashlight) and with the interfering lights present in two dissimilar scenarios where the LEDs might be placed, outdoors (sunlight) and indoors (office light). Results indicate that the generated open circuit voltages are quite similar on the same LED for the different sources of light. So, a good discrimination between the different lights is not possible. However, by adding a resistor in parallel with the LED, an optimum operation point is achieved, which allows a better discrimination between the voltages corresponding to the signal of interest (flashlight) and the interfering lights. This should lead, with the aid of the intermediate stage of Fig. 1, to waking up the MCU only when flashlight illuminates the LED. The value of the resistor has been calculated based on the I-V flashlight characteristic of the LEDs. Based on those results, the most suitable LEDs are red for outdoors and blue for indoors. On the other hand, blue and white LEDs cannot be used outdoors since sunlight originates a higher LED voltage than flashlight.

Work is in progress regarding the design of the appropriate interface circuit between the LED and the MCU to block DC interfering lights and adapt the levels of the generated LED voltages, as well as the circuit that allows a LED to operate as both a light emitter and a receiver. Additionally, it is intended to perform the dynamic characterization of the LEDs operating as photodiodes.

References

[1] E. Ripoll-Vercellone, V. Ferrandiz, J. Aubert and M. Gasulla, "Using LEDs for visible light communication and as a wake-up mechanism in the Internet of Things," in Proc. of the 15th ACM Conf. on Embedded Network Sensor Syst. (SenSys '17), Delft, 2019, pp. 49:1-49-2.

[2] S. Li, A. Pandharipande and F. Willems, "Daylight Sensing LED Lighting System," *IEEE Sensors J.*, vol. 16, no. 9, pp. 3216-3223, 2016.

[3] P. Dietz, W. Yerazunis and D. Leigh, "Very Low-Cost Sensing and Communication Using Bidirectional LEDs," in UbiComp 2003: Ubiquitous Computing, Seattle, Washington, 2003, pp. 175-191.

[4] Y. Acharya, "Spectral and emission characteristics of LED and its application to LED-based sun-photometry," *Optics & Laser Technology*, vol. 37, no. 7, pp. 547-550, 2005.

[5] R. Filippo, E. Taralli and M. Rajteri, "LEDs: Sources and Intrinsically Bandwidth-Limited Detectors," *Sensors*, vol. 17, no. 7, p. 1673, 2017.

[6] M. Kowalczyk and J. Siuzdak, "Photo-reception properties of common LEDs," *Opto-Electronics Review*, vol. 25, no. 3, pp. 222-228, 2017.

LED-Based Wake-Up Circuit for Microcontrollers

Edgar Ripoll-Vercellone, Ferran Reverter, and Manel Gasulla, *Senior Member, IEEE*

***Abstract*— This article proposes, analyzes, and tests a wake-up circuit for a microcontroller (MCU) that uses a light-emitting diode (LED), operating as a photodetector, illuminated by a smartphone flashlight. The wake-up circuit consists of a high-pass filter and a voltage-level translator that interfaces the LED, with a suitable resistor in parallel, to the MCU. When illuminated by a switching flashlight, the LED generates a square voltage that is conveniently converted in logic levels at the output of the wake-up circuit. A firmware embedded into the MCU additionally checks that a predetermined sequence of logic pulses at a given rate is accomplished to activate the MCU. This article includes a theoretical analysis and experimental results that validate the proposed circuit.**

***Index Terms*— Light-emitting diode (LED), low-power mode (LPM), microcontroller (MCU), optical wake-up circuit, photodiode.**

I. Introduction

WIRELESS sensor nodes usually are autonomously powered and have a microcontroller (MCU) unit that controls the electronic modules and processes the information coming from sensors and/or transceivers [1]. To save power, the sensor node is set most of the time in a low-power mode (LPM), which is controlled by the MCU, and only wakes-up occasionally for sensing and transmitting data. MCUs are awaken by internally and/or externally generated interruption signals. Internal interruption signals come from embedded timers and are used by the MCU to carry out periodic tasks [1], [2]. External interruption signals come from, among others, the same sensors in charge of the measurement [3], secondary low-power sensors [4], alarm events [5], or remote radio frequency (RF) signals that trigger a wake-up receiver of the sensor node [6].

Optical wake-up has been proposed using detectors such as light-dependent resistors (LDRs) [4] and photodiodes [7], [8]. In [7], a commercial infrared photodiode was used with a transimpedance amplifier, active, and passive filters, a comparator, and some additional circuitry. Undesired effects of artificial and ambient lights were prevented at the cost of circuit complexity. In [8], a custom CMOS receiver is proposed, where a parasitic photodiode is again surrounded of a complex circuitry. Contrariwise, in [4] a simple voltage divider was used. There, ambient light was the wake-up source and, hence, no circuitry was added to filter it out. However, a current of 3.3 μA was continuously drained and, because no high-pass filter (HPF) was used, generated voltages lying between a logic "0" and "1" could lead to an increase in the MCU power consumption [9]. Light-emitting diodes (LEDs) can also be employed as optical detectors, as demonstrated in [10], and hence for low-cost optical wake-up circuits, as initially proven in [11]. There, an LED was directly connected to the MCU and a smartphone flashlight was used as the wake-up source. Besides, the LED was used for light signaling, thus having a dual function. However, interfering lights, even of low intensity, could also wake-up the MCU and increase its power consumption, as in [4]. In addition, no detailed analysis is provided. Here, an LED-based wake-up circuit activated by a smartphone flashlight and with immunity to interfering lights is proposed, analyzed, and tested. The proposed circuit is much simpler than those suggested in [7] and [8], and solves the limitations of interference sensitivity and current consumption found in [4] and [11].

Manuscript received June 7, 2020; accepted June 22, 2020. Date of publication July 15, 2020; date of current version August 11, 2020. This work was supported in part by the Secretariat of University and Research of the Ministry of Business and Knowledge of the Government of Catalonia and in part by the Spanish State Research Agency (AEI) and the European Regional Development Fund under Project TEC2016-76991-P. The Associate Editor coordinating the review process was Dr. Roman Sotner. *(Corresponding author: Manel Gasulla.)*

Edgar Ripoll-Vercellone is with Idneo Technologies, 08100 Catalonia, Spain (e-mail: edgar.ripoll@idneo.com).

Ferran Reverter and Manel Gasulla are with the Department of Electronic Engineering, Universitat Politècnica de Catalunya, 08860 Catalonia, Spain (e-mail: ferran.reverter@upc.edu; manel.gasulla@upc.edu).

Color versions of one or more of the figures in this article are available online at http://ieeexplore.ieee.org.

Digital Object Identifier 10.1109/TIM.2020.3009340

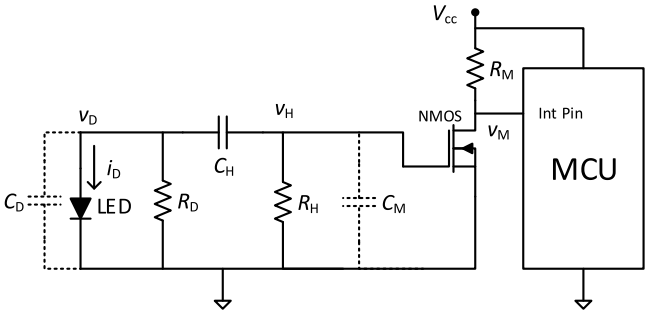

Fig. 1. Circuit for waking up an MCU using an LED.

II. Wake-Up Circuit

The circuit of Fig. 1 is proposed for interfacing an LED to the MCU, which includes several stages as described throughout this section. Similar to a photodiode [10], a voltage across the LED (v_D) is generated in the presence of light, for example that coming from a smartphone flashlight. The value of v_D needs to be high enough to become a logic "1" and wake-up the MCU. However, artificial and ambient interfering lights could also wake-up the MCU. To palliate this, a resistor (R_D) is added in parallel with the LED [12]. In this way, v_D is proportional to the generated LED current (i_D), thus allowing a better discrimination between different light intensities. Even so, dc and low-frequency signals coming from interfering lights either indoors (e.g., office) or outdoors (e.g., sun) can generate values of v_D corresponding to a (false) "1" or to an intermediate level between a logic "0" and "1" that leads to an increase in the MCU power consumption [9]. For this reason, a HPF, consisting of C_H and R_H, is added to suppress these signals. Consequently, a switching wake-up flashlight has to be used to surpass the HPF. When the flashlight turns on, i_D and thus v_D undergo a step increase from an initial value (corresponding to the interfering light) and the voltage step (Δv_D) instantaneously appears in the HPF output (v_H). Since Δv_D may not directly lead to a "1," an inverter voltage level translator (VLT) stage is also added at the output of the HPF. This stage, based on a nMOS transistor and a pull-up resistor (R_M), converts Δv_D at its input to 0 V (a "0") at its output (v_M) and a zero voltage to V_{cc} (a "1"). Finally, the VLT output is connected to an interruption pin of the MCU.

To evaluate the response of the circuit of Fig. 1 in the frequency and time domains, the parasitic capacitances of the LED (C_D) and of the nMOS input (C_M) are considered and represented in dashed lines.

In addition, the LED itself is considered for the analysis as a current source (i_D). To avoid loading effects on R_D and C_H, the conditions $R_H \gg R_D$ and C_D, $C_M \ll C_H$ are imposed. Thus, the Laplace transfer function of the circuit is given by

$$H(s) = \frac{V_H}{I_D} \approx -R_D \frac{s\omega_2}{(s+\omega_1)(s+\omega_2)} \quad (1)$$

which corresponds to a bandpass filter (BPF) with the following cutoff frequencies:

$$f_1 = \frac{\omega_1}{2\pi} = \frac{1}{2\pi\tau_1} \quad (2)$$

$$f_2 = \frac{\omega_2}{2\pi} = \frac{1}{2\pi\tau_2} \quad (3)$$

with $\tau_1 = R_H C_H$ and $\tau_2 = R_D(C_D + C_M)$ where $\tau_1 \gg \tau_2$ and thus $f_1 \ll f_2$.

A wake-up flashlight of frequency f_s will generate a square-wave signal of the same frequency for i_D and thus, assuming $f_s \ll f_2$, for v_D. At a rising edge of v_D, v_H sharply increases from zero to Δv_D and v_M toggles from "1" to "0." Then, v_H exponentially decreases to zero. When v_H crosses the threshold voltage of the nMOS (V_T), v_M toggles again to "1." This process repeats at each rising edge of v_D. For this behavior, v_H is assumed nearly zero before the rising edges of v_D, which can be achieved, assuming a square-wave flashlight of period T_s (=$1/f_s$) and a duty cycle of 50%, with $0.5T_s > 5\tau_1$, leading to

$$f_1 > \frac{5}{\pi} f_s. \quad (4)$$

A firmware activation check (FAC) is embedded into the MCU to reject unwanted wake-up signals coming from interfering lights or even from hacking lights. On the first rising edge of v_M, the MCU is awaken and the FAC is executed. If the result of the FAC is correct, the MCU is kept active; on the contrary, the MCU returns to LPM.

Changes in the parameter values of the components due to their tolerance or temperature drift should not affect the circuit performance thanks to its digital activation mechanism. A lower flashlight intensity or a change in R_D lowers Δv_D but only a value higher than V_T is required, which can also slightly change, altering the duty cycle of v_M but not its frequency. Changes on R_H and C_H alter f_1 but it is easy to accomplish (4) in the worst-case scenario. Finally, the two logic levels of v_M are not affected by voltage drifts on V_{cc} since it powers both the VLT and the MCU.

III. Experimental Results

As a proof-of-concept, a prototype of the circuit in Fig. 1 was designed with the following devices: 1) a low-cost flat-top red LED (150060RS75000, Wurth Electronics) that provides high enough values of Δv_D at indoor and outdoor conditions without requiring very high values of R_D [12]; 2) a small-signal nMOS (RE1C002UN, RHOM) that offers low values of both C_M and V_T; and 3) an STM32L072 MCU with an interruption pin (PA0) that is activated at the rising edge of v_M. For illuminating the LED, we used, depending on the performed tests, either the flashlight of a Motorola Moto X Style (XT1572) smartphone placed at a distance of 1 cm or a high-power white LED that emulated it [12].

A. Static Characterization

Fig. 2 shows the static current/voltage (I/V) characterization of the LED with different types of lights. The Flash curve is the signal of interest, generated here with the emulated flashlight. The rest are interfering lights: Office curve corresponds to compact fluorescent lights placed on the ceiling (~700 lux), Shadow curve to sunlight blocked by an object (~60 W/m2), and Sun curve to direct sunlight (~1000 W/m2). Office and Shadow curves offer the lowest current levels, and Flash curve a higher current level than Sun curve. The Sun + Flash curve is a combination of direct sunlight and flashlight and presents the highest current level.

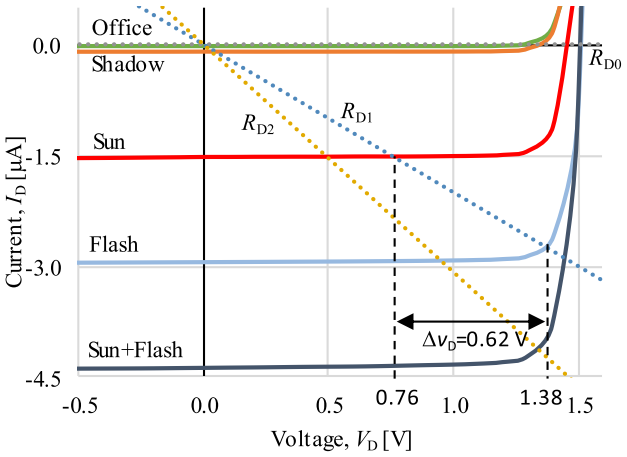

Fig. 2. I/V curves of the LED under test.

TABLE I
VALUES OF v_D AND Δv_D

Light	R_{D0}		R_{D1}		R_{D2}	
	v_D	Δv_D	v_D	Δv_D	v_D	Δv_D
Office	1.17	0.35	0.002	1.38	0.001	1.00
Shadow	1.37	0.15	0.045	1.34	0.035	0.96
Sun	1.46	0.06	0.76	0.62	0.52	0.48
Flash	1.52	–	1.38	–	1.00	–
Sun+Flash	1.52	0.06	1.45	0.69	1.37	0.85

Three lines corresponding to the I/V curves of three different values of R_D are also shown (R_{D0}, R_{D1}, and R_{D2}). Operating values of v_D arise from the intersection of the LED curves with the resistor lines. R_{D1} of 500 kΩ is selected for intersecting with the knee of the Flash curve, resulting in the values of v_D shown in Table I. This selection maximizes Δv_D, also shown in Table I, which refers to the difference between the value of v_D corresponding to the Flash curve and any of the interfering lights. Obviously, the worst case (minimum Δv_D) is for the Sun case, but the resulting value of 0.62 V is still good enough to toggle the VLT output. Smaller (e.g., R_{D2}) or higher values of R_D (e.g., R_{D0}) lead to smaller values of Δv_D. In particular, for R_{D0} (infinite value, equivalent to using no R_D) much smaller values of Δv_D are achieved (e.g., 60 mV), which are not high enough to toggle the VLT output. Hence, this demonstrates the need of using R_D, as pointed out in Section II.

Actually, the flashlight will add to the interfering light, so the Flash curve should add the corresponding interfering curve. Adding Office or Shadow curves to Flash curve does not significantly change it and R_{D1} is still a good choice. However, a significant change appears when adding the Sun curve resulting in the Sun + Flash curve. In this case, R_{D2} of 340 kΩ, which intersects with the knee of the Sun + Flash curve, could seem more optimum, since it leads to $\Delta v_D = 0.85$ V (shown in Table I at the row of Sun + Flash) when changing from Sun to Sun + Flash. However, Δv_D decreases for the other interfering lights with respect to using R_{D1}. Furthermore, the smartphone, when placed near the MCU for activating it, will block any direct interfering light and thus the actual interfering light will be of low intensity, for example like in Shadow or Office (see Section III-C). Thus, R_{D1} is still the best option.

TABLE II

PARAMETERS OF THE WAKE-UP CIRCUIT AND THE CORRESPONDING CUTOFF FREQUENCIES

R_D (kΩ)	C_D [a] (pF)	C_M (pF)	f_2 (kHz)	R_H (MΩ)	C_H (pF)	f_1 (Hz)	R_M (kΩ)	V_{CC} (V)
510	16	25	7.61	5.6	680	41.8	560	3

[a]Measured with an impedance analyzer (E4990A, Keysight).

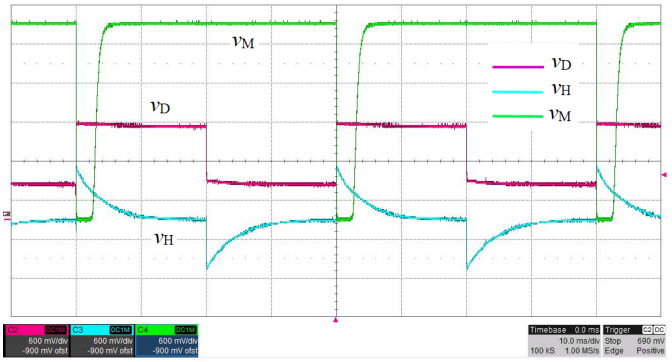

Fig. 3. Dynamic response waveforms of v_D, v_H, and v_M.

B. Dynamic Response

A flashlight with $f_s = 25$ Hz, which is around the upper limit that can be achieved with the smartphone flashlight, and a duty cycle of 50% was generated with the emulated flashlight. Table II shows the value of the remaining circuit parameters in Fig. 1 as well as the calculated cutoff frequencies of the BPF. Frequency f_2 is calculated from (3). Values of the HPF (R_H and C_H) are chosen to accomplish (4) and also $R_H \gg R_D$ and C_D, $C_M \ll C_H$. Then, f_1 is calculated using (2).

Tests were performed outdoors with direct sunlight hitting laterally the LED, apart from the emulated flashlight. Fig. 3 shows the results acquired with an oscilloscope. As can be seen, v_D is a square wave switching from around 500–600 mV when only the sunlight was present to 1.4–1.5 V when the flashlight also illuminated the LED, which is coherent with the values of v_D shown in Table I for R_{D1} (change from Sun to Sun + Flash). A lower voltage with sunlight was now achieved, probably due to a lower intensity of the sunlight than with the case of the static characterization. The effect of the HPF is observed in v_H, where peak voltages (Δv_D) around 800–900 mV were generated, enough to activate the nMOS of the VLT stage and make toggle v_M from 3 V ("1") to 0 V ("0"). Once v_H decreases down V_T, around 400 mV, v_M toggles again to a "1" until the next rising edge of v_D. This emulated situation is a worst-case scenario since the intensity of the interfering light, sunlight, is high. Even so, the system still works as pretended. DC current consumption of the circuit when not switching was around 0.5 nA.

C. Smartphone Test

A test was performed outdoors in a sunny day with the smartphone flashlight and the MCU executing the FAC. Fig. 4 shows the resulting waveforms. Pulses are not perfectly periodic but they slightly vary from pulse to pulse; this is a limitation of the Android Operating System since it is not possible to keep accurate track on short times [13]. The waveforms are still similar to those in Fig. 3 with a main difference: the voltage of v_D corresponding to the interfering light is now much lower, around 100–200 mV (top voltage is still 1.4–1.5 V), because the smartphone, placed above the LED at a distance around 1 cm, blocks the sunlight, reducing the interfering light to much lower levels, for example, comparable to Office or

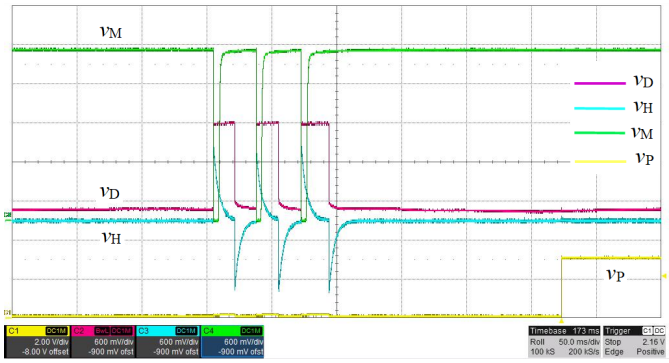

Fig. 4. Waveforms of v_D, v_H, and v_M with the smartphone test.

Shadow lights. This will be the preferred situation since moving away the smartphone reduces the effect of the flashlight and can increase the interfering light. Again, the HPF blocks the effect of the interfering light and the characteristic waveform can be seen in v_H, with a higher peak voltage than before, around 1.3–1.4 V, which is coherent with the values of Δv_D shown in Table I for R_{D1} and Office and Shadow cases. The VLT stage also generates a digital signal for v_M. As a proof of concept, the FAC of the MCU was set to activate a digital output (v_P) when just three rising edges of v_M were detected within a 300-ms time interval. Obviously, a more advanced FAC could be used to increase the system security.

REFERENCES

[1] R. Yan, H. Sun, and Y. Qian, "Energy-aware sensor node design with its application in wireless sensor networks," *IEEE Trans. Instrum. Meas.*, vol. 62, no. 5, pp. 1183–1191, May 2013.

[2] C. Alippi, G. Anastasi, M. Di Francesco, and M. Roveri, "An adaptive sampling algorithm for effective energy management in wireless sensor networks with energy-hungry sensors," *IEEE Trans. Instrum. Meas.*, vol. 59, no. 2, pp. 335–344, Feb. 2010.

[3] E. Sifuentes, R. Gonzalez-Landaeta, J. Cota-Ruiz, and F. Reverter, "Seat occupancy detection based on a low-power microcontroller and a single FSR," *Sensors*, vol. 19, no. 3, p. 699, Feb. 2019.

[4] E. Sifuentes, O. Casas, and R. Pallas-Areny, "Wireless magnetic sensor node for vehicle detection with optical wake-up," *IEEE Sensors J.*, vol. 11, no. 8, pp. 1669–1676, Aug. 2011.

[5] E. Ripoll-Vercellone, V. Ferrandiz, and M. Gasulla, "An add-on electronic device to upgrade mechanical gas meters into electronic ones," *Proceedings*, vol. 2, no. 13, p. 1094, Dec. 2018.

[6] V. Jelicic, M. Magno, D. Brunelli, V. Bilas, and L. Benini, "Benefits of wake-up radio in energy-efficient multimodal surveillance wireless sensor network," *IEEE Sensors J.*, vol. 14, no. 9, pp. 3210–3220, Sep. 2014.

[7] T. Hakkinen and J. Vanhala, "Ultra-low power wake-up circuit for short-range wireless communication," in *Proc. 4th Int. Conf. Intell. Environments (IE)*, Seattle, WA, USA, Jul. 2008, pp. 1–4.

[8] W. Lim, T. Jang, I. Lee, H.-S. Kim, D. Sylvester, and D. Blaauw, "A 380 pW dual mode optical wake-up receiver with ambient noise cancellation," in *Proc. IEEE Symp. VLSI Circuits (VLSI-Circuits)*, Honolulu, HI, USA, Jun. 2016, pp. 1–2.

[9] R. Shreyas, "Solving CMOS transition rate issues using Schmitt triggers," Texas Instrum., Dallas, TX, USA, White paper SLLA364A, 2017.

[10] M. Kowalczyk and J. Siuzdak, "Photo-reception properties of common LEDs," *Opto-Electron. Rev.*, vol. 25, no. 3, pp. 222–228, Sep. 2017.

[11] E. Ripoll-Vercellone, V. Ferrandiz, J. Aubert, and M. Gasulla, "Using LEDs for visible light communication and as a wake-up mechanism in the Internet of Things," in *Proc. 15th ACM Conf. Embedded Netw. Sensor Syst.*, Delft, The Netherlands, Nov. 2017, pp. 1–2.

[12] E. Ripoll-Vercellone, F. Reverter, V. Ferrandiz, and M. Gasulla, "Experimental characterization of off-the-shelf LEDs as photodetectors for waking up microcontrollers," in *Proc. IEEE Int. Instrum. Meas. Technol. Conf. (I2MTC)*, Auckland, New Zealand, May 2019, pp. 1–6.

[13] A. Duque, R. Stanica, H. Rivano, and A. Desportes, "Decoding methods in LED-to-smartphone bidirectional communication for the IoT," in *Proc. Global LIFI Congr. (GLC)*, Paris, France, Feb. 2018, pp. 1–6.

4

Publication VI

4.1 Publication VI: Journal Article III

M. Gasulla, E. Ripoll-Vercellone, and F. Reverter, “A compact Thévenin model for a rectenna and its application to an RF harvester with MPPT,” *Sensors (Switzerland)*, vol. 19, no. 7, 2019, doi: 10.3390/s19071641.

sensors

MDPI

Article

A Compact Thévenin Model for a Rectenna and Its Application to an RF Harvester with MPPT

Manel Gasulla [1,*], Edgar Ripoll-Vercellone [1,2] and Ferran Reverter [1]

[1] e-CAT Research Group, Department of Electronic Engineering, Castelldefels School of Telecommunications and Aerospace Engineering, Universitat Politècnica de Catalunya, c/ Esteve Terradas, 7, 08860 Castelldefels (Barcelona), Spain; edgar.ripoll.vercellone@upc.edu (E.R.-V.); ferran.reverter@upc.edu (F.R.)

[2] Idneo Technologies, c/ Rec de Dalt s/n., 08100 Mollet del Vallès (Barcelona), Spain

* Correspondence: manel.gasulla@upc.edu; Tel.: +34-934-137-092

Received: 28 March 2019; Accepted: 3 April 2019; Published: 6 April 2019

Abstract: This paper proposes a compact Thévenin model for a rectenna. This model is then applied to design a high-efficiency radio frequency harvester with a maximum power point tracker (MPPT). The rectenna under study consists of an L-matching network and a half-wave rectifier. The derived model is simpler and more compact than those suggested so far in the literature and includes explicit expressions of the Thévenin voltage (V_{oc}) and resistance and of the power efficiency related with the parameters of the rectenna. The rectenna was implemented and characterized from −30 to −10 dBm at 808 MHz. Experimental results agree with the proposed model, showing a linear current–voltage relationship as well as a maximum efficiency at $V_{oc}/2$, in particular 60% at −10 dBm, which is a remarkable value. An MPPT was also used at the rectenna output in order to automatically work at the maximum efficiency point, with an overall efficiency near 50% at −10 dBm. Further tests were performed using a nearby transmitting antenna for powering a sensor node with a power consumption of 4.2 µW.

Keywords: RF harvesting; rectenna; Thévenin model; maximum power point tracking; MPPT; L-matching network; sensor node

1. Introduction

Radio frequency (RF) energy harvesting has been extensively proposed to power tiny devices such as RFID tags, autonomous sensors, or Internet of Things (IoT) nodes. RF energy can be harvested either from dedicated sources, such as in the case of RFID devices [1–4], or from the RF energy already present in the ambient environment and coming from unintentional sources such as TV, FM radio, cellular, or WiFi emitters [2,5–10].

Figure 1 shows the block diagram of an RF harvester powering a sensor node. The rectenna (rectifying antenna) transforms the RF signal to a DC voltage and the maximum power point tracker (MPPT) provides the optimum load to the rectenna to transfer the maximum power to the sensor node.

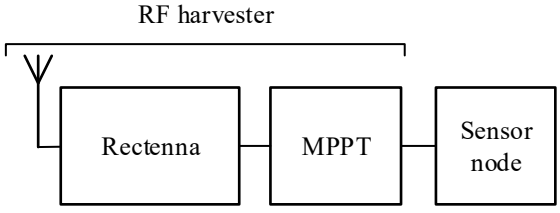

Figure 1. Block diagram of a radio frequency (RF) harvester powering a sensor node.

The rectenna is composed of an antenna, an impedance matching network, and a rectifier. As the available power at the antenna decreases so does the generated voltage. Whenever this voltage is not high enough to properly bias the diodes of the rectifier, power efficiency severely decreases. Several techniques have been proposed to increase the efficiency at low power levels. One of them consists of using an L-matching network for boosting the voltage at the rectifier input [1,3,5,10–21]. As for the MPPT, several works propose its use with rectennas using either commercial chips [6,7] or ad hoc designs [22–25].

With the aim of gaining more insight into the performance of the rectennas, different analytical models are proposed. However, the derived expressions, which in some cases seek to model the rectenna output as an equivalent Thévenin circuit, are rather complex and may require additional simulations or extensive calculations, which hide the influence of the different parameters of the rectenna on its performance [12,18,26–28]. At the other extreme, the Thévenin parameters are sometimes inferred by experimental characterization [25,29–32]. However, in these cases no relationship with the rectenna parameters is established.

Taking into account the previous limitations, this paper proposes a compact Thévenin model for the rectenna with the benefit of achieving manageable expressions of the Thévenin parameters as a function of the parameters of the rectenna so as to gain insight into its operation. In particular, the rectenna under study consists of an L-matching network and of a half-wave rectifier. The proposed model is then experimentally verified and the rectenna further tested in a high-efficency RF harvester with MPPT.

The paper, which continues and expands the work presented in [32], is organized as follows. Section 2 presents the rectenna and the derived Thévenin equivalent. Section 3 describes the MPPT and the sensor node. Section 4 presents the materials and methods and Section 5 provides the experimental results and discussions. Finally, Section 6 concludes the work. Complementarily, two appendices are included. Appendix A presents an analytical development useful for the derivation of the Thévenin equivalent and Appendix B shows simulations of the rectenna with and without the matching network.

2. Rectenna and Its Thévenin Model

Figure 2 shows the schematic circuit of the rectenna under study [33], which includes a high-pass L-matching network (composed of a capacitor C_m and an inductor L_m), a half-wave rectifier, and an output filtering capacitor (C_o). The antenna is modelled by a sinusoidal voltage source v_a of amplitude V_{ap} and frequency f_o with a series radiation resistance R_a. On the other hand, v_{in}, Z_{in}, and P_{in} are, respectively, the sinusoidal voltage, impedance, and power at the input of the rectifier, i_d is the diode current, and V_o, I_o, and P_o are, respectively, the DC voltage, current, and power at the rectenna output. An equivalent resistance R_o is defined as V_o/I_o.

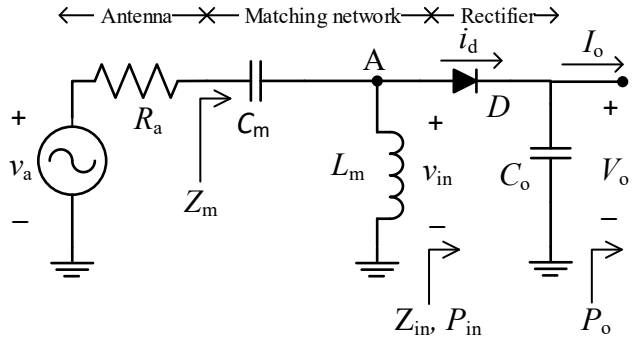

Figure 2. Schematic circuit of the rectenna under study.

The amplitude V_{ap} is given by [12] as follows:

$$V_{ap} = 2\sqrt{2R_a P_{av}}, \quad (1)$$

where P_{av} is the available power at the antenna. The matching network, at matching conditions, that is, $Z_m = R_a$ (where Z_m is defined in Figure 2), boosts the voltage at the input of the rectifier by a voltage gain, G_t, given by [33] as follows:

$$G_t = \frac{V_{inp}}{V_{ap}} = \frac{1}{2}\sqrt{(1+Q^2)}, \tag{2}$$

where V_{inp} is the voltage amplitude of v_{in} and Q is the circuit quality factor given by:

$$Q = \frac{1}{\omega_o C_m R_a}, \tag{3}$$

where $\omega_o = 2\pi f_o$. On the other hand, the value of L_m must comply:

$$L_m = \frac{1}{\omega_o^2}\frac{1}{C_p + C_m Q^2/(1+Q^2)}, \tag{4}$$

where C_p models the parasitic capacitance between node A and ground.

To ease the analysis of the proposed rectenna and also gain more insight into its performance, a compact Thévenin model is provided here. First, the left-hand equivalent circuit of Figure 3 accounts for the antenna, the matching network, and the parasitic elements (R_p-C_p) of the coil, diode, and layout of the circuit. These parasitic elements are derived in Appendix A, where R_p models the losses of the coil and diode and C_p includes the parasitic capacitance of the diode, coil, and layout.

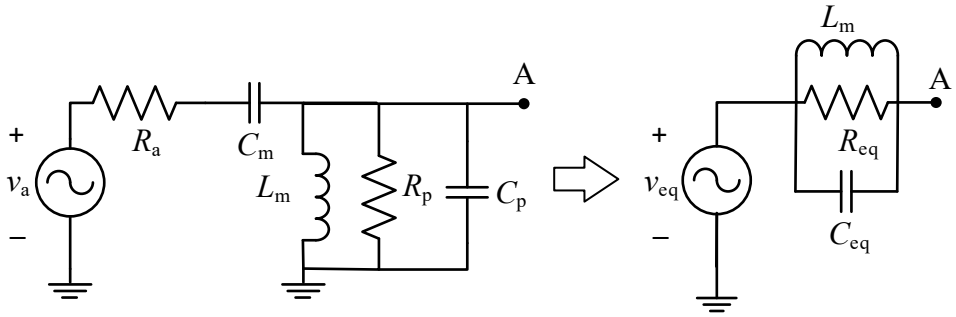

Figure 3. (**left**) Equivalent input circuit of the antenna and L-matching network considering the parasitic effects of the coil and diode and (**right**) its Thévenin equivalent circuit.

Analyzing the left-hand circuit of Figure 3 at f_o, we can achieve the Thévenin equivalent represented by the right-hand circuit of Figure 3, where:

$$\begin{aligned} v_{eq} &= 2G_t v_a \frac{R_p}{4G_t^2 R_a + R_p}, \\ R_{eq} &= \left(4G_t^2 R_a\right) \| R_p, \\ C_{eq} &= C_m \frac{Q^2}{1+Q^2} + C_p. \end{aligned} \tag{5}$$

Next, the Thévenin equivalent of Figure 3 is linked to the next stage of the rectenna, the rectifier, resulting in the left-hand circuit of Figure 4, where the diode does not include its parasitic elements since they have been already considered in the previous derivation (they are included in R_{eq} and C_{eq}). The diode is forward biased when v_{in}, assumed sinusoidal, surpasses V_o. As a result, i_d is pulsed and is composed of the fundamental frequency (f_o) as well as its harmonics and a DC component (I_o). Impedance Z_s (defined in the circuit) is zero at DC (due to the coil L_m) and is equal to R_{eq} at f_o since L_m and C_{eq} form a parallel resonant circuit presenting an infinite impedance. On the other hand, at the harmonics of f_o we have $Z_s << R_{eq}$ (due to C_{eq}) whenever Q is high enough. Therefore, only the current at f_o (i_{in}) originates a voltage drop and v_{in} will be sinusoidal, as assumed before. Thus, apart

from boosting the voltage, the matching network ideally acts as an input band-pass filter that prevents any of the DC current and harmonics to flow through the antenna resistance and dissipate power. This leads to an ideal rectenna efficiency of 100%, assuming no losses in the circuit components and in the diode [34]. Contrariwise, when no matching network is present, maximum rectenna efficiency decreases to 46%, due to the additional losses at R_a originated by the current harmonics generated by the diode pulsed current, as demonstrated in [35]. Appendix B confirms these results via simulations. Finally, the value of C_o has to be much higher than the diode junction capacitance (C_j), as explained in Appendix A, to keep V_o nearly constant, that is, with a low voltage ripple (ΔV_o). This second condition leads to:

$$C_o > \frac{I_o}{\Delta V_o f_o}. \tag{6}$$

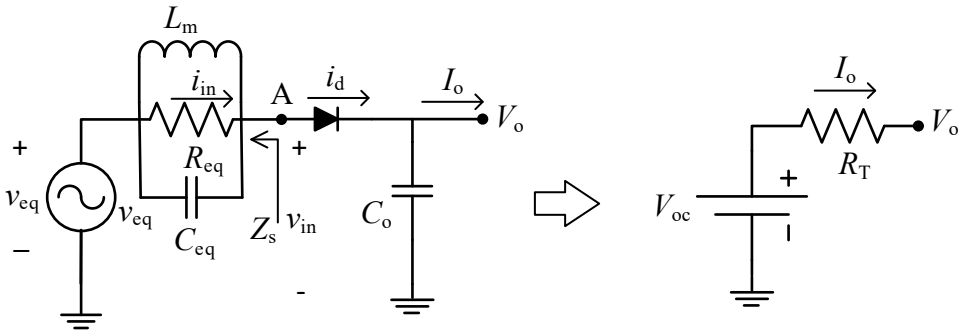

Figure 4. (**left**) Equivalent circuit of the rectenna using the right-hand circuit of Figure 3 and (**right**) its Thévenin equivalent.

The left-hand circuit of Figure 4 leads to the equivalent Thévenin circuit of the rectenna, represented by the right-hand circuit of Figure 4, by linking their output voltage–current relationship. For the left-hand circuit, we have:

$$V_o = V_{inp} - V_\gamma, \tag{7}$$

assuming a fixed forward voltage drop V_γ at the diode and:

$$V_{inp} = V_{eqp} - R_{eq} I_{inp}, \tag{8}$$

where V_{eqp} and I_{inp} are the amplitudes of v_{eq} and i_{in}, respectively. Substituting (8) into (7) provides:

$$V_o = V_{eqp} - V_\gamma - R_{eq} I_{inp}. \tag{9}$$

On the other hand, for the right-hand circuit we have:

$$V_o = V_{oc} - R_T I_o. \tag{10}$$

Then, by equating powers, we obtain:

$$P_{in} = P_o + P_d, \tag{11}$$

where

$$\begin{aligned} P_{in} &= \tfrac{V_{inp} I_{inp}}{2}, \\ P_o &= V_o I_o, \\ P_d &= V_\gamma I_o, \end{aligned} \tag{12}$$

and P_d is the average power dissipated across the diode. Thus, replacing (12) into (11) and using (7), we arrive at the following:

$$I_{inp} = 2 I_o. \tag{13}$$

Finally, using (13) in (9) and equating (9) and (10), we obtain the parameters of the Thévenin model:

$$\begin{aligned} V_{oc} &= V_{eqp} - V_{\gamma}, \\ R_T &= 2R_{eq}, \end{aligned} \tag{14}$$

where V_{eqp} can be derived from v_{eq} in (5), using V_{ap} instead of v_a, resulting in:

$$V_{eqp} = 2G_t V_{ap} \frac{R_p}{4G_t^2 R_a + R_p}. \tag{15}$$

Then, using (15) and R_{eq} of (5) in (14), we have:

$$\begin{aligned} V_{oc} &= 2G_t V_{ap} \frac{R_p}{4G_t^2 R_a + R_p} - V_{\gamma}, \\ R_T &= 2\left[(4G_t^2 R_a) \| R_p\right]. \end{aligned} \tag{16}$$

Therefore, from (16), with an increasing P_{av} and thus V_{ap}, V_{oc} increases whereas R_T holds constant. Next, from (10), we can express I_o as:

$$I_o = (V_{oc} - V_o)/R_T, \tag{17}$$

and the output power P_o over a load resistor R_o can be simply calculated as:

$$P_o = V_o I_o = \frac{V_{oc} V_o - V_o^2}{R_T}, \tag{18}$$

being the power efficiency of the rectenna as:

$$\eta_{rect} = \frac{P_o}{P_{av}} = \frac{V_{oc} V_o - V_o^2}{P_{av} R_T}. \tag{19}$$

Applying the maximum power transfer theorem, maximum power is extracted from the rectenna for $V_o = 0.5V_{oc}$, which is known as the maximum power point (MPP) voltage (V_{MPP}). From (19), the resulting efficiency is as:

$$\eta_{rect,max} = \frac{V_{oc}^2}{4P_{av} R_T}. \tag{20}$$

Thus, using (16) in (20), we arrive at:

$$\eta_{rect,max} = \frac{R_p}{4G_t^2 R_a + R_p} \left(1 - \frac{V_{\gamma}}{\sqrt{2R_a P_{av}}} \frac{4G_t^2 R_a + R_p}{4G_t R_p}\right)^2. \tag{21}$$

As can be seen from (21), $\eta_{rect,max}$ increases with increasing P_{av}. Obviously, with no losses ($R_p = \infty$ and $V_{\gamma} = 0$) $\eta_{rect,max} = 1$ is obtained. On the other hand, the dependence of $\eta_{rect,max}$ on G_t is rather more complex. In [33], an optimum value of G_t was derived arising from the trade-off between the losses introduced by the coil and that due to the voltage drop of the diode. This optimum gain leads, from (16), to a particular value of R_T.

3. MPPT and Sensor Node

In general, a sensor node directly connected to the output of the rectenna will not provide an equivalent resistance $R_o = R_T$, at which the rectenna output operates at the MPP. Thus, an impedance matching stage (in addition to the matching network of the rectenna) is needed between the rectenna output and the sensor node, which can be implemented by a DC/DC converter. An MPPT, which consists of a DC/DC converter plus a tracking algorithm, can be used for automatically searching and

settling that optimum value of R_o, which also corresponds to $V_o = V_{MPP}$. Thus, the overall power efficiency of the RF harvester will be given by the following:

$$\eta_T = \eta_{rect,max}\eta_{MPPT}, \tag{22}$$

where η_{MPPT} is the efficiency of the MPPT and $\eta_{rect} = \eta_{rect,max}$ since the MPPT biases the rectenna at the MPP.

In this work, the fractional open circuit voltage (FOCV) MPPT technique is used, since it leads to simple and power efficient implementations. In this technique, the open circuit voltage (V_{oc}) of the energy transducer (a rectenna here) is first measured and a fraction k of V_{oc} is used to operate at V_{MPP} and thus achieve $\eta_{rect,max}$. Taking into account the analysis in Section 2, a proper choice here is $k = 0.5$ ($V_o = V_{MPP} = 0.5V_{oc}$).

Figure 5 presents the block diagram for the implementation of the FOCV MPPT technique, where C_L, C_{REF}, and C_{load} are capacitors, R_{oc1} and R_{oc2} are resistors, S_1 and S_2 are switches, V_{load} is the output voltage used to power the sensor node, and P_{load} is the power transferred to the sensor node. The operation is the following. First, S_1 closes and S_2 opens (sampling period). For high values of R_{oc1} and R_{oc2}, the output of the rectenna can be considered as open and thus $V_o = V_{oc}$. The voltage divider formed by R_{oc1} and R_{oc2} fixes $V_{MPP} = kV_{oc}$, being $k = 0.5$ here (i.e., $R_{oc1} = R_{oc2}$). The input capacitor (C_L) momentarily stores the incoming harvested energy. Secondly, S_1 opens and S_2 closes (regulation period). Thus, V_{MPP} holds constant thanks to C_{REF}, and the DC/DC converter settles V_o around V_{MPP} and transfers the harvested energy by the rectenna to the sensor node.

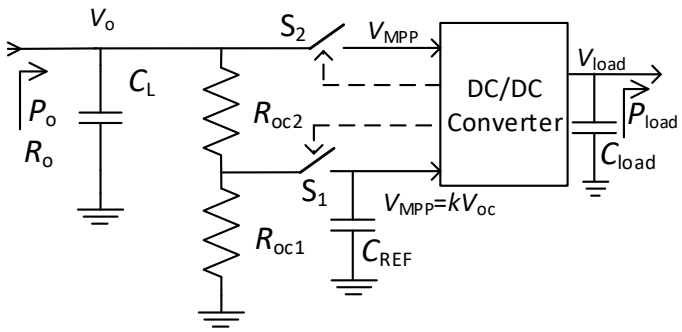

Figure 5. Block diagram for the implementation of the fractional open circuit voltage maximum power point tracking technique.

In order to periodically update V_{oc} (i.e., a change in P_{av} changes V_{oc}), the described sequence is periodically repeated, with the sampling period being much shorter than the regulation period. In this way, V_o will settle most of time at V_{MPP}. To increase the efficiency at light loads, the DC/DC converter uses special control techniques such as pulse frequency modulation (PFM) or burst-mode [36].

Taking into account (22), P_{load} can be related with P_{av} as follows:

$$P_{load} = \eta_T P_{av}. \tag{23}$$

The value of P_{load} and thus of P_{av} must be enough, in average, to power the sensor node, which usually includes a rechargeable storage unit. This unit accounts for the variability of P_{av}, gathering or providing energy whenever P_{av} is higher or lower than required. Storage units can be supercapacitors, batteries, or a combination of both [37]. On the other hand, the required value of P_{load} and thus of P_{av} can be reduced by operating the sensor node in sleep mode most of the time and minimizing its active time.

4. Materials and Methods

The rectenna shown in Figure 2 was implemented on a printed circuit board with Rogers substrate and with the following components: C_m = 0.5 pF (AVX, Fountain Inn, SC, USA), L_m = 27 nH (0603CS model, Coilcraft, Cary, IL, USA), C_o = 1 nF, and a Schottky HSMS-2850 diode (Avago Technologies, San Jose, CA, USA) [33]. The selected value of C_o comfortably accomplished, in order to theoretically have a small ripple (below 1 mV) with the values of I_o shown later in Section 5, as well as the condition stated in Appendix A ($C_o >> C_j$). The circuit of Figure 2 was used for the rectenna characterization, where an RF generator (Agilent E4433B, Santa Clara, CA, USA) was connected at the input instead of the antenna and a Source Measure Unit (SMU, Agilent B2901A, Santa Clara, CA, USA) configured as a voltage sink (quadrant IV) at the output. The generator was set at a tuned optimal frequency of 808 MHz and at different values of P_{av} (−30 dBm, −20 dBm, and −10 dBm). For each value of P_{av}, the SMU was set at different values of V_o while measuring P_o. Then, η_{rect} was obtained as P_o/P_{av}.

As for the FOCV MPPT, a BQ25504 chip (Texas Instruments, Dallas, TX, USA) was used, and in particular an evaluation board provided by the manufacturer. The chip contains a boost converter with PFM control and the board includes, in reference to Figure 5, C_L = 4.8 µF (combination of two ceramic capacitors of 4.7 µF and 100 nF placed in parallel), C_{REF} = 10 nF, and C_{load} = 104.8 µF (combination of three ceramic capacitors of 100 µF, 4.7 µF, and 100 nF placed in parallel). The default values of R_{oc1} and R_{oc2} were modified to 10 MΩ in order to fix k = 0.5 (the default value is set to 0.78). The sampling and regulation periods are prefixed by the chip to 256 ms and 16 s, respectively. Then, the efficiency of the whole RF harvester (rectenna plus MPPT) was characterized by using the RF generator at the input of the rectenna and the SMU set at 3 V at the output of the MPPT (V_{load}). The RF generator was set at different values of P_{av}, from −20 dBm to −5 dBm in steps of 1 dBm, and for each value the SMU measured the output power P_{load}. Then, from (23), η_T was estimated.

For demonstration purposes, the RF harvester including the MPPT was also employed to power a sensor node intended to upgrade a mechanical gas meter to a smart device [38]. For these tests, the node was programmed to stay in a standby mode, consuming 1.4 µA. The input power (P_{av}) was set to keep the voltage supply of the sensor node (V_{load}) at 3 V, thus P_{load} = 4.2 µW. As for the RF harvester input, two configurations were used: (1) an RF generator and (2) a receiving monopole antenna. In the second case, another identical monopole antenna was connected to a nearby RF generator, jointly acting as a wireless energy transmitter. The antennas showed an insertion loss higher than 10 dB at 808 MHz. Figure 6 shows pictures of both setups.

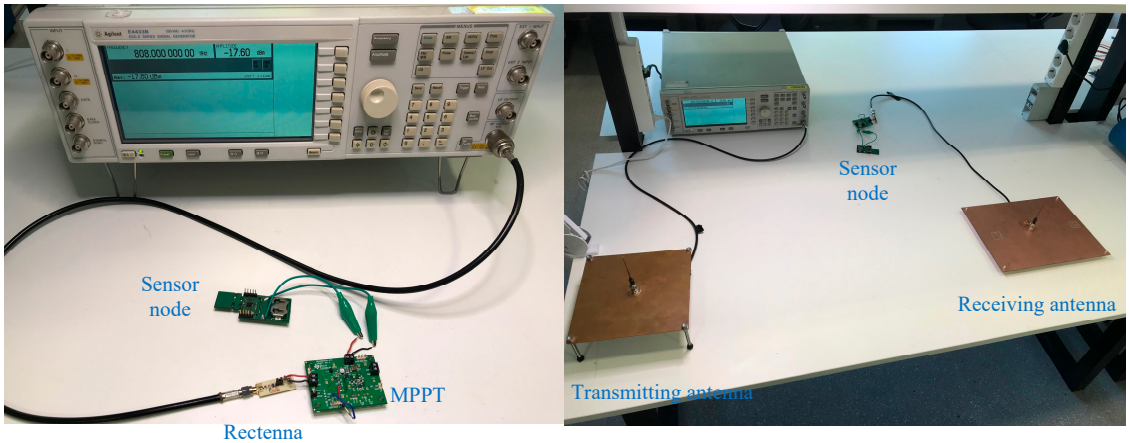

Figure 6. Picture of the setups for powering the sensor node using, for the RF harvester input, (**left**) the RF generator or (**right**) a monopole antenna.

5. Experimental Results and Discussion

As for the proposed rectenna, Figure 7 shows the measured values (in dots) of I_o (blue circles) and η_{rect} (red squares) as a function of V_o at different values of P_{av}. A least-squares fitting of (17) to the experimental data of I_o was performed (blue continuous line) to obtain the Thévenin parameters (V_{oc} and R_T) at each power level, which are shown in Table 1. Calculated values of V_{ap}, from (1), and of V_{eqp}, from (15), are also included in Table 1. This fitting differs from that performed in [32], where the efficiency data (η_{rect}) were used instead, which leads to slight differences in the Thévenin parameters. The new fitting procedure was considered more convenient as both V_{oc} and R_T can be more easily inferred from the fitting curve. As can be seen, the fitting curves match well the experimental data, and more at the highest power of −10 dBm, which confirms that the rectenna can be well approximated by a Thévenin equivalent circuit. Then, V_{oc} and R_T were used to obtain η_{rect} using (19), and the resulting curves are also represented in Figure 7 (red continuous line). The match with the experimental data is good, and again better at −10 dBm.

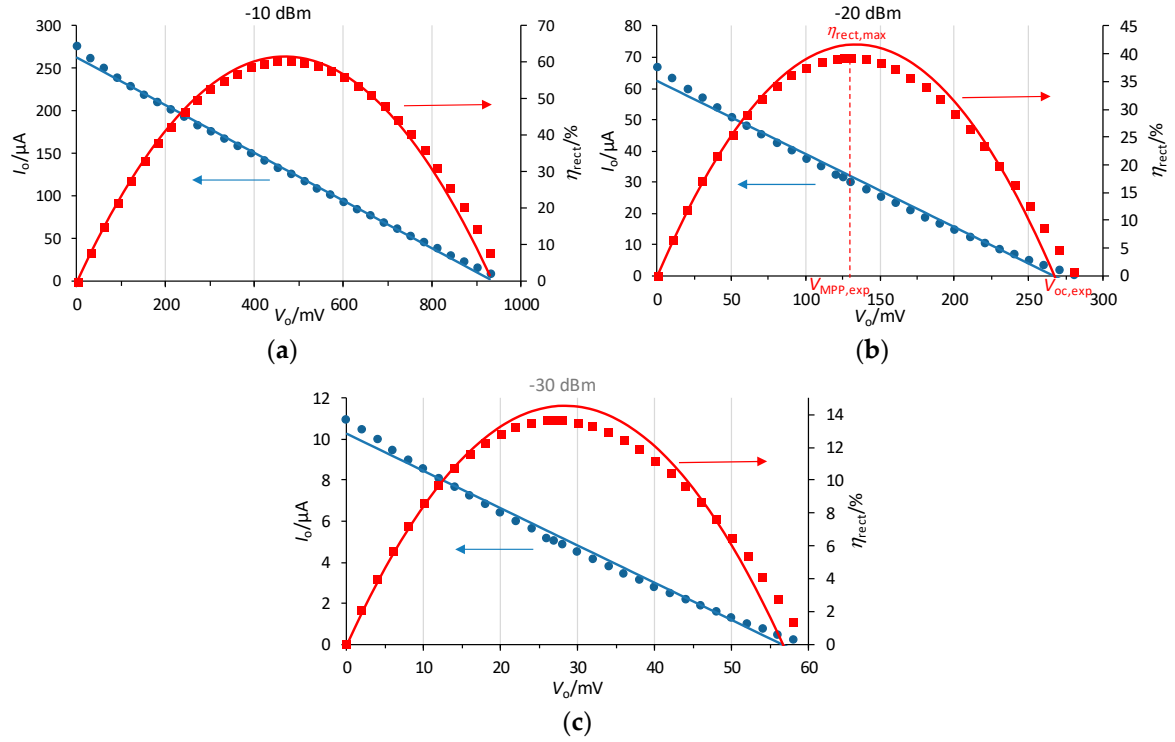

Figure 7. Measured values (dots) and least-squares fittings (continuous lines) of I_o and η_{rect} versus V_o for the rectenna at P_{av} equal to (**a**) −10 dBm, (**b**) −20 dBm, and (**c**) −30 dBm.

Table 1. Inferred values of V_{oc} and R_T and calculated values of V_{eqp} at different values of P_{av}.

P_{av} (dBm)	V_{ap} (mV)	V_{oc} (mV)	R_T (kΩ)	V_{eqp} (mV)
−10	200 mV	937	3.56	1183
−20	63.2 mV	268	4.29	374
−30	20.0 mV	56.6	5.51	118.3

With C_m = 0.5 pF, R_a = 50 Ω, and f_o = 808 MHz, Q = 7.88 results from (3), and G_t = 3.97 from (2). Then, from (16) and assuming the value of R_p = 9.21 kΩ derived in Appendix A, R_T = 4.7 kΩ is obtained, which is within the range of values found in Table 1. The inferred values of R_T moderately change with P_{av} due to the relative low value of Q, which limits the accuracy of the rectenna model proposed in Section 2. However, a higher value of Q, which could be obtained using a lower value of C_m and appropriately readjusting L_m, does not lead to the optimum gain G_t [33], thus decreasing

the power efficiency. On the other hand, V_{oc} in Table 1 increases with increasing P_{av} and thus V_{ap}, which agrees with (16). The values of V_{oc} can be estimated in advance, when necessary, from (16) by calculating V_{eqp} from (15), shown in Table 1, and inferring a value of V_γ from the manufacturer data or from simulations.

From the measured data of η_{rect} (red squares in Figure 7), Table 2 shows the achieved $\eta_{rect,max}$ and its corresponding voltage ($V_{MPP,exp}$), as well as the experimental open circuit voltage ($V_{oc,exp}$) of the rectenna. In Figure 7, $\eta_{rect,max}$, $V_{MPP,exp}$, and $V_{oc,exp}$ are also marked for P_{av} = −20 dBm. As can be seen, $\eta_{rect,max}$ increases with increasing P_{av}, ranging from 13.6% at −30 dBm to 60.3% at −10 dBm, which agrees with (21). The values of $\eta_{rect,max}$ can be estimated in advance, when necessary, from (21) and inferring a value of V_γ from the manufacturer data or from simulations. One particular case is the upper limit, which would be achieved for $P_{av}\to\infty$ (or $V_\gamma\to 0$), in our case 74%. The resulting efficiencies ($\eta_{rect,max}$) are among the highest published in the literature for similar designs [33]. On the other hand, V_{oc} from Table 1 nearly matches $V_{oc,exp}$. Finally, $V_{MPP,exp}$ equates or nearly matches 0.5 $V_{oc,exp}$, the regulated voltage at the input of the MPPT. Thus, the proposed and implemented MPPT will be able to extract the maximum power (or nearly) from the rectenna.

Table 2. Experimental values of $\eta_{rect,max}$, $V_{MPP,exp}$, and $V_{oc,exp}$ at different values of P_{av}.

P_{av} (dBm)	$\eta_{rect,max}$ (%)	$V_{MPP,exp}$ (mV)	$V_{oc,exp}$ (mV)
−10	60.3	480	960
−20	39.3	130	280
−30	13.6	27	60

As for the whole RF harvester (rectenna plus the MPPT), Figure 8 shows the experimental values of η_T versus P_{av}. At −20 dBm, $\eta_{rect,max}$ = 39.3% (Table 2) but η_T = 6.5%, resulting, from (22), in η_{MPPT} = 16.5%. This low value of η_{MPPT} is due to both a low input voltage value (140 mV = 0.5 $V_{oc,exp}$) and a low value of P_o (3.9 μW = $\eta_{rect,max}P_{av}$). Contrariwise, at −10 dBm, $\eta_{rect,max}$ = 60.3% and η_T = 48.6%, resulting in η_{MPPT} = 80.6%, which agrees with the data from the BQ25504 chip's datasheet. At higher values of P_{av} (−5 dBm), η_T reached a value of 55.6%. Compared to [6], where a similar chip for the MPPT was used, η_T is quite higher.

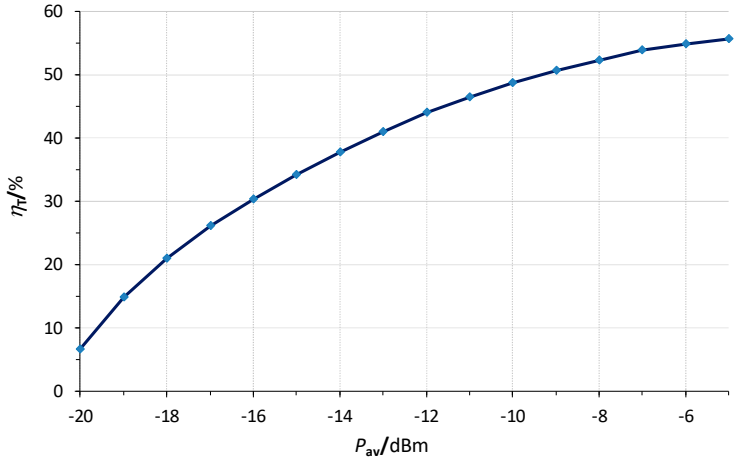

Figure 8. Overall efficiency (η_T) of the RF harvester.

When powering the sensor node, the required value of P_{av} was −17.6 dBm. This value fits well with (23), considering the corresponding efficiency in Figure 8 (≈24%). This performance was also tested with the antennas at a distance of 0.5 and 1 m. The power output of the remote RF generator was tuned at appropriate values so as to operate the node, resulting in 8.0 and 13.2 dBm, respectively. These values accounted for the respective link budgets.

6. Conclusions

This work proposed a compact Thévenin model for a rectenna and its application for designing a high-efficiency RF harvester. The rectenna under study consists of an L-matching network and a half-wave rectifier. Explicit expressions for the Thévenin voltage and resistance were derived that offer insight into the operation of the rectenna. An expression was also provided for the power efficiency. The rectenna was implemented and characterized from −30 to −10 dBm at 808 MHz and the results mainly agreed with the derived model, with differences arising from the limited Q factor of the matching network. High efficiencies were obtained, in particular 60% at −10 dBm. Then, an ensuing MPPT was also added, where the behavior of the rectenna as an equivalent Thévenin circuit allowed the use of a simple FOCV technique. The whole RF harvester (rectenna plus MPPT) showed an overall efficiency near 50% at −10 dBm. Further tests were performed with a nearby transmitting antenna for powering a sensor node with a power consumption of 4.2 μW.

Author Contributions: Conceptualization, M.G.; Formal analysis, M.G. and F.R.; Funding acquisition, M.G. and F.R.; Investigation, M.G. and E.R.-V.; Methodology, M.G.; Project administration, M.G. and F.R.; Writing–original draft, M.G.; Writing–review and editing, M.G. and F.R.

Funding: This work was supported by the Secretariat of University and Research of the Ministry of Business and Knowledge of the Government of Catalonia, by the Spanish State Research Agency (AEI) and by the European Regional Development Fund under Project TEC2016-76991-P.

Acknowledgments: The authors wish to thank Josep Jordana, Francesc-Josep Robert, and Jordi Berenguer for their initial support, and the Castelldefels School of Telecommunications and Aerospace Engineering, Barcelona, Spain, for the RF instrumentation needed to perform the experiments.

Conflicts of Interest: The authors declare no conflict of interest.

Appendix A. Parallel Circuit Model of the Inductor and Diode

The use of a matching network leads to sinusoidal voltage and current waveforms at f_o, as mentioned in Section 2. Here, the equivalent circuit model at f_o is derived from the manufacturer models of the diode (https://docs.broadcom.com/docs/AV02-1377EN) and inductor (https://www.coilcraft.com/pdfs/spice_0603cs.pdf) used for the implemented rectenna and reported in Section 4. This model will be used in the left-hand circuit of Figure 3.

First, the left-hand circuit in Figure A1 shows the equivalent linear circuit model of the diode, connected between node A and the V_o node at Figure 2, together with the output capacitor C_o, where R_s is the parasitic series resistance, C_j is the parasitic junction capacitance, and R_j is the junction resistance. R_j depends inversely on the bias current and makes only sense for modelling small current variations around a bias current. In our case, the diode current is pulsed and thus the inclusion of R_j is not appropriate. Instead, a constant voltage drop will be assumed in Section 2 for the analysis of the circuit of Figure 4.

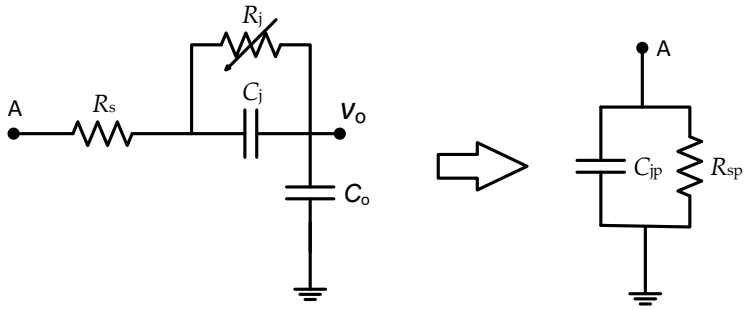

Figure A1. Equivalent linear circuit model of the HSMS-2850 diode together with (**left**) the output capacitor C_o and (**right**) its parallel equivalent circuit.

Using the series-to-parallel equivalent circuit transformation for the left-hand circuit of Figure A1 without R_j and considering $C_o >> C_j$, the right-hand circuit results, where:

$$R_{sp} = R_s \frac{R_s^2 C_j^2 \omega_o^2 + 1}{R_s^2 C_j^2 \omega_o^2}, \tag{A1}$$

$$C_{jp} = \frac{C_j}{R_s^2 C_j^2 \omega_o^2 + 1}. \tag{A2}$$

From the diode datasheet, R_s = 25 Ω and C_{jo} = 0.18 pF (C_{jo} is C_j at zero bias and will be the assumed value for C_j hereafter). With f_o = 808 MHz, R_{sp} = 47.9 kΩ results from (A1) and $C_{jp} \approx C_j$ = 180 fF results from (A2).

As for the inductor, connected between node A and ground at Figure 2, the left-hand circuit of Figure A2 shows the manufacturer model, where $R_v = k\sqrt{f_o}$. Using the series-to-parallel circuit transformation, the circuit in the middle is obtained, where:

$$L_{mp} = L_m \left[1 + \left(\frac{R_v}{\omega_o L_m}\right)^2\right]. \tag{A3}$$

$$R_{vp} = R_v \left[1 + \left(\frac{\omega_o L_m}{R_v}\right)^2\right], \tag{A4}$$

$$R_{1p} = R_1 \frac{R_1^2 C_1^2 \omega_o^2 + 1}{R_1^2 C_1^2 \omega_o^2}, \tag{A5}$$

$$C_{1p} = \frac{C_1}{R_1^2 C_1^2 \omega_o^2 + 1}. \tag{A6}$$

From the coil datasheet, R_1 = 17 Ω, R_2 = 30 mΩ, C_1 = 49 fF, L_m = 27 nH, and $k = 5.75 \times 10^{-5}$. At 808 MHz, R_v = 1.63 Ω and from (A3) to (A6), $L_{mp} \approx L_m$ = 27 nH, R_{vp} = 11.5 kΩ, R_{1p} = 950 kΩ, and $C_{1p} \approx C_1$ = 49 fF. Then, neglecting R_2, since it is very small, the right-hand circuit of Figure A2 is obtained, where $R_{Lp} = R_{vp} \| R_{1p}$ = 11.4 kΩ.

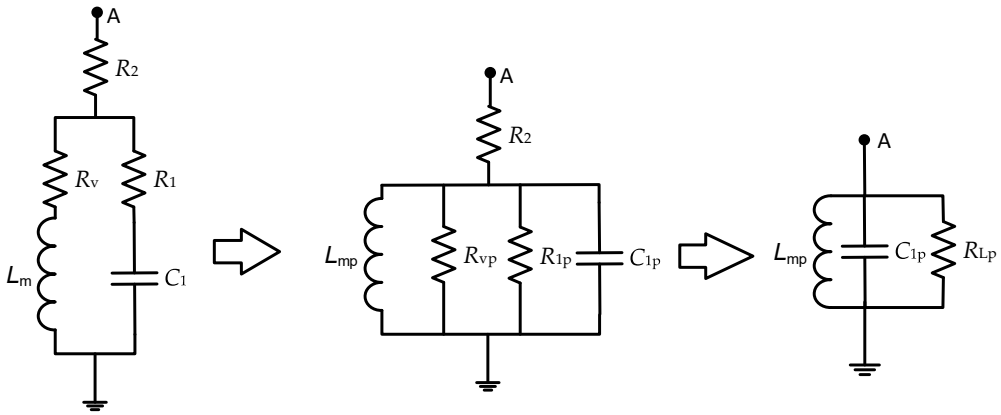

Figure A2. (**left**) Manufacturer model of the inductor and (**middle** and **right**) equivalent circuits.

Joining the right-hand circuits in Figures A1 and A2, and considering the parasitic capacitance from node A to ground arising from the layout (C_{lay}), the circuit in Figure A3 is obtained, where:

$$R_p = R_{sp} \| R_{Lp} = 9.21 \text{ k}\Omega, \tag{A7}$$

$$C_p = C_{jp} + C_{1p} + C_{lay}. \tag{A8}$$

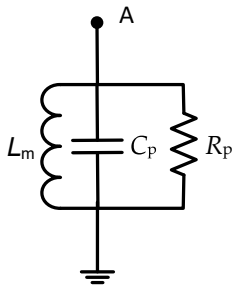

Figure A3. Parallel equivalent circuit of the inductor.

This equivalent circuit is used in the left-hand circuit of Figure 3.

Appendix B. Simulations of the Rectenna Efficiency with and without an L-Matching Network

In order to highlight the benefits of using a matching network, we report simulation results of the rectenna efficiency with and without an L-matching network. For the simulations, the ADS software (Version 2017, Keysight, Santa Rosa, CA, USA) was used. The simulated circuit with the matching network was that of Figure 2 with a resistor R_o connected at its output, in parallel with C_o. Ideal components were used for the matching network with the values reported in Section 4. The diode was modelled without parasitic elements (null series resistance and junction capacitance) but with a saturation current of 3 μA (that corresponding to the HSMS-2850 diode used for the implemented rectenna). For the RF source, a frequency of 808 MHz (that used for the experiments) was used with P_{av} ranging from −10 to 50 dBm in steps of 20 dB. For the circuit without the matching network, the right terminal of R_a was directly connected to the diode anode (node A). For both circuits, a harmonic balance analysis was performed with P_{av} and R_o as sweeping parameters.

Figure A4 shows the simulation results of the rectenna efficiency ($\eta_{rect} = P_o/P_{av}$) plotted against R_o for different values of P_{av}. The left graph shows the results for the circuit with the L-matching network. As can be seen, η_{rect} steeply increases for increasing values of P_{av}, achieving around 99% at P_{av} = 50 dBm. At −10 dBm, efficiency is higher than the corresponding results of Figure 7 because ideal components were used for the simulation. On the other hand, the right graph shows the results for the circuit without the L-matching network. As can be seen, η_{rect} steeply increases for increasing values of P_{av} but now reaches a maximum value around 46%, as predicted theoretically in [35], due to the additional losses at R_a originated by the current harmonics generated by the diode pulsed current. At −10 dBm, efficiency is lower than 4%. Therefore, the use of the matching network allows a notable increase in the rectenna efficiency, because it provides voltage gain and prevents any of the DC current and harmonics to flow through the antenna resistance.

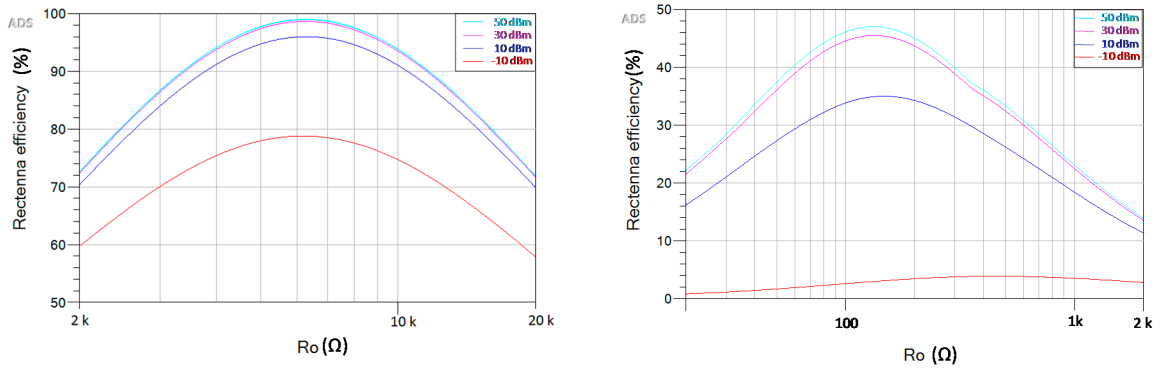

Figure A4. Rectenna efficiency for the circuit (**left**) with and (**right**) without the matching network.

References

1. Shameli, A.; Safarian, A.; Rofougaran, A.; Rofougaran, M.; De Flaviis, F. Power Harvester Design for Passive UHF RFID Tag Using a Voltage Boosting Technique. *IEEE Trans. Microw. Theory Tech.* **2007**, *55*, 1089–1097. [CrossRef]
2. Sample, A.; Smith, J.R. Experimental results with two wireless power transfer systems. In Proceedings of the 2009 IEEE Radio and Wireless Symposium, San Diego, CA, USA, 18–22 January 2009; pp. 16–18.
3. Attaran, A.; Rashidzadeh, R.; Muscedere, R. Chipless RFID tag using RF MEMS switch. *Electron. Lett.* **2014**, *50*, 1720–1722. [CrossRef]
4. Álvarez López, Y.; Franssen, J.; Álvarez Narciandi, G.; Pagnozzi, J.; González-Pinto Arrillaga, I.; Las-Heras Andrés, F. RFID Technology for Management and Tracking: E-Health Applications. *Sensors* **2018**, *18*, 2663. [CrossRef] [PubMed]
5. Singh, G.; Ponnaganti, R.; Prabhakar, T.V.; Vinoy, K.J. A tuned rectifier for RF energy harvesting from ambient radiations. *AEU-Int. J. Electron. Commun.* **2013**, *67*, 564–569. [CrossRef]
6. Talla, V.; Kellogg, B.; Ransford, B.; Naderiparizi, S.; Gollakota, S.; Smith, J.R. Powering the Next Billion Devices with Wi-Fi. In Proceedings of the 11th ACM Conference on Emerging Networking Experiments and Technologies, Heidelberg, Germany, 1–4 December 2015.
7. Piñuela, M.; Mitcheson, P.D.; Lucyszyn, S. Ambient RF energy harvesting in urban and semi-urban environments. *IEEE Trans. Microw. Theory Tech.* **2013**, *61*, 2715–2726. [CrossRef]
8. Di Marco, P.; Stornelli, V.; Ferri, G.; Pantoli, L.; Leoni, A. Dual band harvester architecture for autonomous remote sensors. *Sens. Actuators A Phys.* **2016**, *247*, 598–603. [CrossRef]
9. Shaker, G.; Chen, R.; Milligan, B.; Qu, T. Ambient electromagnetic energy harvesting system for on-body sensors. *Electron. Lett.* **2016**, *52*, 1834–1836. [CrossRef]
10. Stoopman, M.; Keyrouz, S.; Visser, H.J.; Philips, K.; Serdijn, W.A. Co-design of a CMOS rectifier and small loop antenna for highly sensitive RF energy harvesters. *IEEE J. Solid-State Circuits* **2014**, *49*, 622–634. [CrossRef]
11. Soltani, N.; Yuan, F. A High-Gain Power-Matching Technique for Efficient Radio-Frequency Power Harvest of Passive Wireless Microsystems. *IEEE Trans. Circuits Syst. I Regul. Pap.* **2010**, *57*, 2685–2695. [CrossRef]
12. Curty, J.-P.; Joehl, N.; Krummenacher, F.; Dehollain, C.; Declercq, M.J. A model for u-power rectifier analysis and design. *IEEE Trans. Circuits Syst. I Regul. Pap.* **2005**, *52*, 2771–2779. [CrossRef]
13. Jordana, J.; Reverter, F.; Gasulla, M. Power Efficiency Maximization of an RF Energy Harvester by Fine-tuning an L-matching Network and the Load. *Procedia Eng.* **2015**, *120*, 655–658. [CrossRef]
14. Abouzied, M.A.; Ravichandran, K.; Sanchez-Sinencio, E. A Fully Integrated Reconfigurable Self-Startup RF Energy-Harvesting System With Storage Capability. *IEEE J. Solid-State Circuits* **2017**, *52*, 704–719. [CrossRef]
15. Nimo, A.; Grgić, D.; Reindl, L.M. Optimization of Passive Low Power Wireless Electromagnetic Energy Harvesters. *Sensors* **2012**, *12*, 13636–13663. [CrossRef]
16. Chaour, I.; Fakhfakh, A.; Kanoun, O. Enhanced Passive RF-DC Converter Circuit Efficiency for Low RF Energy Harvesting. *Sensors* **2017**, *17*, 546. [CrossRef] [PubMed]
17. Scorcioni, S.; Larcher, L.; Bertacchini, A. Optimized CMOS RF-DC converters for remote wireless powering of RFID applications. In Proceedings of the 2012 IEEE International Conference on RFID (RFID), Orlando, FL, USA, 3–5 April 2012; pp. 47–53.
18. De Carli, L.G.; Juppa, Y.; Cardoso, A.J.; Galup-Montoro, C.; Schneider, M.C. Maximizing the Power Conversion Efficiency of Ultra-Low-Voltage CMOS Multi-Stage Rectifiers. *IEEE Trans. Circuits Syst. I Regul. Pap.* **2015**, *62*, 967–975. [CrossRef]
19. Soyata, T.; Copeland, L.; Heinzelman, W. RF Energy Harvesting for Embedded Systems: A Survey of Tradeoffs and Methodology. *IEEE Circuits Syst. Mag.* **2016**, *16*, 22–57. [CrossRef]
20. Agrawal, S.; Pandey, S.K.; Singh, J.; Parihar, M.S. Realization of efficient RF energy harvesting circuits employing different matching technique. In Proceedings of the Fifteenth International Symposium on Quality Electronic Design, Santa Clara, CA, USA, 3–5 March 2014; pp. 754–761.
21. Wilas, J.; Jirasereeamornkul, K.; Kumhom, P. Power harvester design for semi-passive UHF RFID Tag using a tunable impedance transformation. In Proceedings of the 2009 9th International Symposium on Communications and Information Technology, Icheon, Korea, 28–30 September 2009; pp. 1441–1445.

22. Paing, T.; Shin, J.; Zane, R.; Popovic, Z. Resistor Emulation Approach to Low-Power RF Energy Harvesting. *IEEE Trans. Power Electron.* **2008**, *23*, 1494–1501. [CrossRef]
23. Dolgov, A.; Zane, R.; Popovic, Z. Power Management System for Online Low Power RF Energy Harvesting Optimization. *IEEE Trans. Circuits Syst. I Regul. Pap.* **2010**, *57*, 1802–1811. [CrossRef]
24. Saini, G.; Sarkar, S.; Arrawatia, M.; Baghini, M.S. Efficient power management circuit for RF energy harvesting with 74.27% efficiency at 623 nW available power. In Proceedings of the 2016 14th IEEE International New Circuits and Systems Conference (NEWCAS), Vancouver, BC, Canada, 26–29 June 2016; pp. 1–4.
25. Pizzotti, M.; Perilli, L.; del Prete, M.; Fabbri, D.; Canegallo, R.; Dini, M.; Masotti, D.; Costanzo, A.; Franchi Scarselli, E.; Romani, A. A Long-Distance RF-Powered Sensor Node with Adaptive Power Management for IoT Applications. *Sensors* **2017**, *17*, 1732. [CrossRef] [PubMed]
26. Barnett, R.E.; Liu, J.; Lazar, S. A RF to DC Voltage Conversion Model for Multi-Stage Rectifiers in UHF RFID Transponders. *IEEE J. Solid-State Circuits* **2009**, *44*, 354–370. [CrossRef]
27. Razavi Haeri, A.A.; Karkani, M.G.; Sharifkhani, M.; Kamarei, M.; Fotowat-Ahmady, A. Analysis and design of power harvesting circuits for ultra-low power applications. *IEEE Trans. Circuits Syst. I Regul. Pap.* **2017**, *64*, 471–479. [CrossRef]
28. Ou, J.H.; Zheng, S.Y.; Andrenko, A.S.; Li, Y.; Tan, H.Z. Novel Time-Domain Schottky Diode Modeling for Microwave Rectifier Designs. *IEEE Trans. Circuits Syst. I Regul. Pap.* **2018**, *65*, 1234–1244. [CrossRef]
29. Marian, V.; Adami, S.E.; Vollaire, C.; Allard, B.; Verdier, J. Wireless Energy Transfer Using Zero Bias Schottky Diodes Rectenna Structures. *Adv. Mater. Res.* **2011**, *324*, 449–452. [CrossRef]
30. Saini, G.; Arrawatia, M.; Sarkar, S.; Baghini, M.S. A battery-less power management circuit for RF energy harvesting with input voltage regulation and synchronous rectification. In Proceedings of the 2015 IEEE 58th International Midwest Symposium on Circuits and Systems (MWSCAS), Fort Collins, CO, USA, 2–5 August 2015; pp. 1–4.
31. Marian, V.; Allard, B.; Vollaire, C.; Verdier, J. Strategy for Microwave Energy Harvesting From Ambient Field or a Feeding Source. *IEEE Trans. Power Electron.* **2012**, *27*, 4481–4491. [CrossRef]
32. Gasulla, M.; Robert, F.J.; Jordana, J.; Ripoll-Vercellone, E.; Berenguer, J.; Reverter, F. A High-Efficiency RF Harvester with Maximum Power Point Tracking. *Proceedings* **2018**, *2*, 1049. [CrossRef]
33. Gasulla, M.; Jordana, J.; Robert, F.-J.; Berenguer, J. Analysis of the Optimum Gain of a High-Pass L-Matching Network for Rectennas. *Sensors* **2017**, *17*, 1712. [CrossRef] [PubMed]
34. Gutmann, R.J.; Borrego, J.M. Power Combining in an Array of Microwave Power Rectifiers. *IEEE Trans. Microw. Theory Tech.* **1979**, *27*, 958–968. [CrossRef]
35. Gutmann, R.J.; Borrego, J.M. *Solar Power Satellite Rectenna Design Study: Directional Receiving Elements and Parallel-Series Combining Analysis*; NASA Final Rep. NAS9-15453, Chapter 3; Rensselaer Polytechnic Inst.: Troy, NY, USA, 1978.
36. Reverter, F.; Gasulla, M. Optimal Inductor Current in Boost DC/DC Converters Regulating the Input Voltage Applied to Low-Power Photovoltaic Modules. *IEEE Trans. Power Electron.* **2017**, *32*, 6188–6196. [CrossRef]
37. Penella, M.T.; Gasulla, M. Runtime Extension of Low-Power Wireless Sensor Nodes Using Hybrid-Storage Units. *IEEE Trans. Instrum. Meas.* **2010**, *59*, 857–865. [CrossRef]
38. Ripoll-Vercellone, E.; Ferrandiz, V.; Gasulla, M. An Add-On Electronic Device to Upgrade Mechanical Gas Meters into Electronic Ones. *Proceedings* **2018**, *2*, 1094. [CrossRef]

5

Analysis of the results

The scope of the thesis is the energy challenges that developers experience while designing an IoT device. It does not exist a one-size-fits-all approach to solve these problems, that is why the author worked on different solutions for those challenges. The solutions depended on the form factor, the application, the environment where the node will be installed, the available energy to power the node, etc.

The common subject covered by this thesis was established in the introduction chapter and it was developed with a specific focus in chapters 2 to 4. This chapter explains in further depth the common thread of the entire study effort, i.e., the argument of the thesis, to demonstrate how the articles tackled the challenges. This chapter will also go over the overall research outcomes and assessments.

5.1 Energy challenge 1: Low-power sensing system

The objective related to the energy challenge 1 sought to determine a feasible sensing system alternative for smart gas meters. In addition, it sought to provide an alternative to the long-standing fraud- and error-prone gas meter data collection process. Three versions of an add-on node were developed to completely fulfill this objective, and these are briefly detailed here:

1) Version 1 consisted of a small-size and low-cost add-on node for gas meters. Publication I [198] covered the first version's design, implementation, and study of its limitations.
2) Version 2 fixed the limitations of the prior version, which included a short operating life and communication range.
3) Version 3 was documented in Publication II [199]. It improved the previous versions' sensing system such that it could continue to record the gas consumption while an external magnetic tampering is taking place.

The following part of this section moves on to describe in greater detail the analysis of the findings of each version. Besides it elaborates how the versions achieve the objective set for this challenge. Before proceeding, it is necessary to recall the issues for deploying a Smart Grid:

1) the rollout of this new technology will entail substantial costs, technical challenges, and risks;
2) nodes must be immune to tampering fraud, or at least detect them; and
3) smart gas meters must still comply with the three constraints for IoT nodes.

As described above, the design and implementation of a first version of a small-size and low-cost add-on node for gas meters (Figure 7) was proposed in Publication I [198]. Two relevant approaches were proposed in the literature to design a sensing system to upgrade a mechanical gas meter to a smart one: imaging processing and using magnetic sensors. The magnetic sensors approach was chosen given the benefits described in Section 1.4.3.4: low-power consumption, small-size, low-cost, and allows a

simple installation. The node measured the gas consumption of a metric totalizer with a reed switch. This allowed zero-power consumption of the sensing system while it is not active.

Regarding the collection of the data, the communication technology used was NFC, which has various benefits and limitations when compared to other communication technologies. For instance, a cellular-based connectivity would provide direct communication with the cloud, eliminating the need for an operator to visit each gas meter to gather the reading. Nevertheless, the transceivers required for implementing this communication are too power consuming, as mentioned in Section 1.4.2.3. A thorough study has to be done to assess cellular communication viability. An ISM-RF-based approach might potentially serve this purpose, but it would require the gas providers installing a GW in each building and connect it to the power grid. The GW would gather the data from the nearby nodes, as discussed in Section 1.4.3.4. Gas providers would also need some kind of permission to do this. These solutions do not correctly comply the requirement 1) and 3). Therefore, there are still many challenges to be solved before replacing the one-by-one visit of an operator. Consequently, as a first intermediate stage of a rollout, NFC was chosen as the communication technology. This allowed an improved, faster, more reliable, and error-free collection of the data.

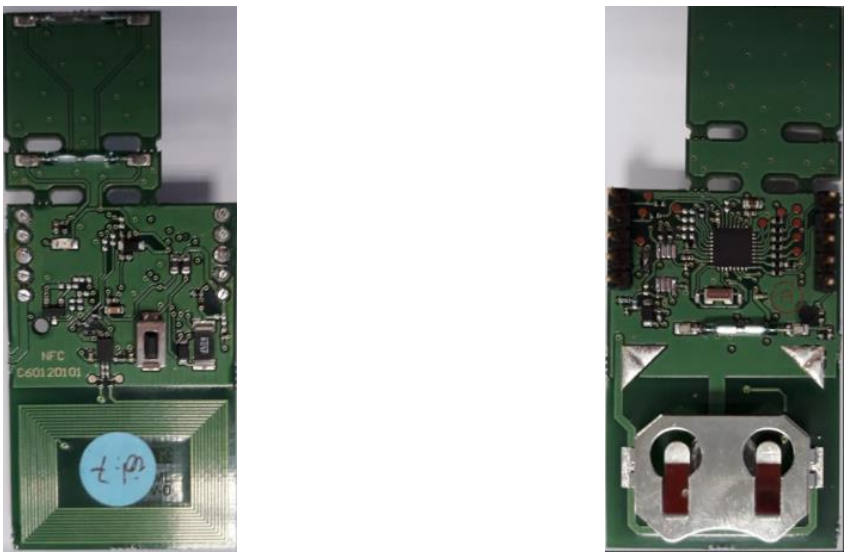

Figure 7: First prototype. Pictures of the front (left) and back (right).

A smartphone was used to interconnect the node with the cloud, which was developed by a third-party company. The smartphone uses an Android application for installing, configuring, activating, managing, and maintaining the node installation. To make the communication secure, the node's EEPROM memory is blocked and, in order to get access to it (read or write), a 128-bits token is sent to a predefined unblocked node's memory section. The token is signed by the cloud with a SHA-256 algorithm using a 32-bit symmetrical secret key and download it to the smartphone with the Android application. The node then validates the token using the secret key with the SHA-256 algorithm and unblock its memory to be accessed for a fixed period of time if the token passes the verification.

Symmetric-key algorithms require both the sender and the recipient of a message to have the same secret key and the secret key was set to be unique for each node. Hence, the cloud has as many secret keys as nodes exists.

Regarding tampering fraud, two relevant cases of utility meter tampering were reviewed in Section 1.4.3.5: node's enclosure tampering and altering the reading using external interfering magnets. Zero-consumption approaches were applied in version 1 of the add-on node. For detecting a node's enclosure tampering, the conventional approach was followed in this work, i.e., a switch button pressed against the lead when the case is closed. Altering the reading using external interfering magnets was detected using a magnetic sensor (reed switch). This method was later improved in the third version of the node.

All in all, the version 1 of the add-on node allowed the energy provider a better reliability in the readings taken by the operator and enabled the user to register the reading themselves. However, there were two problems with the first version of the node: the significant consumption during the sleep mode and the NFC communication range. The autonomy estimated was only one and a half year with a 230 mAh coin cell battery. Further measures were made to locate the power-hungry modules. The results showed the transceiver consumed approximately 7 µA and the microcontroller, 5 µA. The communication range analysis was performed in Publication I [198]. Results showed that the battery holder, placed at the back of the node, generated a considerable interference for the antenna. That impaired its communication range and quality. Although, that was the lowest-cost alternative, the communication needed to be improved.

The product specifications were refined on the basis of the inputs from the first prototype. This stage includes a new loop of development and validation solving all problems detected on the first prototype series and adding those new requirements provided. Figure 8 depicts the improved second version of the add-on node. Since it is a product end-oriented device, the version 2 was manufactured in two shapes, taking into account we worked with two kinds of metric gas meters: Elster and Itron.

Because smaller size was required, the board was divided in two (the main and the antenna boards) and stacked on top of each other, as shown in Figure 8 b). This reduced the node length by 2 cm, at expense of a slightly higher cost as consequence of adding connectors and the additional connection step in the mounting process. The main board consisted of the MCU, the sensors and the battery. The antenna board comprised the communication module, i.e., an NFC printed antenna, a transceiver, and an intelligent switch. They communicated by I2C through a connector. One of the previous findings indicated that a better communication range was achieved with a ferrite layer placed between the antenna and the metal layer (battery holder). This second version continued to have the battery at the back of the antenna, thus a ferrite layer was glued at the back of the antenna board.

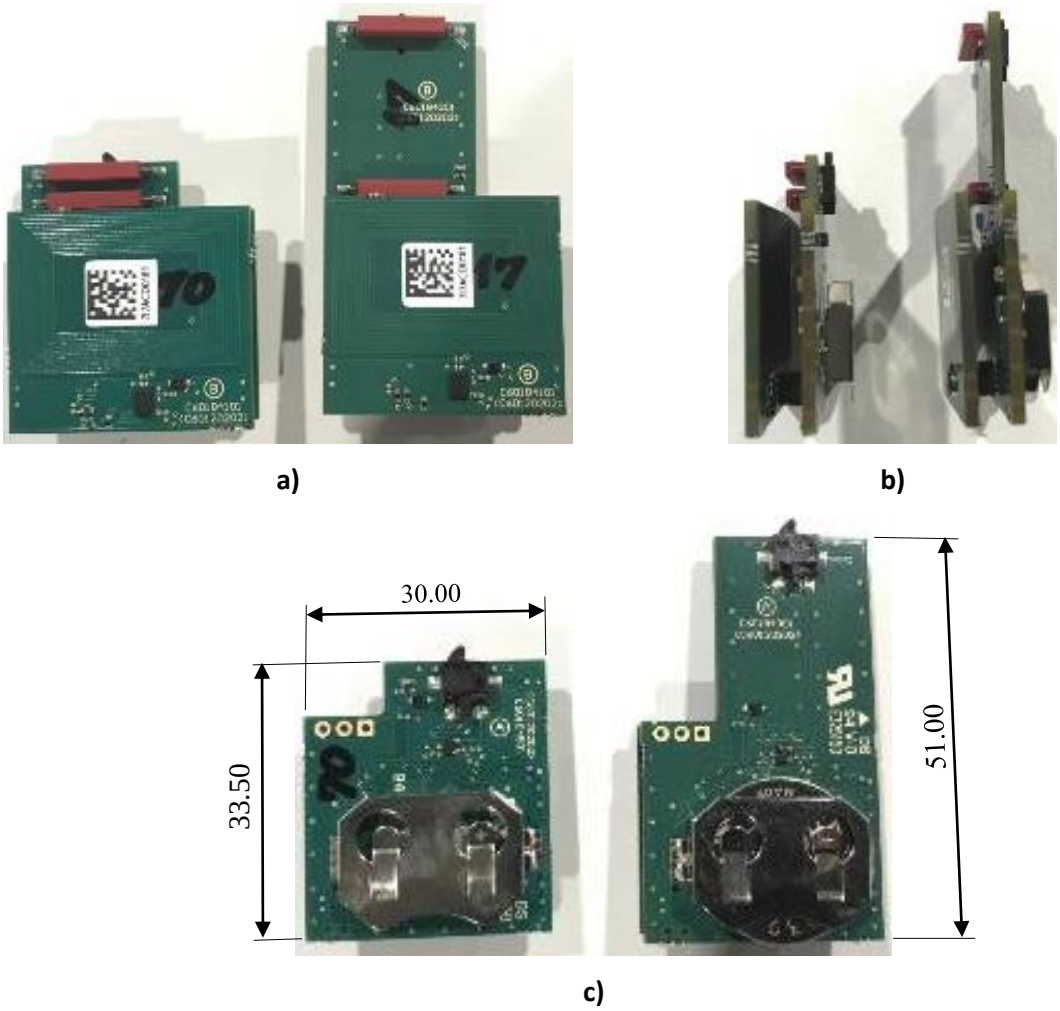

Figure 8: Assembly of the second version of the add-on node: a) front side, b) shows the stack of the main and the antenna boards, and c) back side; measurements in millimeters. The size difference corresponds to two different gas meters: Elster (left) and Itron (right).

The DPM technique was applied in this case using a PMOS as an intelligent switch to cut the energy from the antenna board. A wake-up circuit was used to take energy from the NFC antenna and directly connect it to a MCU pin configured as an external interruption. The MCU then powered the antenna board and communication was established. This reduced the sleep mode consumption by 7 µA, which resulted in an autonomy of the node of more than 5 years.

A reliability trial test was performed in a real environment. The battery life, gas consumption measurement, the data upload to the cloud, and the tampering detection functionalities were validated throughout the month-long study. Around 10 people volunteered to take part in the tests. As this study was carried out within the European project "EnSO" (Energy for Smart Objects), all the volunteers were employees of the company Naturgy. The nodes were installed on the gas meters at their homes as shown in Figure 9 a). The users installed the nodes and were instructed to take three readings every week and to verify that the reading in the meter and the one showed in the application matched. The data were collected through the cloud with the Android application, as shown in Figure 9 b).

a)

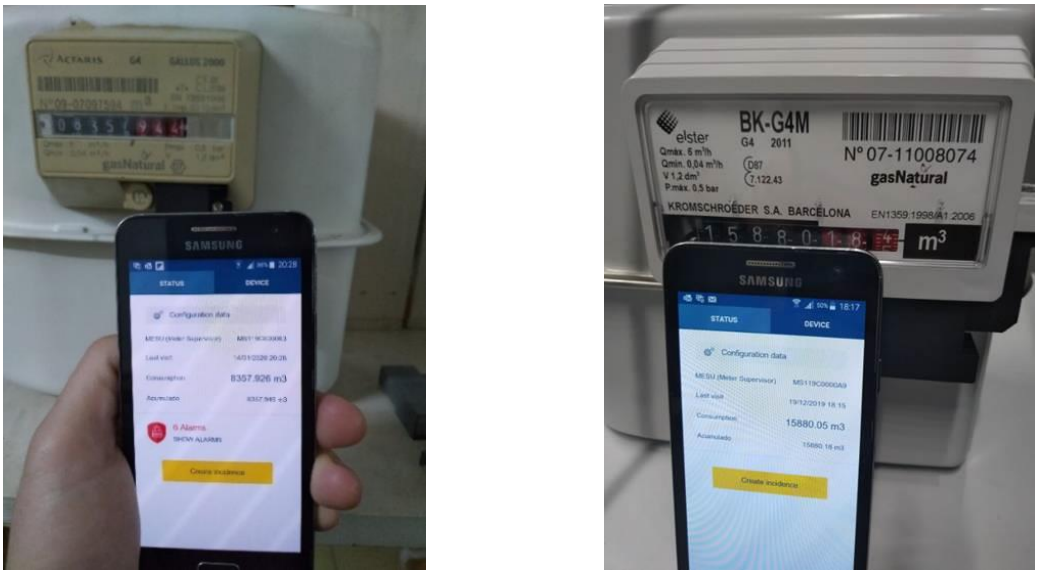

b)

Figure 9: a) Pictures of the add-on node installed in gas meters located in real environments. b) Smartphone reading installed nodes in a Itron (left) and Elster (right) gas meters.

The information of the node was read through NFC, as explained before, and automatically sent to the cloud using the Android application. The information of the node (serial number and configuration), the alarms generated by tampering attempts, and the readings with their corresponding timestamps were shown in the cloud as illustrated in Figure 10 a) and b). Figure 10 c) show a screenshot of the Android application and the serial number of the node is highlighted in a red rectangle. This corresponds with the information in the cloud as shown in Figure 10 b).

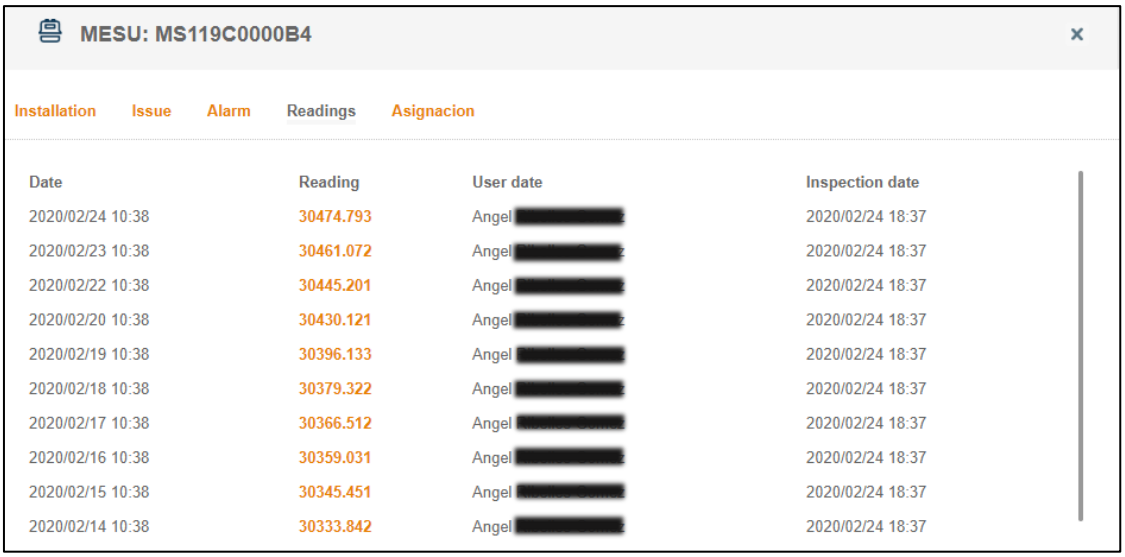

a)

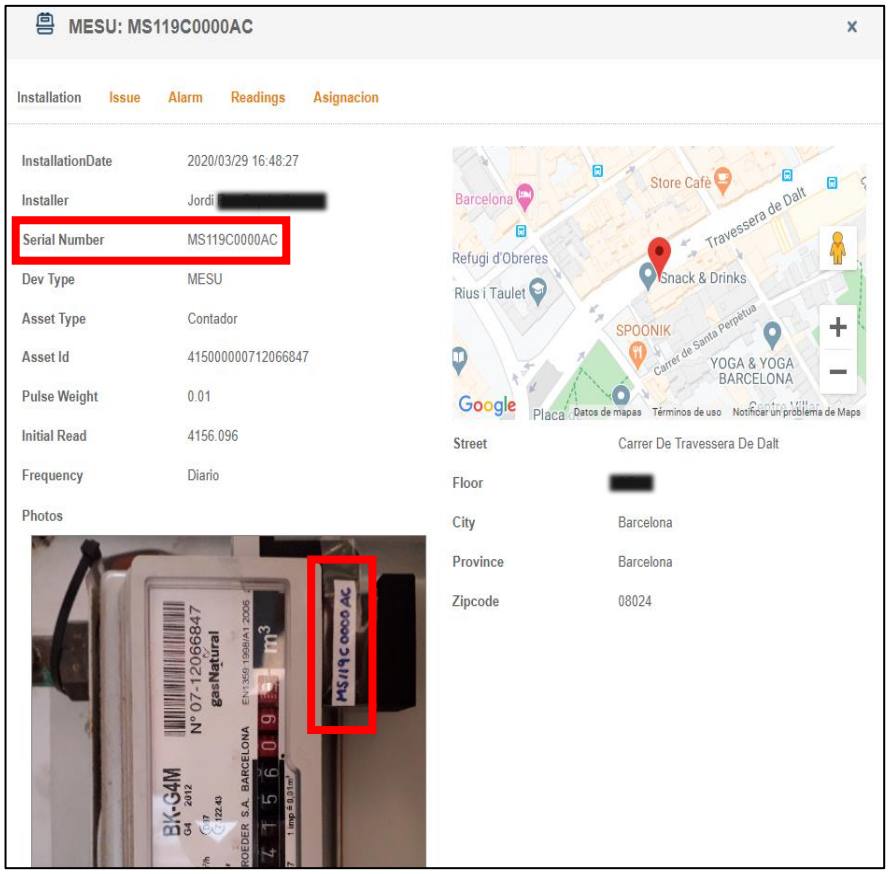

b) **c)**

Figure 10: a) Screenshot of the Android application; b) data of an installed add-on node showed in the cloud; and c) consumption history of an installed device

The tampering detection was also tested. The node proved to detect the interference of an external magnet placed near the gas meter, which can generate incorrect meter readings. The device also proved to detect node's enclosure tampering. Any movement regarding the placement of the node in the

gas meter was detected. This might provide the utility company a hint that something has gone wrong since the installation.

Figure 11: Tampering attempts alarms indicated in the cloud

Even though most of the users were able to properly send the periodic readings, one issue was detected: some users experienced failures in the connection after a long period with the device installed. We saw that some of the batteries were not working as expected and did not last as much as specified in the estimations. Therefore, further reliability test should be performed to solve any firmware bugs that could cause the program to configure the MCU in a higher consumption mode.

Thus far, the second version improved the node such that it complies the 3 challenges for deploying a Smart Grid. However, in regard to challenge 2), the fraud problem against tampering was partially solved since the node is able to detect the node's enclosure tampering and an external interfering magnet, but, as in the majority of the nodes proposed in the literature, the measurement is lost while the tampering is taking place. Therefore, a sensing system immune to external interfering magnets was designed, implemented, and experimentally tested in the Publication II, resulting in the third version of the node. The version 3 differs from version 2 in that it has a dual magnetic sensing circuit and an algorithm coded in the MCU that work together to make the node immune to an external interfering magnet.

Figure 12 [199] depicts the proposed sensing circuit, which is briefly detailed here. As mentioned in Publication II [199], it consists of a dual magnetic sensing: a) primary sensing that relies on reed switches, and b) secondary sensing carried out by Hall-effect sensors. Both sensing strategies have active and passive elements. Overall, the circuit has four sensors: the *primary active sensor* (PAS), the *primary passive sensor* (PPS), the *secondary active sensor* (SAS), and the *secondary passive sensor* (SPS). The PAS and the PPS, as their secondary counterparts, monitor the meter magnet and the interfering effects, respectively. A trade-off had to be made in the positioning of the active and the passive sensors. Sensors too close would not allow differentiate the meter magnet. On the contrary, if they were placed too distant, the passive one could not be able to detect the interfering magnet.

The voltages V_{PAS} and V_{PPS}, correspond to the output voltages of the PAS and the PPS, respectively. The outputs are connected to digital inputs of the MCU configured to generate an external

interruption. The voltages V_{SAS} and V_{SPS} correspond to the output voltages of the SAS and the SPS, respectively. The outputs are connected to analog inputs of the MCU. A digital output (V_{power} in Figure 12) of the MCU powers the secondary sensing.

The primary sensing corresponds to the one implemented in the version 2 of the add-on node. Under normal conditions, i.e., without interfering effects, it is the sensing strategy operating by default. The gas consumption is simply measured in a metric totalizer by increasing a digital counter for every external interruption triggered by the PAS. The resolution of the digital measure is 0.01 m^3, which corresponds to a complete turn of the less significant digit of the mechanical index, where the meter magnet is located. On the other hand, a DPM technique is employed for cutting the power from the secondary sensing (V_{power} = '0'). As a consequence, it has no effect on the node's autonomy in normal operation, and thus, the node works the same manner as version 2.

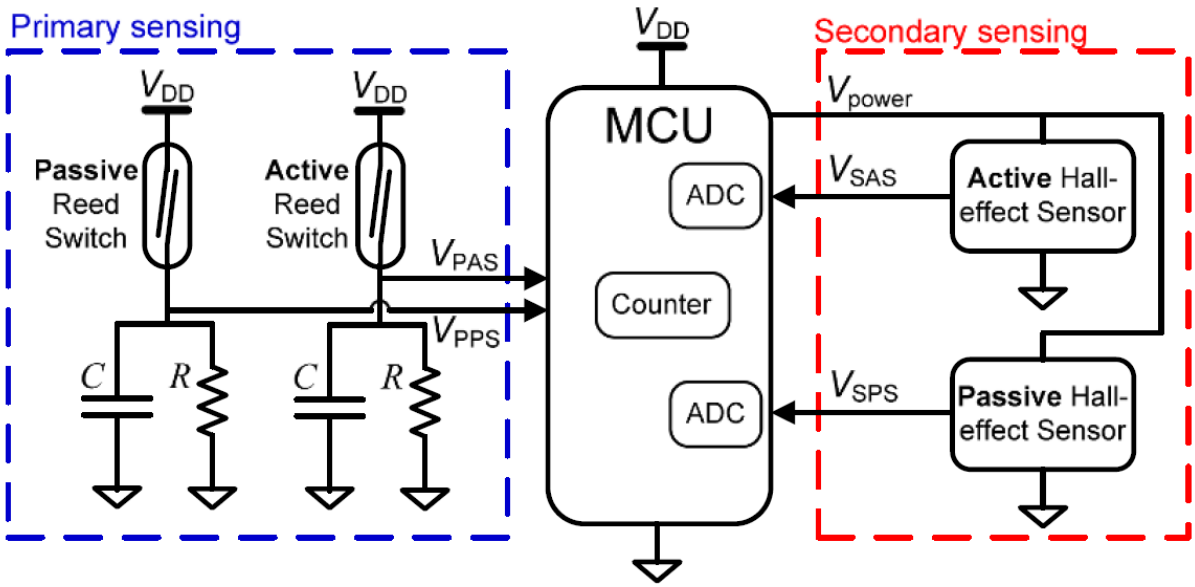

Figure 12: Schematic of the novel dual magnetic sensing circuit. Source [199]**.**

When the PPS detects the interfering effects of an external magnet, the MCU activates the secondary sensing. In this situation, the gas consumption measuring procedure is dictated by the secondary sensing and the algorithm programmed in the MCU. A flowchart of the algorithm executed by the MCU is shown in Figure 13 [199] and it will be briefly recalled here. The algorithm comprises 5 main stages:

- *Stage A*, which is the firmware implementation of the version 2, i.e., the system relies on the primary sensing. As previously noted, this corresponds to the normal operating conditions of the node.
- *Stage B*, which is called when the presence of an interfering magnet was detected. This stage is responsible of detecting when interfering effects has been stabilized, i.e., it is

expected that the external magnet will be placed in a fixed position. Meanwhile, the sensing system waits until the external magnet stops moving. In order to detect that, The MCU checks if V_{SPS} is within an upper and lower threshold. Once stabilized, the difference $V_{SAS} - V_{SPS}$ is stored in the variable ΔV_{ref}.

- *Stage C*, which verifies the removal or movement of the external magnet. If it was removed, the algorithm configures the sensing system to operate in the *Stage A*, and if it was moved, to the *Stage B*. Contrariwise, if it was not removed or moved, the factor $\Delta V = V_{SAS} - V_{SPS} - \Delta V_{ref}$ is computed.
- *Stage D*, which detects the effects of the meter magnet on the SAS. When the meter magnet is aligned with the SAS, V_{SAS} increases and $\Delta V > 0$. If ΔV exceeds a specified threshold the counter is incremented by one. The threshold was experimentally determined by measuring the effects of the meter magnet. Furthermore, an internal variable (M) is set to '1', indicating that the meter magnet has been recognized by the secondary sensing. The purpose of this variable is to lock the digital counter until it is validated that the influence of the meter magnet is no longer detected by the SAS.
- *Stage E*, contrarily to the previous stage, unlocks the counter by resetting M to '0'. This is inferred by comparing ΔV with zero. In the practice, a more conservative approach is considered by comparing ΔV with a value near to zero. The reason is the uncertainty of the measurement based on the ADC's resolution, the sensitivity of the Hall-effect sensors, and the electrical noise.

The algorithm is executed every 50 ms to optimize the energy consumption. In addition, for a more stable result, the measured values of V_{SAS} and V_{SPS} correspond to an average of 10 measurements. The consumption increased 80 µA under a tampering attempt with an external magnet. Although the autonomy is greatly reduced, the sensing system would still allow the node to continue measuring until an operator visits the installation, where he will be notified by the node of a tampering attempt.

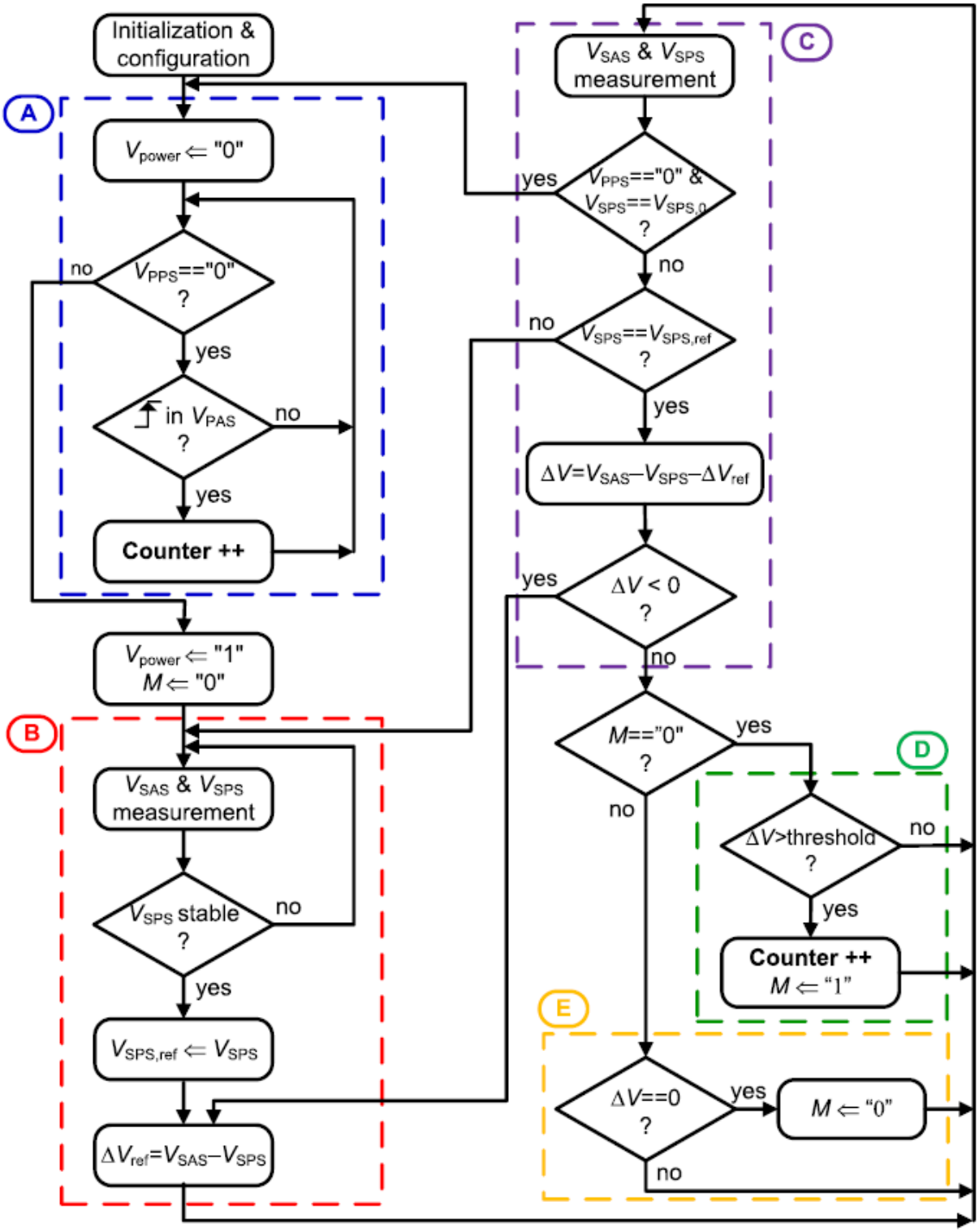

Figure 13: Flowchart of the algorithm executed by the MCU.
Source [199].

The main contributions of this third version can be summarized as follows:

- The dual sensing system combines hardware and an algorithm to carry out the measurement.

- It does not exist in the literature another solution that allows the smart meter to keep recording the gas consumption while an external magnet tampering is happening. The solution it is not fully immune to external magnetic fields because, as expected, the Hall-effect sensors will saturate at some point. The saturation limit was not measured in this work, though. This method could be complemented by shielding the enclosure, as previously described in Section 1.4.3.5, to endure stronger magnetic fields.
- This solution increases the cost of the node at expense of a better functionality. The difference in price would reflect the cost of the two hall-effect sensors (around 1.2 €). The total cost of the node, considering the communication module of version 2, would still be less than 10 €.
- The proposed solution effectively satisfies the three constraints of the IoT nodes.

5.2 Energy challenge 2: Low-power wake-up circuit

The objective for the energy challenge 2 was related to the optimization of the IoT node power consumption when this is not operating. This included the analysis, characterization, and evaluation of a simple low-power wireless circuit for waking up nodes. In Section 1.4.4, the literature was reviewed, and among the technologies used for waking up nodes, optical communication was chosen to design the wake-up circuit. In particular, we proposed the use of commercially available LEDs, illuminated with the flash light of a smartphone, as a contactless wake-up system of the MCU when it is in sleep mode. Two major problems have been identified that hinder the design of an optimal circuit: the lack of information of LEDs operating as photodetectors and the ambient light interference. In that sense, the research has been covered in publications III, IV and V. Publication III contains the preliminary findings of this thesis investigation. It presents the simplest LED-based wake-up circuit, which stands as the foundation for this study. Publication IV provides the characterization of LEDs working as photodiode. Publication V addresses the analysis, design, and evaluation of a LED-based wake-up circuit. The novel circuit is simple, complies with the constraints of nodes for the IoT and is immune to ambient light interference.

All the circuits proposed in this energy challenge were focused on waking an MCU up, i.e., as mentioned in Section 1.4.4, the case where the node is assembled with a battery powering the MCU configured in the lowest consumption mode until a signal wakes it up. However, the study could be extended to activate intelligent switches. Therefore, a lower-power consumption of the node on shelf-time might be achieved since only the intelligent switch would be draining the battery.

The research elaborated in the three publications used the flashlight of a smartphone as signal of interest for the wake-up, and sunlight and office light as ambient light interference. However, the finding of this work could be extended to other sources of light. In addition, while maximizing the

communication bit rate was beyond the scope of this research, the limiting factor was the flashlight of the smartphone flashlight rather than the LEDs.

Publication III has a broad scope and a wide range of use cases. It looked to give both an alternative communication system and a wireless wake-up solution for nodes, which comply with the constraints of the IoT. The design has one major drawback, which is the operation under ambient light conditions. This may cause unwanted turns-on and higher consumption as discussed in Section 1.4.4.2. Nevertheless, the most relevant contribution of this study was that, under the appropriate environment conditions, it is the simplest, lowest-cost, smallest, and lowest-power solution for waking up an MCU. Based on the LED characterization carried out in publications IV and V, suitable environmental conditions are indoor spaces where the LED is not exposed to sunlight or have a cover attached to protect it from sunlight.

Publication IV tackles the LEDs current-voltage characterization problem. An initial characterization of twenty LEDs with a high-power white emitting LED (emulating the smartphone flashlight, as defined in [201]) was first carried out to choose the appropriate ones for the study. The same setup as in [201] was utilized. The difference with the final published study of the characterization was that only the open-circuit voltage (V_{oc}) and photogenerated short-circuit current (I_{sc}) were measured. The selection criteria were to choose two LEDs of each emission color: 1) the cheapest and smallest one and 2) one with a higher emitting power level, preferably with a flat top clear lens. In the case of the GREEN and WHITE LEDs, only one of each was selected because they already met both selection criteria. Table I summarizes the values of the absolute I_{sc} and of the V_{oc}. The highlighted rows indicate the LEDs selected for the article.

Table I: Information about the pre-selected LEDs and their generated open-circuit voltage and short-circuit current.

Emission Color	Part number	Acronym	Emission wavelength[(a)] [nm]	Cost [€]	V_{oc} [V]	$\lvert I_{sc}\rvert$ [µA]
Blue	150060BS75000	BLUE1	470	0.15	1.9	0.1
	MLEROY-A1-0000-000502	-	455	0.82	2.3	3.8
	L135-U450003500000	-	448	1.02	2.3	2.8
	LB Q39G-L2OO-35-1	-	470	0.45	2.1	0.1
	L135-B475003500000	BLUE2	475	1.02	2.2	6.4
Green	GT PSLR31.13-LSLU-T1T2-1-150-R18	-	525	0.73	-0.5	-1.1
	LT G6SP-CBEB-25-1-140-R18-Z	-	528	1.49	1.3	5.4
	XQAGRN-02-0000-000000Z01	-	540	0.6	-0.6	2.4
	SML-D12M8WT86	-	572	0.34	1.6	0.9
	150060VS75000	GREEN	570	0.14	1.6	2.3
Red	GH DASPA2.24-QORK-1-1	-	640	1.17	1.6	105.0
	MLERED-A1-0000-000U01	-	625	1.1	1.6	70.1
	ASMT-QHBD-AFH0E	-	625	1.36	6.4	18.5
	150060RS75000	RED1	625	0.14	1.5	4.9
	SML-D12U8WT86	-	620	0.34	1.5	2.2
	MLESRD-A1-0000-000W01	RED2	618	0.88	1.6	40.8
White	MX3AWT-A1-0000-000E50	-	6000 K	1.08	0.0	1.3
	ASMT-QWBC-NJK0E	-	7250 K	1.93	2.2	0.2
	MLEAWT-A1-R250-0004E3	-	5000 K	0.58	0.0	1.9
	CLM3C-WKW-CWBYA153	WHITE	5500 K	0.2	2.2	0.2

[a.] Except for White LEDs, which specify the CCT[6].

[6] CCT (Correlated Color Temperature): "Term used to describe the color of "white" light sources. Specifically, it is the temperature of the Planckian (black body) radiator, which produces the chromaticity most similar to that produced by the light source in question" [206].

The findings in Publication IV derived in some interesting results:

- The current-voltage characterization of the selected LEDs allowed us to discover that placing a resistor in parallel with the LED allows to better discriminate the signal of interest from interferences.
- The selection of the optimum load resistor is the one that maximizes the difference between the signal of interest and the ambient light. The findings of this study show this occurs (approximately) when the resistor line intersects the knee of the signal of interest. The current-voltage characterization was used to estimate it graphically.
- The sensitivity to a source of light varied according on the emission color of the LEDs. This agrees with the studies in the literature discussed in Section 1.4.4.2, which showed the LEDs' spectral responsivity varies depending on the materials they are fabricated, thus the emission color. The responsivity peak is produced below the peak emission wavelength. Therefore, this inconsistency is due to the peak, the width of the spectral responsivity, and the overlap with the emission spectrum differ from one LED to another. Therefore, some LEDs, such as blue LEDs, skip most of the emission spectrum of the white emitting LED and thus show a low sensitivity to it. On the other hand, red LEDs have a higher overlap with the emission spectrums of the emitting LED and sunlight and thus a higher sensitivity than blue LEDs.
- Higher I_{sc} were generated for bigger LEDs with the same emission color and with the same light source, as expected, since they have a larger photo-sensitive surface.

Publication V continued the work by proposing a simple, low-cost, and low-power, contactless wake-up circuit immune to ambient interference. Only red LEDs were considered for this article since they performed the best both outdoors and indoors. In particular, RED1 was selected over RED2 because derived in the cheapest and smallest solution. To achieve a larger communication range, RED2 LED could be used, at expense of a higher cost and size.

Figure 14 [202] depicts the LED-based wake-up circuit, which is briefly detailed here. The voltage and current generated by the LED are v_D and i_D, respectively. The previously mentioned optimum load resistor R_D is placed in parallel to the LED. A high-pass filter (HPF) is comprised by the capacitor C_H and the resistor R_H. The HPF output is v_H. Finally, a voltage level translator stage, comprised by a NMOS transistor and a pull-up resistor R_M, generates an output v_M and it is connected to the interrupt pin of the MCU. The dotted lines represent the parasitic capacitances of the diode (C_D) and of the NMOS input (C_M).

As mentioned in the literature in section 1.4.4.2, studies showed that ambient interference behaves as a DC offset in the received signal. Basically, there are two approaches suggested in the literature to overcome this: 1) to modulate the signal and 2) to cancel the DC offset. The approach 1)

was implemented in this study by a OOK modulation of the flashlight of a smartphone. For this purpose, a smartphone application was developed in Android Studio to generate pulses from the flashlight. The application allows to select the number of flash pulses to emit and the duration of the period. A Firmware Activation Check (FAC) was coded into the MCU to reject unwanted wake-up signals coming from interfering lights or even from hacking lights. The communication protocol was out of the scope of this research and thus a simple FAC was implemented, but communication protocols as OpenVLC1.0 could be used.

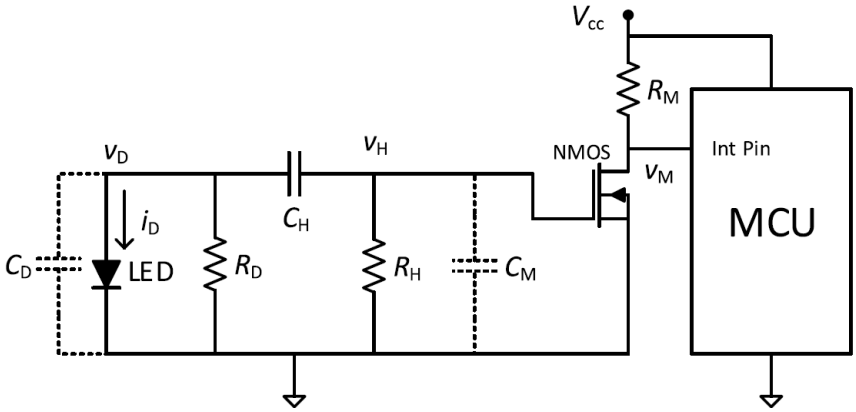

Figure 14: Circuit for waking up an MCU using an LED.
Source [202]

In the literature, the approach 2) consisted of a circuit that, based on an algorithm executed in the MCU, adaptively adds an offset based on the ambient light. In this work, a novel method was implemented instead. A simple HPF was utilized to block the DC ambient interference while allowing the modulated input signal (flashlight) to pass through. When the flashlight turns on, i_D and thus v_D undergo a step increase from an initial value, corresponding to the interfering light (V_{Sun}), to a final value (V_{Flash}) and the voltage step (Δv_D) instantaneously appears in the HPF output. This method does not add computational overhead to the MCU and does not require a complex circuit. It is interesting to note that the information in the input signal is carried in Δv_D as a result of the effects of R_D, as illustrated in Figure 15.

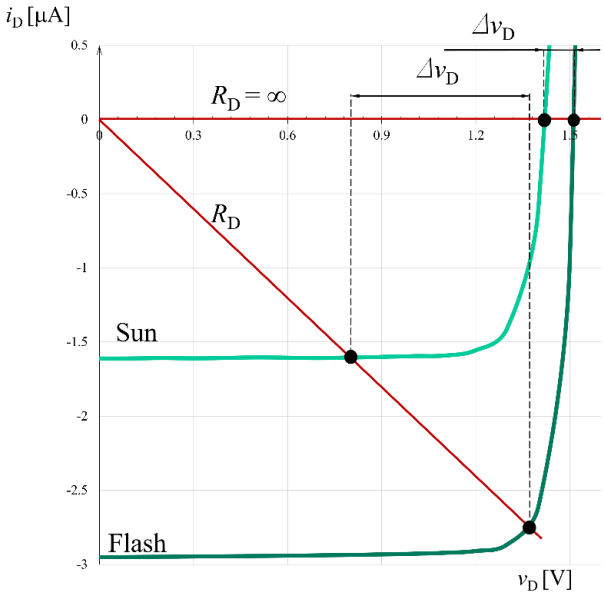

Figure 15: Current-voltage characterization of the LED under study. It shows the operating points with and without R_D and illustrate the effects in the amplitude of the signal information.

In order to select the proper component values, the Laplace transfer function of the circuit is given by (1) with the conditions $R_H >> R_D$ and C_D, $C_M << C_H$ to avoid loading effects on R_D and C_H, stated in [202]:

$$H(s) = \frac{V_H}{I_D} \approx -R_D \frac{s\omega_2}{(s+\omega_1)(s+\omega_2)} \quad (1)$$

which corresponds to a bandpass filter (BPF) with the following cutoff frequencies [202]:

$$f_1 = \frac{\omega_1}{2\pi} = \frac{1}{2\pi R_H C_H} \quad (2)$$

$$f_2 = \frac{\omega_2}{2\pi} = \frac{1}{2\pi R_D (C_D + C_M)} \quad (3)$$

As mentioned before, the signal of interest is a smartphone flashlight. The light signal hits the LED, which generates a photocurrent square wave with the same frequency as the light signal (f_S). The input current signal has a DC offset as a result of the ambient light interference. The square wave is fed to the BPF and processed based on the relation between f_S, f_1 and f_2. Three cases can be distinguished: 1) $f_S > f_2$; 2) $f_1 < f_S < f_2$; and 3) $f_S < f_1$. Figure 16 illustrates the analysis of the steady-state time response of a BPF to the fundamental frequency of a square wave in the case 3). The input signal, $i_D \cdot R_D$, is referred to the right axis. The signal v_H normalized to Δv_D is represented in the left axis. The plot shows that case 3) takes full advantage of the entire amplitude of the input signal ($\pm\Delta v_D$) and ensures the activation of the NMOS. Therefore, the BPF was designed to work in case 3).

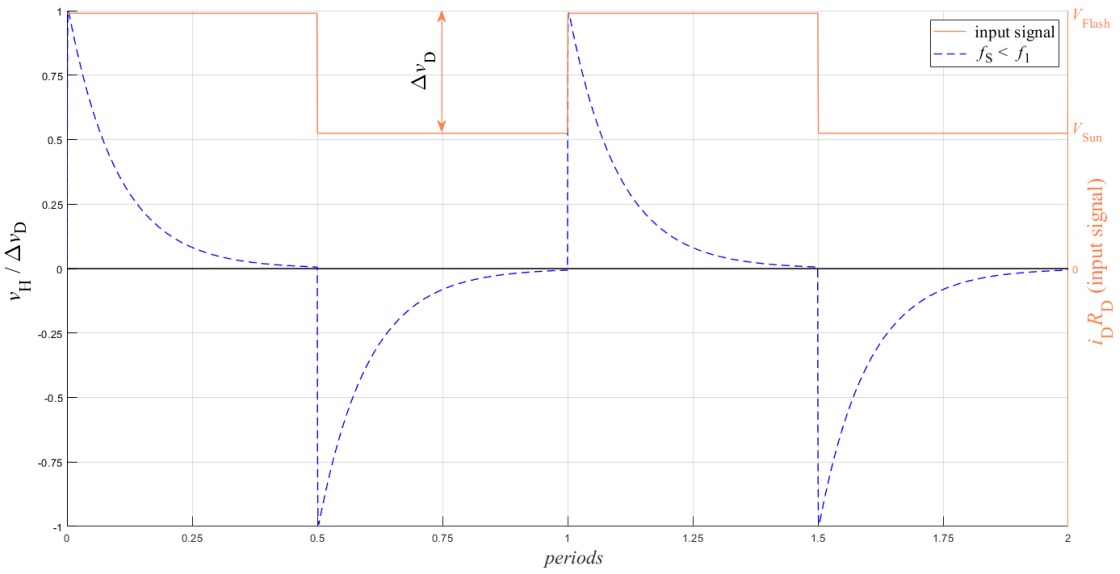

Figure 16: Response of a bandpass filter to different fundamental frequencies of an input square wave signal with a DC offset.

In reviewing the literature, most solutions outperform our contactless wake-up circuit regarding the communication range. However, considering the constraints for the nodes of the IoT and the objective set for this energy challenge, our solution resulted to be 1) simpler because it comprises only an off-the-shelf SMD LED, 3 resistors, 1 capacitor, and 1 NMOS transistor; 2) smaller because the measured footprint of the mentioned components is less than 10 mm^2; 3) lower-cost, which is less than 0.5 €; and 4) with a lower-power consumption (around 0.5 nA).

5.3 Energy challenge 3: High-efficiency energy harvester

The objectives related to the energy challenge 3 have been covered by the publication VI [203]. Here the work was focused on designing a highly efficient energy harvester. Figure 6 showed a block diagram of a generic RF harvester. A particular case was developed in Chapter 4 and showed in Figure 17. The highlighted blocks indicate the differences between the generic and the particular case addressed here.

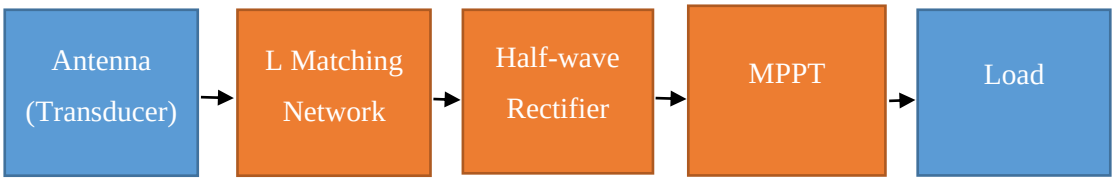

Figure 17: Particular case of the implementation of an RF energy harvester.

The matching network block is an essential part of the RF harvester. The main functions are transferring the maximum power from the antenna to the rectifier and boosting the voltage. It is

interesting to note that the simulations of this study of the rectenna efficiency with and without the L matching network (using ideal components) resulted in an increase of more than 70%. A passive voltage boost was achieved by using a L matching network topology, as suggested in the literature. The matching network values were derived from [196], where it was demonstrated that an optimum voltage gain exists.

As mentioned in Section 1.4.5.4, the rectifier/multiplier block of a RF harvester is often considered as the most critical, since it is the major source of inherent power loss due to biasing the diodes (or MOS transistors). Here, a half-wave rectifier was adopted, which is the simplest implementation of a rectifier.

A rectenna (rectifying antenna) comprises the antenna, the matching network, and the rectifier. The rectenna under study will be briefly outlined here. It is represented in Figure 18 [203]. The antenna was modeled as a sinusoidal voltage source v_a and the series radiation resistance R_a. The matching network comprises the capacitor C_m and the inductor L_m. Following, the diode D as the half-wave rectifier. Finally, an output filter capacitor C_o.

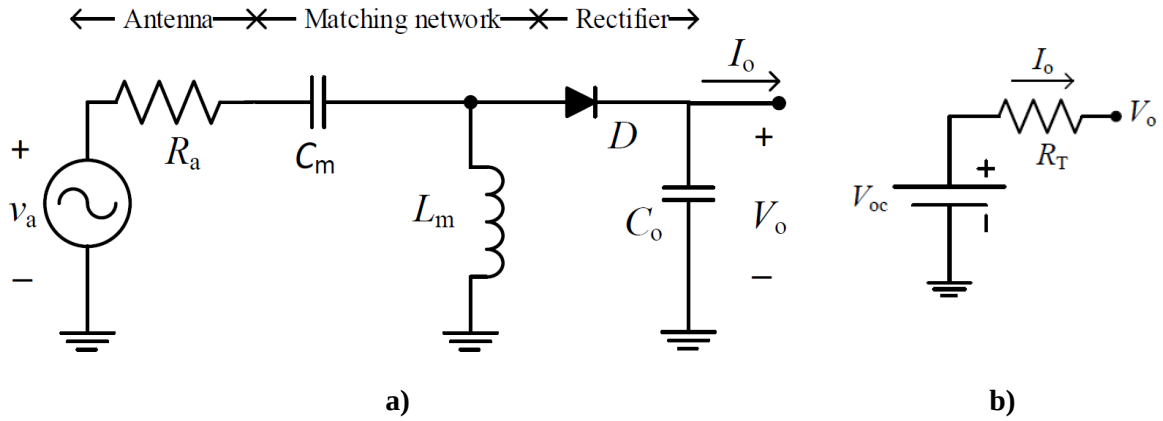

Figure 18: a) Schematic circuit of the rectenna under study and b) its Thévenin equivalent. Source adapted from [203]

The rectenna was modeled as a compact Thévenin circuit, as illustrated in Figure 18, where V_{OC} and R_T are the equivalent voltage and resistance, respectively. The equivalent circuit benefits from others reported in the literature in that it is simpler and includes explicit expressions of the Thévenin voltage (4), resistance (5), and power efficiency (6) [203]:

$$V_{OC} = 2G_t V_{ap} \frac{R_p}{4G_t R_a + R_p} - V_\gamma \quad (4)$$

$$R_T = 2\left[(4G_t^2 R_a)||R_p\right] \quad (5)$$

$$\eta_{rect,max} = \frac{R_p}{4G_t^2 R_a + R_p}\left(1 - \frac{V_\gamma}{\sqrt{2R_a P_{av}}}\frac{4G_t^2 R_a + R_p}{4G_t R_p}\right)^2 \quad (6)$$

where V_{ap} is the voltage amplitude of the antenna, P_{av} is the available power at the antenna, R_a is the antenna series radiation resistance, V_γ is the forward voltage drop at the diode, R_p models the losses of

the coil and diode, G_t is the matching network gain, and $\eta_{rect,max}$ is the maximum rectenna efficiency. From equations (4), (5), and (6), the main results can be summarized as follows:

- With an increasing P_{av}, and thus V_{ap}, V_{OC} increases, whereas R_T remains constant.
- $\eta_{rect,max}$ increases with increasing P_{av}. The dependence on G_t is rather more complex. In a previous work [196], the optimum analytical expression of G_t was derived, resulting in a trade-off between the losses introduced by the coil and that due to the voltage drop of the diode.

Based on the theoretical analysis, the rectenna was implemented and characterized from -30 dBm to -10 dBm. An RF generator (Agilent E4433B) was used as the input instead of the antenna and a Source Measurement Unit (SMU, Agilent B2901A) configured as a voltage sink as the output. Even the design was optimized at 808 MHz, the design can be extrapolated to other frequencies by readjusting the values of the components. From the experimental results, the main findings can be summarized as follows:

- The experimental results were successful as they were able to confirm that the rectenna parameters (V_{OC}, R_T, and $\eta_{rect,max}$) can be well approximated by a Thévenin equivalent circuit. Higher P_{av} values resulted in a better match with the model.
- The resulting efficiencies were among the highest published in the literature for similar designs.

A power conditioning circuit is required for applying an appropriate and steady voltage to the load. In order to reach $\eta_{rect,max}$, the maximum power transfer theorem should be applied, i.e., $R_T = R_O$. In general, the equivalent resistance of a node dynamically varies, as previously shown in Figure 2, in Section 1.4.2, with a generic current consumption profile. In order to apply the theorem, a commercially available MPPT was implemented. Nevertheless, this decreases the overall power efficiency of the RF Harvester (η_T) since the MPPT requires energy to work, too.

The RF harvester including the MPPT was also employed to power a sensor node programmed to stay in a standby mode, consuming 1.4 μA. The P_{av} was adjusted to keep the node's voltage supply at 3 V, thus the power transferred to the node (P_{load}) was 4.2 μW. Two configurations were used for the RF harvester input: (1) an RF generator and (2) a receiving monopole antenna. In the first case, the required value of P_{av} was -17.6 dBm, which agrees with the P_{load} formula:

$$P_{load} = \eta_T P_{av}, \quad (7)$$

considering the corresponding measured data of η_T (≈24%). In the second case, another identical monopole antenna was connected to an RF generator, jointly acting as a wireless energy transmitter. This performance was tested at a distance of 0.5 and 1 m. The remote RF generator's power output was

set at appropriate values so as to operate the node, resulting in 8.0 and 13.2 dBm, respectively. These values accounted for the respective link budgets.

Regarding the constraints of the nodes for the IoT, it was mentioned that employing energy harvesting technology comes with some disadvantages associated, which are cost and size. Consistent with the literature, this research designed an energy harvester with a higher complexity level given the required elements to properly power a node. The greater number of components required to carry out this task resulted in a higher cost and size compared to the primary battery solution. Nevertheless, implementing an RF energy harvester has important implications for prolonging the operation life of the node or even achieving perpetual work. For instance, consider the general current consumption profile of a node, powered at 3 V, shown in Figure 2. Table II contains typical numerical values for each node task, with the exception of the sleep current consumption, which is taken from the experimental test in Publication VI.

Table II: Example values for the current consumption profile of a node.

Tasks	Parameters	Values
Sleep	i_1	1.40 µA
Sensing and processing	i_2	5.00 mA
	$t_{1\text{-}2}$	100.00 ms
Communication	i_3	30.00 mA
	$t_{2\text{-}3}$	5.00 ms

Table III provides the average current consumption for each task and its respective impact on the overall current consumption. The average consumption is calculated for two scenarios: the tasks period (T) is 1) 3600 seconds (1 hour) and 2) 600 seconds (10 minutes). Using equation (7) to calculate P_{av} and taking into account that η_T increases with increasing P_{av}, results show that perpetual work of a node powered by the RF harvester is feasible. Only a 9% increase in P_{av} would be necessary for the task period of 1 hour, considering $\eta_T \approx 25\%$. Whereas, with T = 10 minutes, a 43% increase would be required, considering $\eta_T \approx 30\%$. The resulting P_{av} would be -17.22 dBm and -16.05 dBm, for T = 1 hour and T = 10 minutes, respectively.

Table III: Average current consumption by task and its respective percentage weight in the overall current consumption.

	Period (T)			
	3600 s		600 s	
Tasks	**Average [µA]**	**Percentage [%]**	**Average [µA]**	**Percentage [%]**
Sleep	1.40	88.58	1.40	56.38
Sensing and processing	0.14	8.79	0.83	33.56
Communication	0.04	2.64	0.25	10.07
Total	1.58	100.00	2.48	100.00

Because the RF harvester only supplies the average power, the node would require a storage element, like a supercapacitor or a small rechargeable battery, which would provide the current peaks of the different tasks. A preliminary approximation of the values for the storage elements is performed next. The electric charge (Q_{active}) the node needs to carry out the active tasks, i.e., s*ensing and processing* and *communication*, would be:

$$Q_{\text{active}} = i_2 * t_{1-2} + i_3 * t_{2-3} = 0.65 \text{ mC}, \quad (8)$$

which converted in Ampere-Hour results in the theoretical battery capacity (Q_{batt}) required:

$$Q_{\text{batt}} = \frac{Q_{\text{active}}}{3600} = 0.18 \text{ µAh} \quad (9)$$

Care must be taken with the C-rate[7] of the battery because it may not be able to provide the necessary current peaks. Regarding the supercapacitor, considering a 200 mV drop from the operating voltage, the capacity value (C_{sup}) would be:

$$C_{\text{sup}} = \frac{Q_{\text{active}}}{200 \text{ mV}} = 3.25 \text{ mF} \quad (10)$$

Although there are additional power supply factors to consider, such as the equivalent series resistance (ESR) and the leakage current of the storage elements, the charger efficiency, etc., these calculations provide an estimation of the storage elements required by the node for perpetual work.

[7] C-rate: It is the unit of charge-discharge current density in batteries. 1 C is defined as the current level that fully discharges the fully charged battery in 1 hour. If the battery is discharged at 2 C, it should ideally deliver the full capacity in 30 minutes. However, internal losses decrease the battery capacity. On the contrary, discharging the same battery at 0.5 C, will likely increase the capacity to more than 100%.

6

Conclusion and future work

6.1 Conclusions

The present PhD thesis has offered a framework for the exploration of a broad and diverse set of design challenges of a node for the IoT, that cover from the sensing system, following the node consumption, up to the power supply. In this context, the conclusions from the research carried out in Chapter 2, 3 and 4 will be listed next. The section ends with some general conclusions.

The research carried out in Chapter 2 was oriented to define a feasible sensing system alternative for smart gas meters and to improve the collection process of data. The main conclusions of the research conducted to achieve this objective are:

- The present study provides the earliest comprehensive assessment of a dual magnetic sensing system for gas meters. The method consists of a) a low-cost, low-power primary sensing via reed switches, b) a secondary sensing using Hall-effect sensors, and c) a dynamically adjusted algorithm embedded in the MCU. The suggested sensor system has been demonstrated to be independent of static magnetic fields produced by interfering magnets.
- This study has gone some way towards improving the data collection process of gas meters. An add-on node for upgrading mechanical gas meters to smart ones was developed. The add-on smart gas meters benefit of the accuracy and the long-term stability of the conventional gas meters and the advantages of the node upgrade. This enhances the smart gas meter's stability and reliability, ensuring a reduction in energy theft. This proposal can be incorporated in the scenario of an intermediate rollout strategy.

With respect the optimization of the IoT node power consumption when it is not operating, a contactless wake-up system for MCU using commercially available LEDs as photodiodes has been proposed in Chapter 3. The following conclusions may be drawn from the current investigation:

- The preliminary findings of this study presents the simplest, lowest-cost, smallest, and lowest-power solution for waking up an MCU. Nevertheless, its identified limitation is the operation under ambient light conditions, which may cause unwanted turns-on and a higher consumption of the node.
- The findings of this investigation complement those of earlier studies with an I-V characterization of commercially available LEDs of different colors. The characterization has been carried out with the flashlight of a smartphone and with the interfering lights present in two dissimilar scenarios where the LEDs might be placed, outdoors (sunlight) and indoors (office light). Results indicate that the generated open circuit voltages are quite similar on the same LED for the different sources of light. So,

a good discrimination between the different lights is not possible. However, by adding a resistor in parallel with the LED, an optimum operation point is achieved, which allows a better discrimination between the voltages corresponding to the signal of interest (flashlight) and the interfering lights. The value of the resistor has been calculated based on the I-V flashlight characteristic of the LEDs.

- The findings of this study suggest that the most suitable LEDs are red for outdoors and blue for indoors (not exposed to sunlight). On the other hand, blue and white LEDs cannot be used outdoors since sunlight originates a higher LED voltage than flashlight. These findings contribute to our understanding of LEDs as photosensors.
- Based on the previous findings, a circuit with the additional capability to be immune to ambient light interference was proposed. The study proposed a novel method consisting of an optimum load resistor and a HPF that suppress the DC offset generated by the ambient light while allowing the modulated input signal to pass through.

As for the challenge of the high-efficiency energy harvester, Chapter 4 has provided a theoretical and experimental study of a compact Thévenin model of a rectenna implemented into an RF energy harvester. The rectenna under study consists of an LC-matching network and a half-wave rectifier. The study may lead to the following conclusions:

- One of the more significant findings to emerge from this study is that explicit expressions for the Thévenin voltage, resistance, and power efficiency were derived that offer insight into the operation of the rectenna and its efficiency. The research results of this doctoral thesis represent a further step in the study of RF energy harvesting.
- The rectenna was implemented and characterized from -30 to -10 dBm at 808 MHz and the results mainly agreed with the derived model. High efficiencies were obtained, in particular 60% at -10 dBm.
- Then, an ensuing MPPT was also added, where the behavior of the rectenna as an equivalent Thévenin circuit allowed the use of a simple fractional open circuit voltage (FOCV) technique. The whole RF harvester (rectenna plus MPPT) showed an overall efficiency near 50% at -10 dBm.

As has been exposed throughout the different objectives of this thesis, the findings from this study make several contributions to the current literature. The doctoral research was undertaken to design and implement wireless nodes in the field of IoT. Despite the research was always focused on complying with the three constraints for IoT nodes, a tradeoff between them had to be made depending on the application. In that sense, the following conclusions can be drawn:

- The add-on node is in line with the three constraints in normal operation conditions. The cost of the device resulted to be around 10 €, to have a service life of 5 years with

only a small 230 mAh coin cell battery and a size of 51 mm x 30 mm (Itron version) and 30 mm x 30 mm (Elster version). In case longer service life is required, a higher capacity battery could be used at expense of a higher cost and size.

- The wake-up circuit achieves the optimal balance of the 3 constraints, it successfully reaches an equilibrium between functionality and performance. In comparison with other solutions reviewed in the literature and considering the constraints for nodes of the IoT and the objective set for this energy challenge, our solution resulted to be: 1) simpler because it comprises only an off-the-shelf SMD LED, 3 resistors, 1 capacitor, and 1 NMOS transistor; 2) smaller because the measured footprint of the mentioned components is less than 10 mm2; 3) lower-cost, which is less than 0.5 €; and 4) with a lower-power consumption (around 0.5 nA). The communication range of 1 cm was the solution's major limitation.
- Finally, the research in chapter 4 resulted in a high-efficiency RF energy harvester that can be implemented in nodes that are not cost and size constrained but need to extend their operating life as much as possible. Tests were performed with a nearby transmitting antenna for powering a sensor node with a power consumption of 4.2 µW.

6.2 Future work

Several research topics have emerged from the realization and composition of this doctorate thesis, though the following are the key concerns for future work.

6.2.1 Energy challenge 1: Low-power sensing system

The main lines of future research work related to the energy challenge 1 are:

- Further investigation and experimentation into the reliability of the add-on node is strongly recommended. Primary tests were conducted, but much more work will be required to determine the extent to which the add-on node measures without error.
- The NFC communication module should be integrated to the add-on with the dual magnetic sensing method.
- The operating life of the add-on node could be extended using an energy harvesting module.
- The primary sensing with reed switches has a setback. If the meter magnet stops while activating the reed switch, the battery starts draining through the pull-down resistor. A solution could be implemented so once the pulse is detected, the sensor stops consuming energy.

- Further research should be undertaken to explore how the sensing system could be immune to dynamic magnetic fields generated by AC interfering sources.

6.2.2 Energy challenge 2: Low-power wake-up circuit

A natural progression of the work related to the energy challenge 2 would be:

- The analysis and implementation of the wake-up circuit alongside with a bidirectional communication feature.
- Further work should be done in developing a more secure wake-up FAC, which could be based in open protocols, such as OpenVLC1.0.
- Implementing a camera-to-LED communication would be a fruitful area for further work.
- The optimum value of the resistor varies with the light applied; an interesting further work would be to dynamically change the load resistor.

6.2.3 Energy challenge 3: High-efficiency energy harvester

In regard to energy challenge 3, primary areas of future study are:

- Further work needs to be done on the miniaturization of the solution that could be use in a practical application.
- It is interesting to extend the analysis to other standard frequencies, like 433 MHz, 2.4 GHz, 5 GHz, etc.

References

[1] D. Daji, K. Ghule, S. Gagdani, A. Butala, P. Talele, and H. Kamat, "Cloud-based asset monitoring and predictive maintenance in an industrial IoT system," *2020 International Conference for Emerging Technology, INCET 2020*, Jun. 2020, doi: 10.1109/INCET49848.2020.9154148.

[2] Y. Li, J. Tan, and M. Wang, "Design and implementation of enterprise asset management system based on IOT technology," *Proceedings of 2015 IEEE International Conference on Communication Software and Networks, ICCSN 2015*, pp. 384–388, Oct. 2015, doi: 10.1109/ICCSN.2015.7296188.

[3] A. H. Alquhali, M. Roslee, M. Y. Alias, and K. S. Mohamed, "IOT Based Real-Time Vehicle Tracking System," *2019 IEEE Conference on Sustainable Utilization and Development in Engineering and Technologies, CSUDET 2019*, pp. 265–270, Nov. 2019, doi: 10.1109/CSUDET47057.2019.9214633.

[4] M. Desai and A. Phadke, "Internet of Things based vehicle monitoring system," *IFIP International Conference on Wireless and Optical Communications Networks, WOCN*, Oct. 2017, doi: 10.1109/WOCN.2017.8065840.

[5] M. Hassanalieragh *et al.*, "Health Monitoring and Management Using Internet-of-Things (IoT) Sensing with Cloud-Based Processing: Opportunities and Challenges," *Proceedings - 2015 IEEE International Conference on Services Computing, SCC 2015*, pp. 285–292, Aug. 2015, doi: 10.1109/SCC.2015.47.

[6] R. K. Kodali, G. Swamy, and B. Lakshmi, "An implementation of IoT for healthcare," *2015 IEEE Recent Advances in Intelligent Computational Systems, RAICS 2015*, pp. 411–416, Jun. 2016, doi: 10.1109/RAICS.2015.7488451.

[7] A. R. Al-Ali, T. Landolsi, M. H. Hassan, M. Ezzeddine, M. Abdelsalam, and M. Baseet, "An IoT-Based Smart Utility Meter," *2nd International Conference on Smart Grid and Smart Cities, ICSGSC 2018*, pp. 80–83, Nov. 2018, doi: 10.1109/ICSGSC.2018.8541314.

[8] F. Abate, M. Carratù, C. Liguori, M. Ferro, and V. Paciello, "Smart meter for the IoT," *I2MTC 2018 - 2018 IEEE International Instrumentation and Measurement Technology Conference: Discovering New Horizons in Instrumentation and Measurement, Proceedings*, pp. 1–6, Jul. 2018, doi: 10.1109/I2MTC.2018.8409838.

[9] G. R. Nagarjuna, R. Shashidhar, S. B. Puneeth, and B. N. Arunakumari, "IoT enabled smart traffic system for public and emergency mobility in smart city," *Proceedings of the 4th International Conference on IoT in Social, Mobile, Analytics and Cloud, ISMAC 2020*, pp. 53–59, Oct. 2020, doi: 10.1109/I-SMAC49090.2020.9243489.

[10] M. Kural, F. K. Tuncer, D. Memis, and M. N. Dai, "A Smart Mobility Platform for Electric Vehicles with Event Processing," *IEEE 5th World Forum on Internet of Things, WF-IoT 2019 - Conference Proceedings*, pp. 480–484, Apr. 2019, doi: 10.1109/WF-IOT.2019.8767225.

[11] Kalpanaseelam, C. Jayalakshmi, and K. Prasanti, "Smart Vehicle Connectivity for Safety Applications using IOT," *Proceedings of the 3rd International Conference on Inventive Systems and Control, ICISC 2019*, pp. 363–367, Jan. 2019, doi: 10.1109/ICISC44355.2019.9036363.

[12] N. Mostofa, K. Fullin, S. Zehtabian, S. Bacanli, L. Boloni, and D. Turgut, "IoT-Enabled Smart Mobility Devices for Aging and Rehabilitation," *IEEE International Conference on Communications*, vol. 2020-June, Jun. 2020, doi: 10.1109/ICC40277.2020.9149442.

[13] P. Bogdan, M. Pajic, P. P. Pande, and V. Raghunathan, "Making the Internet-of-Things a reality: From smart models, sensing and actuation to energy-efficient architectures," in *2016 International Conference on Hardware/Software Codesign and System Synthesis, CODES+ISSS 2016*, 2016, pp. 1–10. doi: 10.1145/2968456.2973272.

[14] J. H. Pikul and H. Ning, "Powering the Internet of Things," *Joule*, vol. 2, no. 6. 2018. doi: 10.1016/j.joule.2018.06.005.

[15] A. Musaddiq, Y. bin Zikria, O. Hahm, H. Yu, A. K. Bashir, and S. W. Kim, "A Survey on Resource Management in IoT Operating Systems," *IEEE Access*, vol. 6. 2018. doi: 10.1109/ACCESS.2018.2808324.

[16] S. Abbate, M. Avvenuti, D. Cesarini, and A. Vecchio, "Estimation of energy consumption for TinyOS 2.x-based applications," in *Procedia Computer Science*, 2012, vol. 10. doi: 10.1016/j.procs.2012.06.167.

[17] R. Lajara, J. Pelegrí-Sebastiá, and J. J. Perez Solano, "Power consumption analysis of operating systems for wireless sensor networks," *Sensors*, vol. 10, no. 6, 2010, doi: 10.3390/s100605809.

[18] E. Sifuentes, O. Casas, and R. Pallas-Areny, "Wireless magnetic sensor node for vehicle detection with optical wake-up," *IEEE Sensors Journal*, vol. 11, no. 8, 2011, doi: 10.1109/JSEN.2010.2103937.

[19] M. O. Ojo, S. Giordano, G. Procissi, and I. N. Seitanidis, "A Review of Low-End, Middle-End, and High-End Iot Devices," *IEEE Access*, vol. 6. 2018. doi: 10.1109/ACCESS.2018.2879615.

[20] D. Blaauw *et al.*, “IoT design space challenges: Circuits and systems,” in *Digest of Technical Papers - Symposium on VLSI Technology*, 2014, pp. 1–2. doi: 10.1109/VLSIT.2014.6894411.

[21] Q. Sun *et al.*, “A Comprehensive Review of Smart Energy Meters in Intelligent Energy Networks,” *IEEE Internet of Things Journal*, vol. 3, no. 4, pp. 464–479, Aug. 2016, doi: 10.1109/JIOT.2015.2512325.

[22] F. Cascetta and P. Vigo, “The future domestic gas meter: Review of current developments,” *Measurement*, vol. 13, no. 2, pp. 129–145, Apr. 1994, doi: 10.1016/0263-2241(94)90006-X.

[23] “How do we read the gas meter? | Endesa.” https://www.endesa.com/en/blogs/endesa-s-blog/air-conditioning/read-gas-meter (accessed Jul. 14, 2021).

[24] M. Tewolde, J. C. Fritch, and J. P. Longtin, “High-resolution meter reading technique for appliance gas usage monitoring for the smart grid,” in *2011 8th International Conference and Expo on Emerging Technologies for a Smarter World, CEWIT 2011*, 2011, pp. 1–6. doi: 10.1109/CEWIT.2011.6135876.

[25] S. Cai, S. Zhang, D. Huang, and S. Yu, “Remote gas meter reading system based on zigbee networks,” in *2012 Spring World Congress on Engineering and Technology, SCET 2012 - Proceedings*, 2012, pp. 1–4. doi: 10.1109/SCET.2012.6341903.

[26] F. I. Wiratama, M. Syaifuddin, I. K. Wibowo, F. Ardilla, and A. Purnomo, “Gas billing system based on automatic meter reading on diaphragm gas meter with email notification,” in *International Electronics Symposium on Knowledge Creation and Intelligent Computing, IES-KCIC 2018 - Proceedings*, 2019, pp. 395–402. doi: 10.1109/KCIC.2018.8628521.

[27] Y. Mahmood, N. Kama, A. Azmi, and S. Ya’acob, “An IoT based home automation integrated approach: Impact on society in sustainable development perspective,” *International Journal of Advanced Computer Science and Applications*, vol. 11, no. 1, 2020, doi: 10.14569/ijacsa.2020.0110131.

[28] R. Piyare, A. L. Murphy, C. Kiraly, P. Tosato, and D. Brunelli, “Ultra Low Power Wake-Up Radios: A Hardware and Networking Survey,” *IEEE Communications Surveys and Tutorials*, vol. 19, no. 4, pp. 2117–2157, Oct. 2017, doi: 10.1109/COMST.2017.2728092.

[29] M. T. Penella, J. Albesa, and M. Gasulla, “Powering wireless sensor nodes: Primary batteries versus energy harvesting,” *2009 IEEE Intrumentation and Measurement Technology Conference, I2MTC 2009*, pp. 1625–1630, 2009, doi: 10.1109/IMTC.2009.5168715.

[30] G. Shaker, R. Chen, B. Milligan, and T. Qu, “Ambient electromagnetic energy harvesting system for on-body sensors,” *Electronics Letters*, vol. 52, no. 22, 2016, doi: 10.1049/el.2016.3123.

[31] V. Talla, B. Kellogg, B. Ransford, S. Naderiparizi, S. Gollakota, and J. R. Smith, "Powering the next billion devices with Wi-Fi," in *Proceedings of the 11th ACM Conference on Emerging Networking Experiments and Technologies, CoNEXT 2015*, 2015, pp. 1–13. doi: 10.1145/2716281.2836089.

[32] M. Stoopman, S. Keyrouz, H. J. Visser, K. Philips, and W. A. Serdijn, "Co-design of a CMOS rectifier and small loop antenna for highly sensitive RF energy harvesters," *IEEE Journal of Solid-State Circuits*, vol. 49, no. 3, pp. 622–634, 2014, doi: 10.1109/JSSC.2014.2302793.

[33] P. di Marco, V. Stornelli, G. Ferri, L. Pantoli, and A. Leoni, "Dual band harvester architecture for autonomous remote sensors," *Sensors and Actuators A: Physical*, vol. 247, pp. 598–603, Aug. 2016, doi: 10.1016/J.SNA.2016.06.040.

[34] M. Piñuela, P. D. Mitcheson, and S. Lucyszyn, "Ambient RF energy harvesting in urban and semi-urban environments," *IEEE Transactions on Microwave Theory and Techniques*, vol. 61, no. 7, pp. 2715–2726, 2013, doi: 10.1109/TMTT.2013.2262687.

[35] G. Singh, R. Ponnaganti, T. v. Prabhakar, and K. J. Vinoy, "A tuned rectifier for RF energy harvesting from ambient radiations," *AEU - International Journal of Electronics and Communications*, vol. 67, no. 7, pp. 564–569, Jul. 2013, doi: 10.1016/J.AEUE.2012.12.004.

[36] Y. Á. López, J. Franssen, G. Á. Narciandi, J. Pagnozzi, I. G.-P. Arrillaga, and F. L.-H. Andrés, "RFID Technology for Management and Tracking: e-Health Applications," *Sensors 2018, Vol. 18, Page 2663*, vol. 18, no. 8, p. 2663, Aug. 2018, doi: 10.3390/S18082663.

[37] A. Attaran, R. Rashidzadeh, and R. Muscedere, "Chipless RFID tag using RF MEMS switch," *Electronics Letters*, vol. 50, no. 23, pp. 1720–1722, Nov. 2014, doi: 10.1049/el.2014.3075.

[38] A. Sample and J. R. Smith, "Experimental results with two wireless power transfer systems," *RWS 2009 IEEE Radio and Wireless Symposium, Proceedings*, pp. 16–18, 2009, doi: 10.1109/RWS.2009.4957273.

[39] A. Shameli, A. Safarian, A. Rofougaran, M. Rofougaran, and F. de Flaviis, "Power harvester design for passive UHF RFID tag using a voltage boosting technique," *IEEE Transactions on Microwave Theory and Techniques*, vol. 55, no. 6, pp. 1089–1096, Jun. 2007, doi: 10.1109/TMTT.2007.896819.

[40] G. Singh, R. Ponnaganti, T. v. Prabhakar, and K. J. Vinoy, "A tuned rectifier for RF energy harvesting from ambient radiations," *AEU - International Journal of Electronics and Communications*, vol. 67, no. 7, pp. 564–569, Jul. 2013, doi: 10.1016/J.AEUE.2012.12.004.

[41] T. Soyata, L. Copeland, and W. Heinzelman, "RF Energy Harvesting for Embedded Systems: A Survey of Tradeoffs and Methodology," *IEEE Circuits and Systems Magazine*, vol. 16, no. 1, pp. 22–57, Jan. 2016, doi: 10.1109/MCAS.2015.2510198.

[42] J. P. Curty, N. Joehl, F. Krummenacher, C. Dehollain, and M. J. Declercq, "A model for μ-power rectifier analysis and design," *IEEE Transactions on Circuits and Systems I: Regular Papers*, vol. 52, no. 12, pp. 2771–2779, Dec. 2005, doi: 10.1109/TCSI.2005.854294.

[43] M. Pizzotti *et al.*, "A Long-Distance RF-Powered Sensor Node with Adaptive Power Management for IoT Applications," *Sensors 2017, Vol. 17, Page 1732*, vol. 17, no. 8, p. 1732, Jul. 2017, doi: 10.3390/S17081732.

[44] ISO/IEC JTC 1, "Internet of Things (IoT) Preliminary Report 2014," 2015. Accessed: Jan. 30, 2022. [Online]. Available: https://www.iso.org/files/live/sites/isoorg/files/developing_standards/docs/en/internet_of_things_report-jtc1.pdf

[45] H. Puttnies, V. Altmann, F. Golatowski, and D. Timmermann, "Cost-efficient universal approach for remote meter reading using web services and computer vision," in *Proceedings of the WoWMoM 2015: A World of Wireless Mobile and Multimedia Networks*, 2015, pp. 1–6. doi: 10.1109/WoWMoM.2015.7158205.

[46] M. Andersen, "Trends in internet of things platforms," *XRDS: Crossroads, The ACM Magazine for Students*, vol. 22, no. 2, 2015, doi: 10.1145/2845153.

[47] Y. Álvarez López, J. Franssen, G. Álvarez Narciandi, J. Pagnozzi, I. González-Pinto Arrillaga, and F. Las-Heras Andrés, "RFID technology for management and tracking: E-health applications," *Sensors (Switzerland)*, vol. 18, no. 8, 2018, doi: 10.3390/s18082663.

[48] "EnSO." http://enso-ecsel.eu/ (accessed Jul. 10, 2021).

[49] "Worldsensing, Sensors & data loggers for Smart building." https://www.worldsensing.com/ (accessed Jul. 10, 2021).

[50] F. Molaei, E. Rahimi, H. Siavoshi, S. G. Afrouz, and V. Tenorio, "A Comprehensive Review on Internet of Things (IoT) and its Implications in the Mining Industry," *American Journal of Engineering and Applied Sciences*, vol. 13, no. 3, pp. 499–515, Sep. 2020, doi: 10.3844/AJEASSP.2020.499.515.

[51] A. Q. Gbadamosi *et al.*, "IoT for predictive assets monitoring and maintenance: An implementation strategy for the UK rail industry," *Automation in Construction*, vol. 122, p. 103486, Feb. 2021, doi: 10.1016/J.AUTCON.2020.103486.

[52] R. Kanan, O. Elhassan, and R. Bensalem, "An IoT-based autonomous system for workers' safety in construction sites with real-time alarming, monitoring, and positioning strategies," *Automation in Construction*, vol. 88, pp. 73–86, Apr. 2018, doi: 10.1016/J.AUTCON.2017.12.033.

[53] W. W. S. Chung, S. Tariq, S. R. Mohandes, and T. Zayed, "IoT-based application for construction site safety monitoring," *https://doi.org/10.1080/15623599.2020.1847405*, pp. 1–17, 2020, doi: 10.1080/15623599.2020.1847405.

[54] P. Shankara, P. Mahanta, E. Arora, and G. Srinivasamurthy, "Impact of Internet of Things in the Retail Industry," *Lecture Notes in Computer Science (including subseries Lecture Notes in Artificial Intelligence and Lecture Notes in Bioinformatics)*, vol. 9416, pp. 61–65, Oct. 2015, doi: 10.1007/978-3-319-26138-6_9.

[55] The IoT 2020 project team in the IEC Market Strategy Board, "IoT 2020 Smart and Secure IoT Platform," 2016.

[56] M. A. Kamal Zill-E-Huma and Salahuddin, "Introduction to Wireless Sensor Networks," in *Wireless Sensor and Mobile Ad-Hoc Networks: Vehicular and Space Applications*, A. Benhaddou Driss and Al-Fuqaha, Ed. New York, NY: Springer New York, 2015, pp. 3–32. doi: 10.1007/978-1-4939-2468-4_1.

[57] Sandeep Verma, "Network Topologies in Wireless Sensor Networks: A Review 1," *International Journal of Electronics & Communication Technology*, vol. 4, no. 3, 2013, doi: 10.1.1.308.796.

[58] "A guide to Edge IoT analytics: Internet of Things blog." https://www.ibm.com/blogs/internet-of-things/edge-iot-analytics/ (accessed Jul. 10, 2021).

[59] M. T. Penella-López and M. Gasulla-Forner, *Powering Autonomous Sensors*. 2011. doi: 10.1007/978-94-007-1573-8.

[60] F. K. Shaikh and S. Zeadally, "Energy harvesting in wireless sensor networks: A comprehensive review," *Renewable and Sustainable Energy Reviews*, vol. 55. 2016. doi: 10.1016/j.rser.2015.11.010.

[61] K. Halim, G. Mohamed, and G. Ali, "Enhancing DPM techniques in outdoor industrial WSN applications," *International Journal of Distributed Sensor Networks*, vol. 12, no. 7, 2016, doi: 10.1177/155014771350246.

[62] A. S. Ali, C. Coté, M. Heidarinejad, and B. Stephens, "Elemental: An open-source wireless hardware and software platform for building energy and indoor environmental monitoring and control," *Sensors (Switzerland)*, vol. 19, no. 18, 2019, doi: 10.3390/s19184017.

[63] D. Hall, D. C. Ranasinghe, B. Jamali, and P. H. Cole, “Turn-on circuits based on standard CMOS technology for active RFID labels,” in *VLSI Circuits and Systems II*, 2005, vol. 5837. doi: 10.1117/12.624882.

[64] C. Julien, A. Mauger, A. Vijh, and K. Zaghib, “Lithium Batteries: Science and Technology,” *Lithium Batteries: Science and Technology*, pp. 1–619, Oct. 2015, doi: 10.1007/978-3-319-19108-9.

[65] “Shenzhen Honcell Energy Co., Ltd.” http://www.honcell.com/ (accessed Oct. 17, 2021).

[66] “Saft Batteries | We energize the world.” https://www.saftbatteries.com/ (accessed Oct. 17, 2021).

[67] “Batteries | #1 Trusted Battery Brand | Duracell.” https://www.duracell.com/en-us/ (accessed Oct. 17, 2021).

[68] “Tadiran lithium batteries offer PROVEN 40 year operating life.” https://www.tadiranbat.com/ (accessed Oct. 17, 2021).

[69] “Panasonic Batteries | High quality alkaline, zinc & rechargable batteries.” https://www.panasonic-batteries.com/en (accessed Oct. 17, 2021).

[70] Z. Abdin and K. R. Khalilpour, “Single and Polystorage Technologies for Renewable-Based Hybrid Energy Systems,” *Polygeneration with Polystorage: For Chemical and Energy Hubs*, pp. 77–131, Jan. 2019, doi: 10.1016/B978-0-12-813306-4.00004-5.

[71] A. Ameur, A. Berrada, K. Loudiyi, and R. Adomatis, “Performance and energetic modeling of hybrid PV systems coupled with battery energy storage,” *Hybrid Energy System Models*, pp. 195–238, Jan. 2021, doi: 10.1016/B978-0-12-821403-9.00008-1.

[72] K. J. Kim, M. Balaish, M. Wadaguchi, L. Kong, and J. L. M. Rupp, “Solid-State Li–Metal Batteries: Challenges and Horizons of Oxide and Sulfide Solid Electrolytes and Their Interfaces,” *Advanced Energy Materials*, vol. 11, no. 1, p. 2002689, Jan. 2021, doi: 10.1002/AENM.202002689.

[73] M. H. Braga, N. S. Grundish, A. J. Murchison, and J. B. Goodenough, “Alternative strategy for a safe rechargeable battery,” *Energy & Environmental Science*, vol. 10, no. 1, pp. 331–336, Jan. 2017, doi: 10.1039/C6EE02888H.

[74] S. Roberts, “DC/DC Book of Knowledge - Practical tips for the User,” *Recom*, 2016.

[75] C. N. Nayar, S. M. Islam, H. Dehbonei, and K. Tan, “Power Electronics Handbook - Devices, Circuits, and Applications (3rd Edition),” *Power Electronics Handbook: Devices, Circuits, and Applications*, pp. 673–716, 2011, Accessed: Nov. 14, 2021. [Online]. Available:

http://app.knovel.com/hotlink/pdf/id:kt008U4541/power-electronics-handbook/basics-photovoltaics

[76] M. Potocny *et al.*, "Low-Voltage DC-DC Converter for IoT and On-Chip Energy Harvester Applications," *Sensors 2021, Vol. 21, Page 5721*, vol. 21, no. 17, p. 5721, Aug. 2021, doi: 10.3390/S21175721.

[77] W. Hwang, K. Yoo, D. van Thai, W. Lee, and K.-H. Baek, "Design of a DC–DC Converter Customized for Ultra-Low Voltage Operating IoT Platforms," *Energies 2020, Vol. 13, Page 461*, vol. 13, no. 2, p. 461, Jan. 2020, doi: 10.3390/EN13020461.

[78] V. Ivanov, "Design of Powerful DCDC Converters with Nanopower Consumption," *Low-Power Analog Techniques, Sensors for Mobile Devices, and Energy Efficient Amplifiers*, pp. 31–57, 2019, doi: 10.1007/978-3-319-97870-3_3.

[79] S. Mohsen, A. Zekry, K. Youssef, and M. Abouelatta, "A Self-powered Wearable Wireless Sensor System Powered by a Hybrid Energy Harvester for Healthcare Applications," *Wireless Personal Communications*, vol. 116, no. 4, 2021, doi: 10.1007/s11277-020-07840-y.

[80] S. Mohsen, A. Zekry, M. Abouelatta, and K. Youssef, "A self-powered wearable sensor node for iot healthcare applications," in *Proceedings of the 8th International Japan-Africa Conference on Electronics, Communications and Computations, JAC-ECC 2020*, 2020, pp. 70–73. doi: 10.1109/JAC-ECC51597.2020.9355925.

[81] N. H. Zamora, J. C. Kao, and R. Marculescu, "Distributed power-management techniques for wireless network video systems," in *Proceedings -Design, Automation and Test in Europe, DATE*, 2007, pp. 1–6. doi: 10.1109/DATE.2007.364653.

[82] S. Bhatti and J. Xu, "Survey of target tracking protocols using wireless sensor network," in *5th International Conference on Wireless and Mobile Communications, ICWMC 2009*, 2009, pp. 110–115. doi: 10.1109/ICWMC.2009.25.

[83] B. Brock and K. Rajamani, "Dynamic power management for embedded systems [SOC design]," in *Proceedings - IEEE International SOC Conference, SOCC 2003*, 2003, pp. 416–419. doi: 10.1109/SOC.2003.1241556.

[84] P. S. Sausen, M. A. Spohn, and A. Perkusich, "Broadcast routing in wireless sensor networks with dynamic power management and multi-coverage backbones," *Information Sciences*, vol. 180, no. 5, 2010, doi: 10.1016/j.ins.2009.11.016.

[85] N. H. Zamora and R. Marculescu, "Coordinated distributed power management with video sensor networks: Analysis, simulation, and prototyping," in *2007 1st ACM/IEEE International*

Conference on Distributed Smart Cameras, ICDSC, 2007, pp. 4–11. doi: 10.1109/ICDSC.2007.4357499.

[86] Yingqi Xu, J. Winter, and Wang-Chien Lee, "Dual prediction-based reporting for object tracking sensor networks," in *The First Annual International Conference on Mobile and Ubiquitous Systems: Networking and Services, 2004. MOBIQUITOUS 2004.*, 2004, pp. 154–163. doi: 10.1109/MOBIQ.2004.1331722.

[87] S. Friedrichs, U. Kulau, and L. Wolf, "Energy-efficient voltage scheduling of peripheral components on wireless sensor nodes," in *2014 IEEE International Conference on Communications Workshops, ICC 2014*, 2014, pp. 860–865. doi: 10.1109/ICCW.2014.6881308.

[88] W. Dargie, "Dynamic power management in wireless sensor networks: State-of-the-art," *IEEE Sensors Journal*, vol. 12, no. 5, 2012, doi: 10.1109/JSEN.2011.2174149.

[89] W. Dargie, "Analysis of the power consumption of a multimedia server under different DVFS policies," in *Proceedings - 2012 IEEE 5th International Conference on Cloud Computing, CLOUD 2012*, 2012, pp. 779–785. doi: 10.1109/CLOUD.2012.31.

[90] H. Aydin, V. Devadas, and D. Zhu, "System-level energy management for periodic real-time tasks," in *Proceedings - Real-Time Systems Symposium*, 2006, pp. 313–322. doi: 10.1109/RTSS.2006.48.

[91] P. Pillai and K. G. Shin, "Real-time dynamic voltage scaling for low-power embedded operating systems," *Operating Systems Review (ACM)*, vol. 35, no. 5, 2001, doi: 10.1145/502059.502044.

[92] V. Raghunathan, C. Schurgers, S. Park, and M. B. Srivastava, "Energy-aware wireless microsensor networks," *IEEE Signal Processing Magazine*, vol. 19, no. 2, 2002, doi: 10.1109/79.985679.

[93] P. Levis *et al.*, "TinyOS: An operating system for sensor networks," in *Ambient Intelligence*, 2005. doi: 10.1007/3-540-27139-2_7.

[94] E. Baccelli, O. Hahm, M. Gunes, M. Wahlisch, and T. Schmidt, "RIOT OS: Towards an OS for the Internet of Things," in *2013 IEEE Conference on Computer Communications Workshops (INFOCOM WKSHPS)*, 2014, pp. 79–80. doi: 10.1109/infcomw.2013.6970748.

[95] A. Dunkels, B. Grönvall, and T. Voigt, "Contiki - A lightweight and flexible operating system for tiny networked sensors," in *Proceedings - Conference on Local Computer Networks, LCN*, 2004, pp. 455–462. doi: 10.1109/LCN.2004.38.

[96] M. Kovatsch, S. Duquennoy, and A. Dunkels, “A low-power CoAP for Contiki,” *Proceedings - 8th IEEE International Conference on Mobile Ad-hoc and Sensor Systems, MASS 2011*, pp. 855–860, 2011, doi: 10.1109/MASS.2011.100.

[97] K. Geissdoerfer, M. Chwalisz, and M. Zimmerling, “Taking a Deep Dive Into The Batteryless Internet of Things With Shepherd,” *GetMobile: Mobile Computing and Communications*, vol. 24, no. 3, pp. 5–8, 2021, doi: 10.1145/3447853.3447855.

[98] K. Geissdoerfer, M. Chwalisz, and M. Zimmerling, “Shepherd: A portable testbed for the batteryless IoT,” in *SenSys 2019 - Proceedings of the 17th Conference on Embedded Networked Sensor Systems*, 2019, pp. 83–95. doi: 10.1145/3356250.3360042.

[99] J. Ylinen, M. Koskela, L. Iso-Anttila, and P. Loula, “Near field communication network services,” *Proceedings of the 3rd International Conference on Digital Society, ICDS 2009*, pp. 89–93, 2009, doi: 10.1109/ICDS.2009.43.

[100] S. Kamath and J. Lindh Keywords, “Measuring Bluetooth® Low Energy Power Consumption”, Accessed: Jan. 23, 2022. [Online]. Available: www.ti.com/lit/zip/SWRA347.

[101] J. S. Lee, M. F. Dong, and Y. H. Sun, “A preliminary study of low power wireless technologies: ZigBee and Bluetooth Low Energy,” *Proceedings of the 2015 10th IEEE Conference on Industrial Electronics and Applications, ICIEA 2015*, pp. 135–139, Nov. 2015, doi: 10.1109/ICIEA.2015.7334098.

[102] A. Lavric, A. I. Petrariu, and V. Popa, “Long Range SigFox Communication Protocol Scalability Analysis under Large-Scale, High-Density Conditions,” *IEEE Access*, vol. 7, pp. 35816–35825, 2019, doi: 10.1109/ACCESS.2019.2903157.

[103] Y. Lykov, A. Paniotova, V. Shatalova, and A. Lykova, “Energy Efficiency Comparison LPWANs: LoRaWAN vs Sigfox,” *2020 IEEE International Conference on Problems of Infocommunications Science and Technology, PIC S and T 2020 - Proceedings*, pp. 485–490, Oct. 2021, doi: 10.1109/PICST51311.2020.9468026.

[104] “Low data rate, low power sub-1GHz transceiver,” SPIRIT1, DocID022758 Rev. 11, ST Microelectronics, Aug. 2021. Accessed: Jan. 27, 2022. [Online]. Available: https://www.st.com/resource/en/datasheet/spirit1.pdf

[105] “CC1201 Low-Power, High-Performance RF Transceiver,” SWRS154B, Rev. B, TI, Oct. 2014. Accessed: Jan. 29, 2022. [Online]. Available: https://www.ti.com/lit/gpn/cc1201

[106] “High Performance, ISM Band, FSK/ASK Transceiver IC,” ADF7020. Rev. E, Analog Devices, Sep. 2016. Accessed: Jan. 29, 2022. [Online]. Available: https://www.analog.com/media/en/technical-documentation/data-sheets/ADF7020.pdf

[107] “ATA8510/ATA8515 - UHF ASK/FSK Transceiver,” 9315G-INDCO-08/15, Atmel, Aug. 2015. Accessed: Jan. 29, 2022. [Online]. Available: https://ww1.microchip.com/downloads/en/DeviceDoc/Atmel-9315-Smart-RF-ATA8510-ATA8515_Datasheet.pdf

[108] H. A. H. Alobaidy, J. S. Mandeep, R. Nordin, N. F. Abdullah, C. G. Wei, and M. L. S. Soon, “Real-World Evaluation of Power Consumption and Performance of NB-IoT in Malaysia,” *IEEE Internet of Things Journal*, pp. 1–1, Nov. 2021, doi: 10.1109/JIOT.2021.3131160.

[109] H. Tu, X. Zhao, and J. Ban, “SIM7080G Hardware Design,” Rev. 1.04, SIMCom, Sep. 2020. Accessed: Jan. 28, 2022. [Online]. Available: https://www.simcom.com/service-86.html

[110] L. Liu, D. Du, H. Ding, and R. Wang, “BG96 Hardware Design - LPWA Module Series,” Rev 1.4, Quectel, Aug. 2019. Accessed: Jan. 29, 2022. [Online]. Available: https://www.quectel.com/download_file/1409

[111] “SARA-R5 series - LTE-M / NB-IoT modules with secure cloud - Data sheet,” UBX-19016638, Rev. 11, u-blox, Dec. 2021. Accessed: Jan. 29, 2022. [Online]. Available: https://www.u-blox.com/en/ubx-viewer/view/SARA-R5_DataSheet_UBX-19016638?url=https%3A%2F%2Fwww.u-blox.com%2Fsites%2Fdefault%2Ffiles%2FSARA-R5_DataSheet_UBX-19016638.pdf

[112] “Cinterion® EXS62-W/EXS82-W Hardware Interface Description,” EXS62-W_EXS82-W_HID_v01.100a, Thales, Sep. 2020. Accessed: Feb. 12, 2022. [Online]. Available: https://m2m-communication.gemalto.com/Thales_EXS62W_EXS82W_HID

[113] “SARA-R5 series - LTE-M / NB-IoT modules with secure cloud - System integration manual,” UBX-19041356, Rev. 08, u-blox, Dec. 2021. Accessed: Feb. 12, 2022. [Online]. Available: https://www.u-blox.com/en/docs/UBX-19041356

[114] K. Mekki, E. Bajic, F. Chaxel, and F. Meyer, “A comparative study of LPWAN technologies for large-scale IoT deployment,” *ICT Express*, vol. 5, no. 1, pp. 1–7, Mar. 2019, doi: 10.1016/J.ICTE.2017.12.005.

[115] B. Xiong and R. Wang, “EG91 Series Hardware Design - LTE Standard Module Series,” Rev. 2.1, Quectel, Jul. 2021. Accessed: Jan. 29, 2022. [Online]. Available: https://www.quectel.com/download_file/19845

[116] Y. Chen, D. Du, F. Wang, and L. Xu, “EM05 Hardware Design - LTE Standard Module Series,” Rev. 1.2, Quectel, Jan. 2020. Accessed: Jan. 29, 2022. [Online]. Available: https://www.quectel.com/download_file/14485

[117] “Cinterion® ELS31-V Hardware Interface Description,” ELS31-V_HID_v4.3.3.0fb, v. 4.3.3.0fb, Thales, Apr. 2020. Accessed: Jan. 29, 2022. [Online]. Available: https://m2m-communication.gemalto.com/Thales_ELS31V_HID

[118] “Cinterion® PDS6 Hardware Interface Description,” PDS6_HID_v04.003, v. 04.003, Thales, May 2020. Accessed: Jan. 29, 2022. [Online]. Available: https://m2m-communication.gemalto.com/Thales_PDS6_HID

[119] “Cinterion® ELS81-US Hardware Interface Description,” els81-us_hid_v04.000b, Thales, Apr. 2020. Accessed: Feb. 12, 2022. [Online]. Available: https://m2m-communication.gemalto.com/Thales_ELS81US_HID

[120] Z. Chen, X. Liu, Y. Xia, and J. Liu, “A7672X Series Hardware Design,” Rev. 1.01, SIMCom, Nov. 2021. Accessed: Jan. 29, 2022. [Online]. Available: https://www.simcom.com/service-1385.html

[121] Q. Jin Bai, “A7602E-H&A7608SA-H Hardware Design,” Rev. 1.00, Jun. 2021. Accessed: Jan. 29, 2022. [Online]. Available: https://www.simcom.com/service-1405.html

[122] J. Mathews, M. Barnes, and D. K. Arvind, “Low power free space optical communication in wireless sensor networks,” *12th Euromicro Conference on Digital System Design: Architectures, Methods and Tools, DSD 2009*, pp. 849–856, 2009, doi: 10.1109/DSD.2009.234.

[123] I. Sohn, Y. H. Jang, and S. H. Lee, “Ultra-low-power implantable medical devices: Optical wireless communication approach,” *IEEE Communications Magazine*, vol. 58, no. 5, pp. 77–83, May 2020, doi: 10.1109/MCOM.001.1900609.

[124] J. Mathews, M. Barnes, A. Young, and D. K. Arvind, “Low power wake-up in Wireless Sensor Networks using Free Space Optical communications,” *Proceedings - 4th International Conference on Sensor Technologies and Applications, SENSORCOMM 2010*, pp. 256–261, 2010, doi: 10.1109/SENSORCOMM.2010.47.

[125] L. Klaver and M. Zuniga, “Shine: A step towards distributed multi-hop visible light communication,” in *Proceedings - 2015 IEEE 12th International Conference on Mobile Ad Hoc and Sensor Systems, MASS 2015*, 2015, pp. 235–243. doi: 10.1109/MASS.2015.78.

[126] Q. Wang, S. Yin, O. Gnawali, and D. Giustiniano, “Demo: OpenVLC1.0 Platform for Research in Visible Light Communication Networks,” in *Proceedings of the 21st Annual International Conference on Mobile Computing and Networking - MobiCom ’15*, 2015, vol. 20, no. 3.

[127] S. Schmid, G. Corbellini, S. Mangold, and T. R. Gross, “LED-to-LED Visible Light Communication networks,” in *Proceedings of the International Symposium on Mobile Ad Hoc Networking and Computing (MobiHoc)*, 2013, p. 1. doi: 10.1145/2491288.2491293.

[128] P. Dietz, W. Yerazunis, and D. Leigh, “Very Low-Cost Sensing and Communication Using Bidirectional LEDs,” *Lecture Notes in Computer Science (including subseries Lecture Notes in Artificial Intelligence and Lecture Notes in Bioinformatics)*, vol. 2864, pp. 175–191, Oct. 2003, doi: 10.1007/978-3-540-39653-6_14.

[129] S. Schmid, T. Bourchas, S. Mangold, and T. R. Gross, “Linux light bulbs: Enabling internet protocol connectivity for light bulb networks,” in *VLCS 2015 - Proceedings of the 2nd International Workshop on Visible Light Communications Systems, co-located with MobiCom 2015*, 2015, pp. 3–8. doi: 10.1145/2801073.2801074.

[130] J. Henrie, J. Evans, and T. Minh, “Apparatus and method for wireless communication between a host and a selectively removable module electrically connected to the host,” 2001

[131] G. Leenders, G. Callebaut, L. van der Perre, and L. de Strycker, “An Experimental Evaluation of Energy Trade-Offs in Narrowband IoT,” 2020. doi: 10.1109/WF-IoT48130.2020.9221010.

[132] M. Lauridsen, R. Krigslund, M. Rohr, and G. Madueno, “An Empirical NB-IoT Power Consumption Model for Battery Lifetime Estimation,” in *IEEE Vehicular Technology Conference*, 2018, vol. 2018-June. doi: 10.1109/VTCSpring.2018.8417653.

[133] “Primary Lithium Battery - LS 26500,” Doc. No 31016-2-0510, Saft, May 2010. Accessed: Feb. 12, 2022. [Online]. Available: https://www.saftbatteries.com/download_file/6X7JMGAnv3Fm6HdmtEv%252B2gtlbZ1bRRVHkjS11M6md92GD2EF7vU%252F3Oybbz3WOlG%252BxR8srpA5iCdJ%252FV3IQzTVHQyiTucngZKEg9KkYCLkowAvgaG1huro9WKJ3UfO703Xe15DCKhtHpMt4rQJ6fDjUHI87SAtgmvKaGFh1ARccxABR6hW1Q%253D%253D/LS26500_0510.45639c68-11ea-4d97-8a55-aeea8be04354.pdf

[134] R. Grezaud, L. Sibeud, F. Lepin, J. Willemin, J. C. Riou, and B. Gomez, “A robust and versatile,-40°C to +180°C, 8Sps to 1kSps, multi power source wireless sensor system for aeronautic applications,” *IEEE Symposium on VLSI Circuits, Digest of Technical Papers*, pp. C310–C311, Aug. 2017, doi: 10.23919/VLSIC.2017.8008520.

[135] S. Oh *et al.*, “Low-Power Resistive Bridge Readout Circuit Integrated in Two Millimeter-Scale Pressure-Sensing Systems,” *Low-Power Analog Techniques, Sensors for Mobile Devices, and Energy Efficient Amplifiers*, pp. 111–128, 2019, doi: 10.1007/978-3-319-97870-3_6.

[136] M. Liu, K. Pelzers, R. van Dommele, A. van Roermund, and P. Harpe, “Nanopower SAR ADCs with Reference Voltage Generation,” *Low-Power Analog Techniques, Sensors for Mobile Devices, and Energy Efficient Amplifiers*, pp. 59–82, 2019, doi: 10.1007/978-3-319-97870-3_4.

[137] F. Reverter, “Rail-to-Rail Timer-Based Demodulator for AM Sensor Signals,” *IEEE Transactions on Instrumentation and Measurement*, vol. 68, no. 1, pp. 306–308, Jan. 2019, doi: 10.1109/TIM.2018.2879127.

[138] F. Reverter and M. Gasulla, “Demodulating AM Square Signals via a Digital Timer for Sensor Applications,” *IEEE Transactions on Instrumentation and Measurement*, vol. 69, no. 5, pp. 2593–2601, May 2020, doi: 10.1109/TIM.2020.2964075.

[139] F. Reverter and M. Gasulla, “Using a digital timer to demodulate AM triangular signals for sensor applications,” *I2MTC 2020 - International Instrumentation and Measurement Technology Conference, Proceedings*, May 2020, doi: 10.1109/I2MTC43012.2020.9128788.

[140] L. Areekath, B. George, and F. Reverter, “A simple direct microcontroller interface for capacitively-coupled resistive sensors,” *I2MTC 2020 - International Instrumentation and Measurement Technology Conference, Proceedings*, May 2020, doi: 10.1109/I2MTC43012.2020.9128801.

[141] M. W. Ahmad, M. Mourshed, D. Mundow, M. Sisinni, and Y. Rezgui, “Building energy metering and environmental monitoring - A state-of-the-art review and directions for future research,” *Energy and Buildings*, vol. 120. 2016. doi: 10.1016/j.enbuild.2016.03.059.

[142] G. Spasov, M. Kutseva, G. Petrova, and V. Tsvetkov, “A Smart Solution for Electrical Power Monitoring Based on MCP39F501 Sensor,” in *2019 28th International Scientific Conference Electronics, ET 2019 - Proceedings*, 2019, pp. 1–4. doi: 10.1109/ET.2019.8878502.

[143] R. A. Stewart *et al.*, “Integrated intelligent water-energy metering systems and informatics: Visioning a digital multi-utility service provider,” *Environmental Modelling and Software*, vol. 105, 2018, doi: 10.1016/j.envsoft.2018.03.006.

[144] E. & Young, “Cost-benefit analysis for the comprehensive use of smart metering,” 2013. Accessed: Jan. 16, 2022. [Online]. Available: https://www.bmwi.de/Redaktion/EN/Publikationen/cost-benefit-analysis-for-the-comprehensive-use-of-smart-metering-systems.html

[145] “Pilot natural gas remote meter reading scheme in El Papiol (Barcelona) | Conócenos.” https://www.nedgia.es/conocenos/en/pilot-natural-gas-remote-meter-reading-scheme-in-el-papiol-barcelona/ (accessed Jul. 14, 2021).

[146] “EN 16314:2013 - Gas meters - Additional functionalities.” https://standards.iteh.ai/catalog/standards/cen/979f0c31-e88c-433c-bc73-63686b18b643/en-16314-2013 (accessed Oct. 21, 2021).

[147] J. Crihfield, “gas meter.” stock.adobe.com.

[148] Christian, “Abstract image of an old UK gas meter.” stock.adobe.com.

[149] Z. He, Y. He, Y. Yang, and M. Gao, “A low-cost direct reading system for gas meter based on machine vision,” in *Proceedings of the 2017 12th IEEE Conference on Industrial Electronics and Applications, ICIEA 2017*, 2018, vol. 2018-February. doi: 10.1109/ICIEA.2017.8283020.

[150] H. U. R. Siddiqui, R. Brown, S. Dudley, and M. F. Mushtaq, “Gas Metering Using Optical Sensor,” in *ICETAS 2019 - 2019 6th IEEE International Conference on Engineering, Technologies and Applied Sciences*, 2019, pp. 1–5. doi: 10.1109/ICETAS48360.2019.9117567.

[151] Y. Jiang, Y. Liang, Y. Cui, L. He, Y. Cao, and C. Hu, “Wireless digital gas meter with lower power consumption,” in *Proceedings - 5th International Conference on Frontier of Computer Science and Technology, FCST 2010*, 2010, pp. 192–197. doi: 10.1109/FCST.2010.113.

[152] O. Rorato, S. Bertoldo, C. Lucianaz, M. Allegretti, and R. Notarpietro, “An Ad-Hoc Low Cost Wireless Sensor Network for Smart Gas Metering,” *Wireless Sensor Network*, vol. 05, no. 03, 2013, doi: 10.4236/wsn.2013.53008.

[153] M. Tewolde and J. P. Longtin, “High-resolution meter reading system for gas utility meter,” in *Proceedings of IEEE Sensors*, 2010, pp. 849–852. doi: 10.1109/ICSENS.2010.5690859.

[154] A. Babuta, B. Gupta, A. Kumar, and S. Ganguli, “Power and energy measurement devices: A review, comparison, discussion, and the future of research,” *Measurement: Journal of the International Measurement Confederation*, vol. 172. 2021. doi: 10.1016/j.measurement.2020.108961.

[155] B. C. Puig and J. Carmona, “Bridging the gap between energy consumption and distribution through non-technical loss detection,” *Energies*, vol. 12, no. 9, 2019, doi: 10.3390/en12091748.

[156] M. Mesganaw, “Case Tamper Detection Reference Design Using Inductive Sensing”, Accessed: Sep. 30, 2021. [Online]. Available: www.ti.com

[157] F. J. Boudreau and M. Kraus, “Electronic Tamper Detection in a Utility Meter Using Magnetics,” U.S. Patent, US9274146B2, Aug. 13, 2016 Accessed: Sep. 30, 2021. [Online]. Available: https://patents.google.com/patent/US9274146B2

[158] M. A. Murphy, “A system and method for detecting tampering of a utility meter,” U.S. Patent, US7847690B2, Jul. 09, 2009 Accessed: Sep. 30, 2021. [Online]. Available: https://patents.google.com/patent/US7847690B2

[159] S. Zigovszki and M. A. Thomas, “Magnetic sensing to detect tampering with a utility meter,” Art. no. U.S. Patent, US9671254B2, Sep. 2014, Accessed: Sep. 30, 2021. [Online]. Available: https://patents.google.com/patent/US9671254B2/

[160] Texas Instruments, “Magnetic Tamper Detection Using Low-Power Hall Effect,” TI, TIDA-00839, 2016. Accessed: Jan. 16, 2022. [Online]. Available: https://www.ti.com.cn/cn/lit/ug/tidub69/tidub69.pdf

[161] “Rotary gas meter series TAR”, Accessed: Sep. 30, 2021. [Online]. Available: www.tormenegroup.com

[162] A. D. Ramirez, “Magnetic Tampering Detection in a Utility Meter,” Art. no. U.S. Patent, US9658254B2, Jun. 2013, Accessed: Sep. 30, 2021. [Online]. Available: https://patents.google.com/patent/US9658254

[163] R. Budampati and J. Becker, “Methods and systems for activating sealed sensors in the field,” U.S. Patent, US10018487B2, 2018 Accessed: Jan. 16, 2022. [Online]. Available: https://patents.google.com/patent/US10018487B2

[164] “XC6194 Series | Your analog power IC and the best power management, TOREX.” https://www.torexsemi.com/products/push-button-controllers/series/?name=xc6194 (accessed Oct. 31, 2021).

[165] D. J. Knapp, “Optical communication device, method and system,” U.S. Patent, US20100061734A1, 2010 Accessed: Jan. 16, 2022. [Online]. Available: https://patents.google.com/patent/US20100061734

[166] K. Karren and A. Gkourlias, “System and method for activating an isolated device,” U.S. Patent, US8928190B2, 2011 Accessed: Jan. 16, 2022. [Online]. Available: https://patents.google.com/patent/US8928190

[167] Y. Li *et al.*, “A near-short-wave IR tunable InGaAs nanomembrane PhotoFET on flexible substrate for lightweight and wide-angle imaging applications,” *Digest of Technical Papers - Symposium on VLSI Technology*, vol. 2018-June, pp. 159–160, Oct. 2018, doi: 10.1109/VLSIT.2018.8510702.

[168] A. Pérez-Tomás, A. Lima, Q. Billon, I. Shirley, G. Catalan, and M. Lira-Cantú, “A Solar Transistor and Photoferroelectric Memory,” *Advanced Functional Materials*, vol. 28, no. 17, p. 1707099, Apr. 2018, doi: 10.1002/ADFM.201707099.

[169] M. Kowalczyk and J. Siuzdak, “Photo-reception properties of common LEDs,” *Opto-Electronics Review*, vol. 25, no. 3, pp. 222–228, Sep. 2017, doi: 10.1016/J.OPELRE.2017.06.009.

[170] J. Sticklus, P. A. Hoeher, and M. Hieronymi, “Experimental Characterization of Single-Color Power LEDs Used as Photodetectors,” *Sensors 2020, Vol. 20, Page 5200*, vol. 20, no. 18, p. 5200, Sep. 2020, doi: 10.3390/S20185200.

[171] T. Li, C. An, Z. Tian, A. T. Campbell, and X. Zhou, “Human sensing using visible light communication,” in *Proceedings of the Annual International Conference on Mobile Computing and Networking, MOBICOM*, 2015, vol. 2015-Septe. doi: 10.1145/2789168.2790110.

[172] Z. Yang, Z. Wang, J. Zhang, C. Huang, and Q. Zhang, “Wearables can afford: Light-weight indoor positioning with visible light,” in *MobiSys 2015 - Proceedings of the 13th Annual International Conference on Mobile Systems, Applications, and Services*, 2015, pp. 465–465. doi: 10.1145/2742647.2745924.

[173] S. Yin and O. Gnawali, “Towards embedded visible light communication robust to dynamic ambient light,” in *2016 IEEE Global Communications Conference, GLOBECOM 2016 - Proceedings*, 2016, pp. 1–6. doi: 10.1109/GLOCOM.2016.7842344.

[174] Z. Tian, K. Wrighty, and X. Zhou, “Lighting up the internet of things with DarkVLC,” in *HotMobile 2016 - Proceedings of the 17th International Workshop on Mobile Computing Systems and Applications*, 2016, pp. 33–38. doi: 10.1145/2873587.2873598.

[175] Y. Zhao and J. Vongkulbhisal, “Design of visible light communication receiver for on-off keying modulation by adaptive minimum-voltage cancelation,” *Engineering Journal*, vol. 17, no. 4, 2013, doi: 10.4186/ej.2013.17.4.125.

[176] “Photosensing with ambient background - EDN.” https://www.edn.com/photosensing-with-ambient-background/ (accessed Jul. 14, 2021).

[177] M. Heydariaan, S. Yin, O. Gnawali, D. Puccinelli, and D. Giustiniano, “Embedded Visible Light Communication: Link Measurements and Interpretation,” *Proceedings of the MadCom: New Wireless Communication Paradigms for the Internet of Things Workshop (MadCom 2016)*, 2016.

[178] S. Sudevalayam and P. Kulkarni, “Energy harvesting sensor nodes: Survey and implications,” *IEEE Communications Surveys and Tutorials*, vol. 13, no. 3, 2011, doi: 10.1109/SURV.2011.060710.00094.

[179] S. Chalasani and J. M. Conrad, “A survey of energy harvesting sources for embedded systems,” *Conference Proceedings - IEEE SOUTHEASTCON*, pp. 442–447, 2008, doi: 10.1109/SECON.2008.4494336.

[180] A. R. M. Siddique, S. Mahmud, and B. van Heyst, “A review of the state of the science on wearable thermoelectric power generators (TEGs) and their existing challenges,” *Renewable and Sustainable Energy Reviews*, vol. 73, pp. 730–744, Jun. 2017, doi: 10.1016/J.RSER.2017.01.177.

[181] A. Kadechkar, J. R. Riba, M. Moreno-Eguilaz, and J. Perez, "SmartConnector: A Self-Powered IoT Solution to Ease Predictive Maintenance in Substations," *IEEE Sensors Journal*, vol. 20, no. 19, pp. 11632–11641, Oct. 2020, doi: 10.1109/JSEN.2020.2998157.

[182] T. Sanislav, G. D. Mois, S. Zeadally, and S. C. Folea, "Energy Harvesting Techniques for Internet of Things (IoT)," *IEEE Access*, vol. 9, pp. 39530–39549, 2021, doi: 10.1109/ACCESS.2021.3064066.

[183] J. Wang, S. Zhou, Z. Zhang, and D. Yurchenko, "High-performance piezoelectric wind energy harvester with Y-shaped attachments," *Energy Conversion and Management*, vol. 181, pp. 645–652, Feb. 2019, doi: 10.1016/J.ENCONMAN.2018.12.034.

[184] X. Zhao, J. Cai, Y. Guo, C. Li, J. Wang, and H. Zheng, "Modeling and experimental investigation of an AA-sized electromagnetic generator for harvesting energy from human motion," *Smart Materials and Structures*, vol. 27, no. 8, p. 085008, Jul. 2018, doi: 10.1088/1361-665X/AACDC4.

[185] P. Vincent *et al.*, "Indoor-type photovoltaics with organic solar cells through optimal design," *Dyes and Pigments*, vol. 159, pp. 306–313, Dec. 2018, doi: 10.1016/J.DYEPIG.2018.06.025.

[186] F. Mateen, M. Ahsan Saeed, J. Won Shim, and S. K. Hong, "Indoor/outdoor light-harvesting by coupling low-cost organic solar cell with a luminescent solar concentrator," *Solar Energy*, vol. 207, pp. 379–387, Sep. 2020, doi: 10.1016/J.SOLENER.2020.06.104.

[187] W. Ma *et al.*, "A flexible self-charged power panel for harvesting and storing solar and mechanical energy," *Nano Energy*, vol. 65, p. 104082, Nov. 2019, doi: 10.1016/J.NANOEN.2019.104082.

[188] "Photovoltaic modules - Panneaux Solaires au Silicium | Solems.com." https://www.solems.com/en/photovoltaic-modules (accessed Oct. 30, 2021).

[189] R. la Rosa, C. Dehollain, A. Burg, M. Costanza, and P. Livreri, "An Energy-Autonomous Wireless Sensor with Simultaneous Energy Harvesting and Ambient Light Sensing," *IEEE Sensors Journal*, 2021, doi: 10.1109/JSEN.2021.3068134.

[190] V. Talla, B. Kellogg, B. Ransford, S. Naderiparizi, S. Gollakota, and J. R. Smith, "Powering the Next Billion Devices with Wi-Fi," *Proceedings of the 11th ACM Conference on Emerging Networking Experiments and Technologies*, pp. 1–13, Dec. 2015, doi: 10.1145/2716281.2836089.

[191] M. Piñuela, P. D. Mitcheson, and S. Lucyszyn, "Ambient RF energy harvesting in urban and semi-urban environments," *IEEE Transactions on Microwave Theory and Techniques*, vol. 61, no. 7, pp. 2715–2726, 2013, doi: 10.1109/TMTT.2013.2262687.

[192] A. Sample and J. R. Smith, “Experimental results with two wireless power transfer systems,” *RWS 2009 IEEE Radio and Wireless Symposium, Proceedings*, pp. 16–18, 2009, doi: 10.1109/RWS.2009.4957273.

[193] I. Chaour, A. Fakhfakh, and O. Kanoun, “Enhanced Passive RF-DC Converter Circuit Efficiency for Low RF Energy Harvesting,” *Sensors 2017, Vol. 17, Page 546*, vol. 17, no. 3, p. 546, Mar. 2017, doi: 10.3390/S17030546.

[194] T. Soyata, L. Copeland, and W. Heinzelman, “RF Energy Harvesting for Embedded Systems: A Survey of Tradeoffs and Methodology,” *IEEE Circuits and Systems Magazine*, vol. 16, no. 1, pp. 22–57, Jan. 2016, doi: 10.1109/MCAS.2015.2510198.

[195] M. R. Shokrani, M. Khoddam, M. N. B. Hamidon, N. A. Kamsani, F. Z. Rokhani, and S. bin Shafie, “An RF energy harvester system using UHF micropower CMOS rectifier based on a diode connected CMOS transistor,” *The Scientific World Journal*, vol. 2014, 2014, doi: 10.1155/2014/963709.

[196] M. Gasulla, J. Jordana, F.-J. Robert, and J. Berenguer, “Analysis of the Optimum Gain of a High-Pass L-Matching Network for Rectennas,” *Sensors 2017, Vol. 17, Page 1712*, vol. 17, no. 8, p. 1712, Jul. 2017, doi: 10.3390/S17081712.

[197] A. Astigarraga *et al.*, “A 21 m operation range RFID tag for ‘pick to light’ applications with a photovoltaic harvester,” *Micromachines*, vol. 11, no. 11, 2020, doi: 10.3390/mi11111013.

[198] E. Ripoll-Vercellone, V. Ferrandiz, and M. Gasulla, “An Add-On Electronic Device to Upgrade Mechanical Gas Meters into Electronic Ones,” *Proceedings*, vol. 2, no. 13, 2018, doi: 10.3390/proceedings2131094.

[199] E. Ripoll-Vercellone, M. Gasulla, and F. Reverter, “Electronic reading of a mechanical gas meter based on dual magnetic sensing,” *Measurement Science and Technology*, vol. 32, no. 9, p. 097001, Jun. 2021, doi: 10.1088/1361-6501/AC00E8.

[200] E. Ripoll Vercellone, V. Ferrandiz, J. Aubert, and M. Gasulla, “Using LEDs for Visible Light Communication and as a Wake-up Mechanism in the Internet of Things,” *Proceedings of the 15th ACM Conference on Embedded Network Sensor Systems*, 2017, doi: 10.1145/3131672.

[201] E. Ripoll-Vercellone, F. Reverter, V. Ferrandiz, and M. Gasulla, “Experimental characterization of off-the-shelf LEDs as photodetectors for waking up microcontrollers,” in *I2MTC 2019 - 2019 IEEE International Instrumentation and Measurement Technology Conference, Proceedings*, 2019, vol. 2019-May. doi: 10.1109/I2MTC.2019.8826967.

[202] E. Ripoll-Vercellone, F. Reverter, and M. Gasulla, "LED-Based Wake-Up Circuit for Microcontrollers," *IEEE Transactions on Instrumentation and Measurement*, vol. 69, no. 9, 2020, doi: 10.1109/TIM.2020.3009340.

[203] M. Gasulla, E. Ripoll-Vercellone, and F. Reverter, "A compact thévenin model for a rectenna and its application to an RF harvester with MPPT," *Sensors (Switzerland)*, vol. 19, no. 7, 2019, doi: 10.3390/s19071641.

[204] *A Dictionary of Physics*. 2019. doi: 10.1093/acref/9780198821472.001.0001.

[205] "Directive 2011/65/EU of the European Parliament and of the Council of 8 June 2011 on the restriction of the use of certain hazardous substances in electrical and electronic equipment (recast) (Text with EEA relevance)," *Official Journal L174*, pp. 88–110, Jul. 2011, doi: 10.3000/17252555.L_2011.174.eng.

[206] "Correlated color temperature," *Encyclopedic Dictionary of Polymers*, pp. 232–232, 2007, doi: 10.1007/978-0-387-30160-0_2905.